NASA Cooperative Agreement NCC 2-1209

Distributed and Centralized Conflict Management Under Traffic Flow Management Constraints

Dr. Karl Bilimoria, Technical Monitor
Eric Feron, Principle Investigator

Final report

Laboratory for Information and Decision Systems
International Center for Air Transportation
Massachusetts Institute of Technology

To

The National Aeronautics and Space Administration
Ames Research Center

February 5, 2003

Contents

List of Figures

Chapter 1

Introduction

1.1 Background

1.1.1 Current Air Traffic Control system

Current air transportation in the United States relies on a system born half a century ago. While demand for air travel has kept increasing over the years, technologies at the heart of the National Airspace System (NAS) have not been able to follow an adequate evolution. For instance, computers used to centralize flight data in airspace sectors run a software developed in 1972. Safety, as well as certification and portability issues arise as major obstacles for the improvement of the system.

The NAS is a structure that has never been designed, but has rather evolved over time. This has many drawbacks, mainly due to a lack of integration and engineering leading to many inefficiencies and losses of performance. To improve the operations, understanding of this complex needs to be built up to a certain level. This work presents research done on Air Traffic Management (ATM) at the level of the en-route sector.

1.1.2 Major issues

Today's air operations are characterized by an overwhelming emphasis on safety, with little relatively attention paid to performance of the service provided by Air Traffic Control (ATC) facilities. Although safety will always remain the most important task to be performed by ATC, experts agree that some efficiency awareness is needed in the system.

System-wide

The most obvious consequences of the NAS inefficiencies are the almost inevitable delays experienced by commercial flights in the US. As the system handles an ever increasing number of daily operations due to higher demand (see Fig. 1-1), it also nears a capacity limit - although this number remains an unknown. The variation in the last few years has shown that delays were increasing noticeably faster than

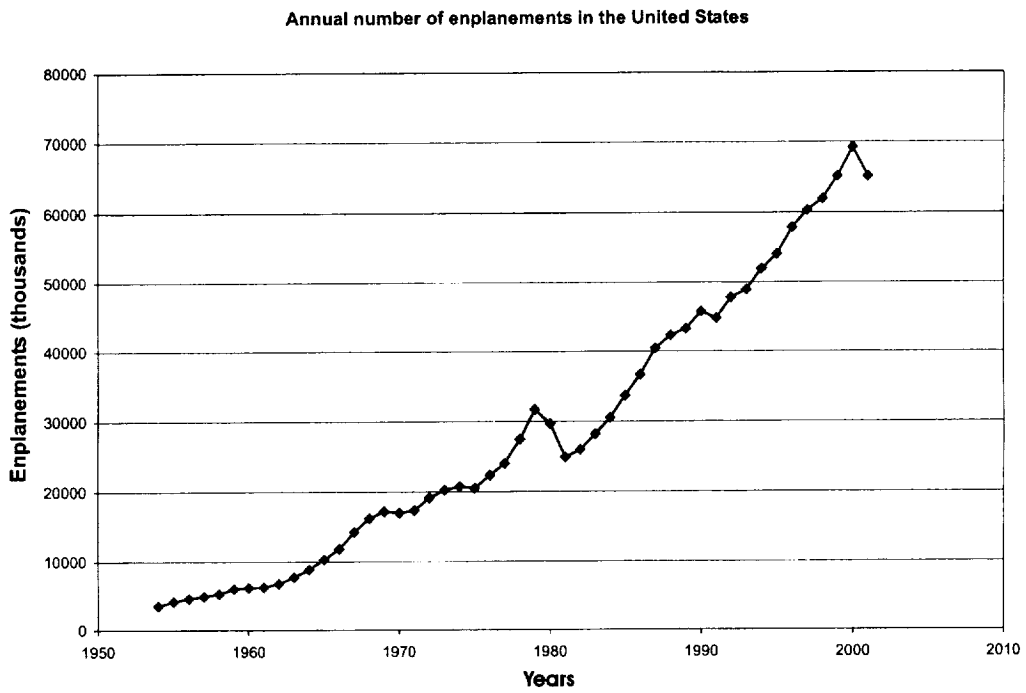

Figure 1-1: Number of enplanements over the last 50 years

the number of daily operations. This high sensitivity is a sure indication of a system approaching gridlock.

Summer 2000 delays During the summer of 2000, the delay problem became widely publicized and public awareness was raised regarding the issues faced by the air transportation community. Weather-related restrictions severely impacted the system at that time and translated into dramatic delays. This amplification is a phenomenon characterizing the lack of robustness attained when reaching the limit.

Fig. 1-2 shows the evolution of delays over the last few years. Since the terrorists attacks of September 11th, 2001, air traffic has globally decreased, and so did the delays.

System sensitivity and delay back-propagation The state of congestion attained by the NAS is illustrated by the following situation, which occurred in June 2000. On a clear weather day, a small demand/capacity imbalance at Newark Airport (one of New York City's airports) propagated restrictions throughout the country in 15 minutes. Initially 5 aircraft in excess of the usual Newark landing capacity (45 aircraft per hour) led to 250 aircraft being held at airports or on holding patterns throughout the country. Fig. 1-3 shows the evolution of the propagation in time.

Sector-wise

As the NAS is divided into smaller entities called sectors, the problems encountered at the higher scale map to local areas. Human air traffic controllers are in charge

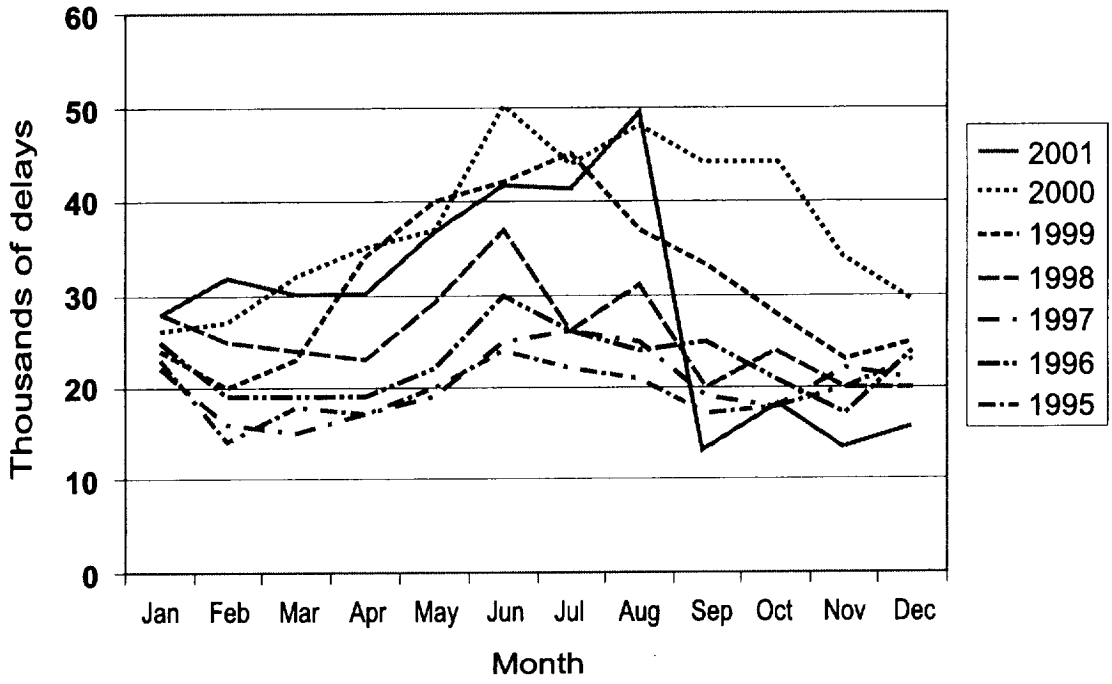

Figure 1-2: Monthly delay data over the last 7 years. A flight is delayed if it arrives at destination more than 15 min later than its scheduled time of arrival.

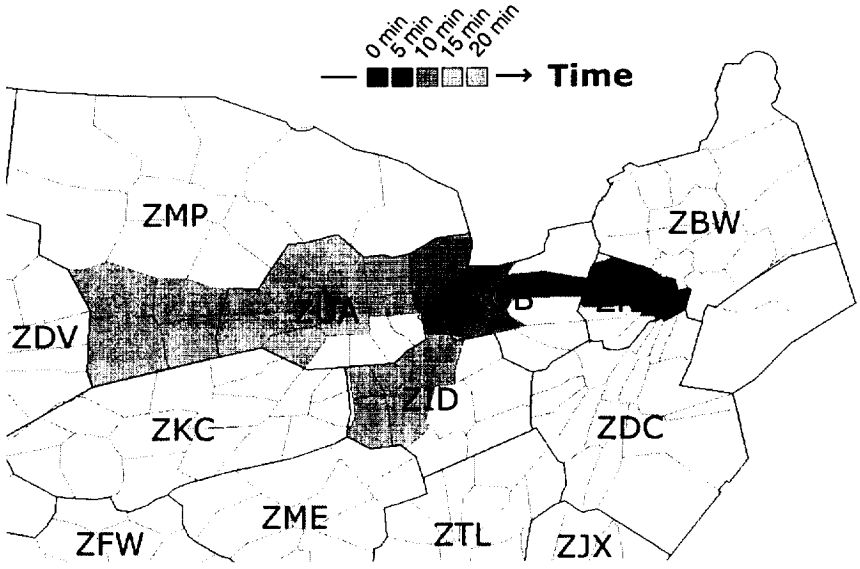

Figure 1-3: Propagation of a restriction in New York Air Route Traffic Control Center throughout the country. (Source [39]).

of managing aircraft in their sector, i.e. directing them from an entry point to an exit point while keeping each airplane separated from one another throughout their flight. This separation is a minimum standard prescribed by the Federal Aviation Administration (FAA) in the US, which forbids en-route aircraft to get closer than 5 nautical miles (nm) from each other at any time of their flight. En-route sectors are sectors handling aircraft at cruising altitude (usually above 18,000 ft). Terminal area sectors, also called TRACONs, are centered on one or more airports, and control aircraft up to a certain altitude.

Capacity limitations due to human controllers Because controllers are human beings, they have a finite capacity to handle aircraft. Their main goal is to guarantee safety, thus to maintain separation. Performance, and expeditious handling of aircraft are only dealt with when time permits. Moreover, an upper limit on the number of aircraft that can be handled simultaneously exists, although it is hard to compute. References [18, 17] bring about the notion of complexity of a sector to explain why this number varies with each particular situation.

Non-optimality of current control schemes The current concept of control of air traffic relies on a fully centralized decision process. Control is performed at the controller's level while aircraft are only the actuators. Such a centralized policy, for all the safety it guarantees, does not perform well from an economic standpoint. From the aircraft perspective, optimal parameters of flights (due to winds, aircraft loading, optimal altitude or speed) are not always those actually flown.

1.1.3 Future improvements

Because of these system flaws, a lot of research and development work is currently under way to improve the overall concept of operations. The certification process, inherent to any safety-critical system, may delay for years the time when new concepts will start being implemented nation-wide. A brief overview of these concepts follows.

Concepts

Free Flight Because of the centralized system inefficiencies mentioned above, the ATM community focuses part of its work on the Free Flight concept. In this scheme, every aircraft out of the terminal areas (departure and arrival sectors) is solely responsible for maintaining separation with surrounding aircraft. The upside of this constraint is the freedom gained by these aircraft to choose their flight path independently. The assumption is that the aircraft decision makers - either the flight deck, the airline operations center (AOC), or both - will optimize their flight path according to their cost function.

This raises many questions about extreme situations. One critical scenario would occur if a conflict encounter gets to a level of complexity beyond the capacities of any implemented conflict resolution algorithm. The control would then be handed over to stand-by human air traffic controllers, who then would be faced with an unusually

complex situation. There is concern about the accuracy and safety of the reaction of the human controllers.

The foundation of the concept itself might be discussed in terms of efficiency. Studies have been done to determine under which assumptions decentralized control is more efficient than the current, centralized scheme (see [6, 25]). A priori, this result is not intuitive as the greediness of individual decisions may lead to an overall higher number of conflicts that increases the time spent for conflict avoidance on a typical flight (due to the creation of a non-organized flow by this scheme, contrary to the well-structured flow of today's network of beacons and airways - see [38]).

Distributed Air-Ground Traffic Management (DAG-TM) Building on the idea of Free Flight, an entire concept of operation has been developed, where air traffic control service providers, airline operations centers and flight deck interact (see [1, 24]). DAG-TM is an advanced ATM concept where decision processes are decentralized and distributed among this triad of agents, which have different responsibilities.

Tools

Advances in the Air Traffic Management concepts heavily rely on new means of communication, positioning and guidance. The following introduces some of these.

Satellite Positioning System - Wide Area Augmentation System (WAAS) Satellite Positioning technology lies at the heart of the envisioned air traffic system. This technology has been popularized in the last decade with the American Global Positioning System (GPS), as well as its Russian counterpart (Glonass) and the future European system (Galileo). To gain in precision, the GPS has been augmented with WAAS in the US. This, in conjunction with current ground facilities (radar, navigation aids), is expected to deliver the level of accuracy and redundancy required for the safe operations of aircraft.

Automatic Dependent Surveillance - Broadcast (ADS-B) To supplement ground-based radar on the way to perform self-separation, one needs to know the positions of surrounding aircraft. This is achieved by broadcasting the position obtained through the previously described system, and listening for neighbors' positions. This system is in its demonstration phase and is expected to be first implemented in radar-deprived areas, such as the Pacific Ocean, Siberia and polar regions. (see [2])

Center-TRACON Automation System (CTAS) A set of ATM tools has been developed at NASA Ames Research Center under the name of CTAS. These tools present real-time data to the controller in order for him to take appropriate and optimal actions. As of today, they do not interact directly with the aircraft.

They currently mostly deal with the arrival and departure processes:

- A Terminal Management Advisor (TMA), managing the arrival sequence of aircraft;

- A Descent Advisor (DA), generating times of descent for optimal sequencing in the terminal area;

- A Final Approach Spacing Tool (FAST), sequencing final approach paths and runway assignments;

- A Surface Management System (SMS), for surface movements management.

Other tools exists, such as the Direct-To (D2) tool that proposes en-route clearances to be delivered by the controller, taking separations issues into account. This alone can save precious minutes of flight and should be greatly appreciated by the ATC customers.

Some of these tools were field-tested at Dallas-Fort Worth airport and encountered a great success on the controllers' side.

1.2 Motivation

Motivation for the present work arises from the ATM current state-of-the-art, and is described next. It was conducted with the intention of gaining insight into modeled scenarios of operations, on specific issues encountered by the system.

1.2.1 Worst-case scenarios

To deliver meaningful results of stability, worst-case scenarios were preferred to probabilistic analyses. The number of daily operations (40,000 in the US alone) and the certification requirements justify inquiring the more pessimistic scenarios.

For instance, if a flow of aircraft is supposed to carry aircraft separated at least by the minimum separation distance D_{sep}, we will assume that they are separated by exactly D_{sep} over an extended period of time. We also make sure that such hypotheses do not overlook even worse cases. Stability results are derived from formal analysis rather than from an extended number of simulations.

1.2.2 Separation

One part of this work concentrates on the problem of intersecting flows of aircraft. Two or three flows intersect and each aircraft in each flow has to maintain separation with all others. Centralized and decentralized processes of decision are analyzed and stability proofs are given where available.

1.2.3 Scheduling and system overflow

A second part deals with the problem of input/output imbalance, and restriction back-propagation, much in the way described in Section 1.1.2. An analysis of a sector capacity is formally derived.

Chapter 2

Models

2.1 Aircraft

2.1.1 Kinematics

The mathematical approach of this work requires some simplifying assumptions. Aircraft motion can be modeled in very different ways, and to very different levels of realism. A purely kinematic model of the aircraft is used, ignoring the mass and inertia parameters.

Consequently, an aircraft A_i is associated with a state-space vector $(\mathbf{x_i}, \mathbf{v_i})$, i.e. position and speed. This fully characterizes the vehicle. With kinematics only, any action on the speed vector $\mathbf{v_i}$ is instantaneous. These actions, called *maneuvers*, consist of turns or speed changes and happen immediately.

2.1.2 Maneuver library

Conflict avoidance maneuvers

For conflict avoidance purposes, three models of maneuvers were used (see Fig. 2-1). These models will be used mostly in Chapter 3.

- Lateral displacement: the controlled aircraft performs an instantaneous change of position perpendicular to its route of flight. Its speed remains unchanged. (Fig. 2-1-a)

- Heading change: the controlled aircraft changes heading instantaneously, modifying the direction of the speed vector. (Fig. 2-1-b)

- Offset maneuver: the controlled aircraft performs two successive heading changes, while keeping its speed at a constant value. Both heading changes are of same amplitude χ, but opposite in direction. After the maneuver, the speed vector returns to its original direction. (Fig. 2-1-c and [3])

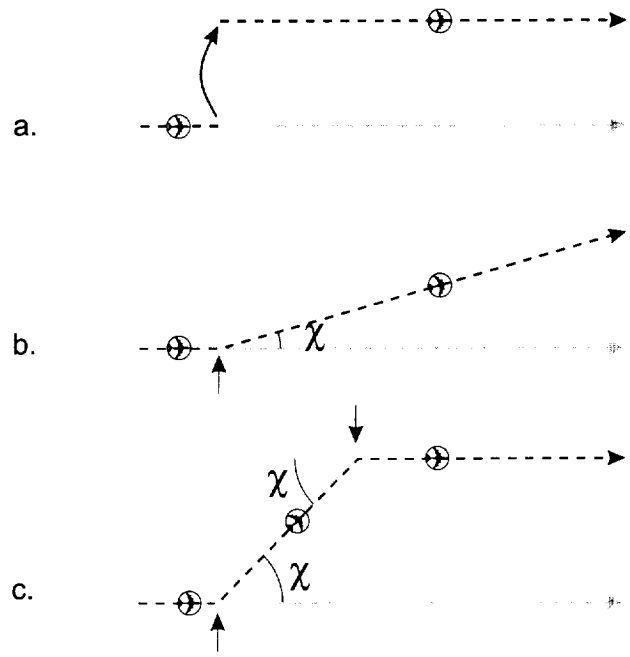

Figure 2-1: Maneuvers: a. Lateral displacement. b. Heading change. c. Offset maneuver

Speed

As we tackle the problems of aircraft scheduling in Chapter 4, we also need to model aircraft speed changes. Unless otherwise mentioned, instantaneous speed changes are considered. These speed changes are constrained to remain in the acceptable envelope of flight of an en-route aircraft. Mach number on the upper side and buffet on the lower side limit the acceptable speed to a certain range $[v_{min}, v_{max}]$, usually 400-500 knots (kt) (see [31]).

2.1.3 Two-dimensional model

To simplify the analysis of aircraft flows and to derive analytical results, we conducted our work in two dimensions. This framework is justified in the real-world by various considerations:

- Airspace representation to the controller is on a radar screen, thus in two dimensions;
- The vertical en-route structure should be modified in last resort only;
- Inefficiencies arise from fuel burn used to perform altitude changes;
- Passenger comfort is disrupted when performing climbs or descents.

2.1.4 Safety distance

To account for the FAA separation distance of $D_{sep} = 5$ nm, a 2.5 nm-radius safety zone is attached to each aircraft. The 5 nm separation standard is thus violated if two of these circular zones intersect.

Although a vertical separation limit of 2000 ft (1000 ft under the new Reduced Vertical Spacing Minimum program) exists in the real world, it is not be taken into account here because of the two-dimensional model explained above.

2.2 Sector and aircraft arrival

In both Chapters 3 and 4, aircraft need to meet a certain kind of requirement at a given point. In Chapter 3, this requirement consists in maintaining separation at the intersection of two or three aircraft flows. In Chapter 4, a scheduling constraint exists at the exit of a sector.

This translates into zones of control of a certain length D. In the case of aircraft flows intersection, we thus have a circular sector of radius D, whose center is the intersection (see also [9]). In the scheduling case, we have a rectangular sector, of length D, and width w: the scheduling constraint has to be met at a distance D from the entry fix.

Aircraft enter the sector at prescribed entry points, mimicking the network of fixes existing in the real world. The only assumption on their arrival is a guarantee that inter-arrival spacing is at least D_{sep}: this is a reasonable assumption stating that aircraft are not in conflict when entering.

2.3 Control schemes

Control is applied to aircraft in flows, whether centralized or decentralized. Except when otherwise mentioned, an aircraft receives only one instruction through its entire flight in the sector. Depending on the situation, this one instruction is either a maneuver or a change in speed, as described in Section 2.1.2.

2.3.1 Decentralized

A decentralized control scheme is applied when possible. Each aircraft makes its own, greedy maneuver to perform adequate separation or scheduling requirement. This models the Free Flight distributed concept of operations.

2.3.2 Centralized

A centralized control scheme is used in Section 3.4. This is an exact parallel with what is done today in the ATC system, where the controller performs centralized control.

2.3.3 First In - First Out policy

A First-In First-Out policy is implemented in all of our models. Aircraft leave the sector in the order they entered, i.e. no overtaking is allowed. This policy is widely recognized as the fairest.

2.4 Metrics

Precise stability and metrics description are further explained in Chapters 3 and 4. Following is only a quick overview of the ideas.

2.4.1 Stability

We characterize stability of aircraft flows under constraints as the state in which no conflict occurs at any time using acceptable maneuvers of bounded amplitude.

2.4.2 Capacity

Capacity is a number of aircraft that can be processed by a sector for a particular task (e.g., delaying aircraft).

Chapter 3

Control of intersecting flows under separation constraints

3.1 Background

Conflict Detection and Resolution (CD&R) has attracted considerable attention over the last decade. A 2000 survey [26] related the existence of 68 different CD&R modeling methods.

The research community addressed problems related to Air Traffic Management in a great variety of approaches. In line with today's concept of operations, centralized control approaches are used to provide globally optimal control of pools of aircraft operating in the same airspace. Different mathematical formulations are taken, such as semi-definite programming [15], mixed integer programming [37], optimal control [19], genetic algorithms [16], or a combination of the above [32]. These approaches provide optimal path planning for a finite number of aircraft performing online computations. Some innovative approaches make use of other fields of research: hybrid systems [4], optical networks theory [33], or self-organized criticality [27].

Decentralized control is also addressed in a number of papers to provide theoretical background to the future Free-Flight concept (see Section 1.1.3). Once again, different approaches are taken, such as: mixed integer linear programming [36], analytical geometry [5, 28, 29, 30], or hybrid systems [20]. Procedure-based control appears in a few papers such as [8, 20].

The present work concentrates on an infinite number of aircraft involved in potential conflicts. Aircraft are organized along airways in infinite flows that intersect. Potential conflicts occur at the intersection and aircraft maneuver independently to avoid violating safety distances. One originality of this work lies in the proof of stability (i.e. safety) of the control law over any amount of time and with any number of aircraft in each flows.

Section 3.2 shows the stability of two intersecting flows when aircraft use the offset maneuver to perform conflict avoidance. Section 3.3 presents the same result for aircraft using heading changes, although the proof is more involved than in Section 3.2. Section 3.4 addresses the problem of three intersecting flows. Because the decentral-

ized control used in the two preceding sections does not yield stability in that case, centralized control is used to create a procedure-based, stable scheme.

This chapter presents results that appeared in [11] and [12]. Appendix A gives a summary of simulations appearing in this thesis.

3.2 Two flows using offset maneuver

The problem of two intersecting flows of aircraft that must maintain separation is addressed in this section. Considering the offset maneuver for conflict avoidance (see Section 2.1.2), simulations are performed and a stability analysis is provided.

3.2.1 Model

The following model of operations is considered: two flows of aircraft intersect at the center O of a sector of radius D, called *control volume*. Each flow enters through a fix, either W (West) or N (North), with the intention of leaving the sector through E (East) and S (South) respectively. All aircraft fly at constant and uniform speed. Each aircraft can observe the state of all aircraft already inside the control volume (using an idealization of ADS-B, for instance). Each aircraft can take a single maneuver at the instant it enters the control volume. This maneuver must have minimal amplitude and must be conflict-free; this assumption models a real-world system in which pilots make safe, lowest-cost, decentralized decisions.

Offset maneuver and lateral displacement The offset maneuver is shown in Fig. 2-1-c and with more details in Fig. 3-1. It consists of two successive heading changes of fixed amplitude $\pm\chi$. This type of maneuver is considered realistic and air traffic controllers use it to handle conflicts. The amplitude of the maneuver is modulated by the length of "inclined" leg.

Comparing with the lateral displacement model (see Fig. 2-1-a), the offset maneuver considered in this section is equivalent to a lateral jump of size d and a longitudinal, backward jump of size $d\tan(\chi/2)$ (see Fig. 3-1). This important remark simplifies the stability analysis by making the proofs presented in [29] almost directly applicable to the current model. One difficulty arises here as the inclined leg is not included in the conflict resolution analysis, and must still be conflict-free. Therefore, we assume the offset maneuver area is sufficiently far from the conflict itself. Under these conditions, the maneuver reduces to choosing a position, when entering the control volume, along a line inclined at an angle of value $\pm(\pi/2+\chi/2)$ with respect to the direction of flow. This angle is positive if the deviation occurs to the left and negative to the right.

We wish to derive the largest lateral deviation necessary for conflict resolution. As in the analysis presented in [29], we define a corridor of width d_{max}, within which each aircraft can maneuver (Fig. 3-3). It is shown that for d_{max} large enough, there always exists a maneuver within that corridor such that any conflict can be solved.

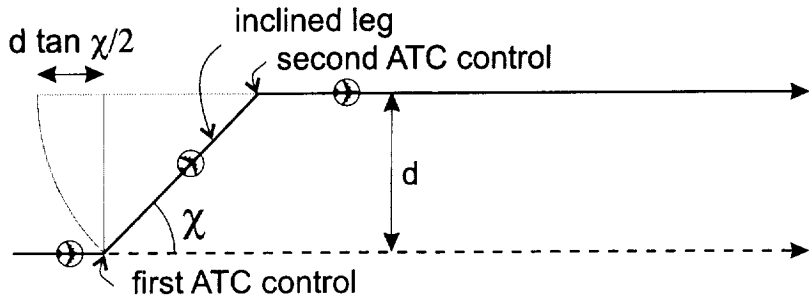

Figure 3-1: Offset maneuver

3.2.2 Simulations

Fig. 3-2 shows the result of a simulation using 250 aircraft in both flows, with an initial separation subject to a uniform distribution on the interval $[5, 15]$ nm. A plot of the population of deviations is given along with a snapshot of the control volume at one instant during the simulation. Data from a set of 20 simulations are available, although only one instance is represented here. This data show a recurring characteristic appearing in the deviation distribution: no aircraft ever deviated more than ≈ 7.5 nm. Equivalently, all aircraft found conflict-free path by performing an offset maneuver that took them no further than 7.5 nm away from their original planned trajectory.

This result, as well as the overall geometry of the control volume, should be paralleled with that of Mao *et al.* (see [28, 29, 30]).

3.2.3 Stability proof

Existence of a bounded conflict resolution offset maneuver draws from the analysis found in [29]. Parameters of interest are the separation distance D_{sep} and the encounter angle (90 deg, in this case).

Consider an aircraft entering the control volume. Assume without loss of generality that this aircraft is eastbound and denote it A_i, as in Fig. 3-3. We show that this aircraft can always execute a bounded offset maneuver of amplitude less than or equal to d_{max}, if $d_{max} = \sqrt{2}D_{sep}$, which results in a conflict-free trajectory.

We prove this fact by contradiction, assuming in the first place that such a maneuver does not exist.

Hypothesis: A_i cannot find a conflict-free maneuver of amplitude smaller than d_{max}

Each aircraft within the control volume projects an "aisle" (oriented at a 45 degree angle in the case of orthogonal aircraft flows), such that no aircraft from the opposite flow can enter this aisle without creating a conflict.

The aisles created by the eastbound aircraft ahead of A_i should not cover the protected circle of A_i, wherever A_i is located within its maneuver corridor. Indeed, if the converse were true, A_i could hide behind the aircraft by moving sideways and thus find a conflict-free trajectory with an offset maneuver of amplitude d less than d_{max}

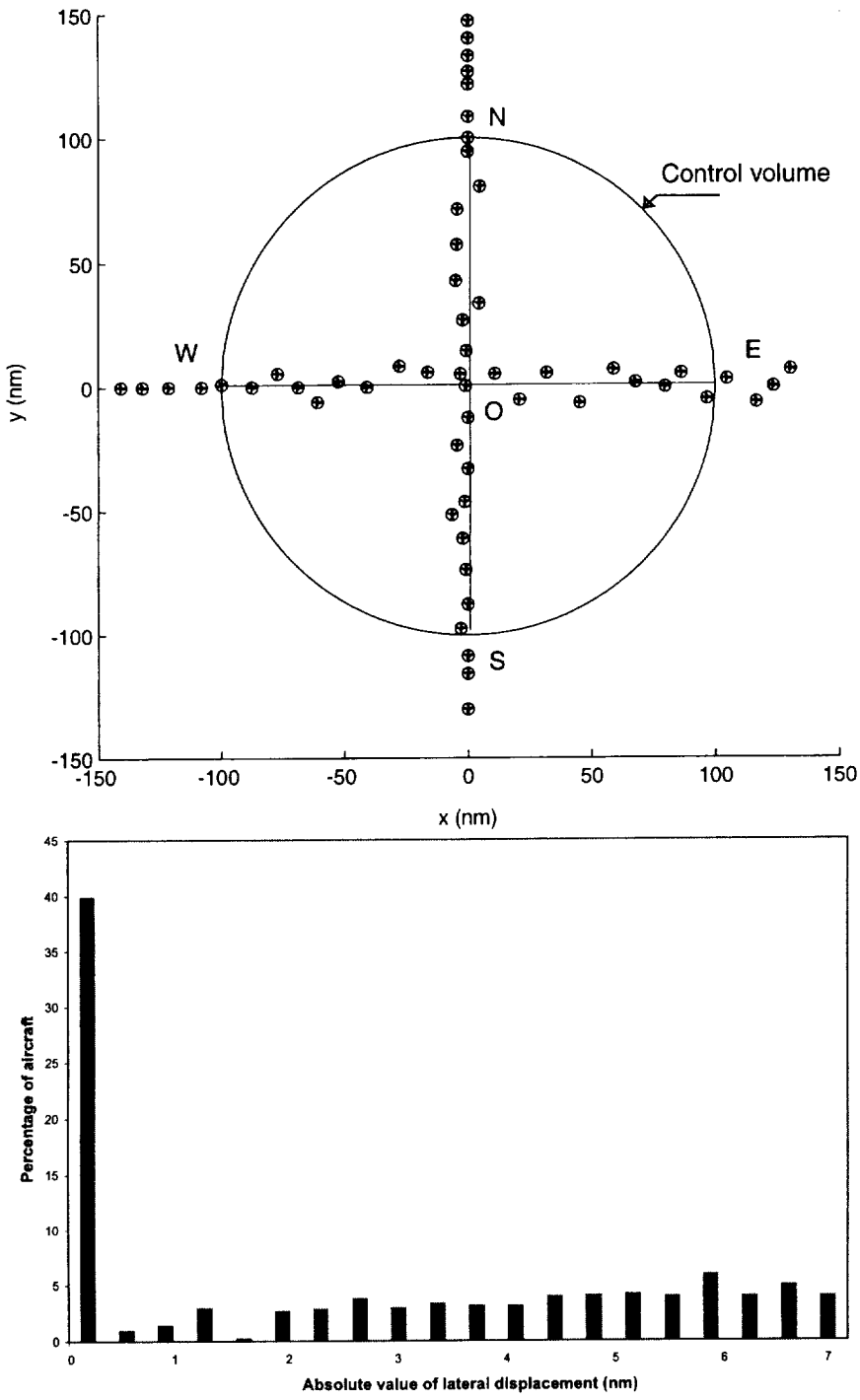

Figure 3-2: Simulation for random arrival using offset maneuvers. Original separation is uniformly distributed on $[5, 15]$ nm. 250 aircraft are simulated in each flow. Top: Snapshot of the simulation. Bottom: Aircraft deviation distribution.

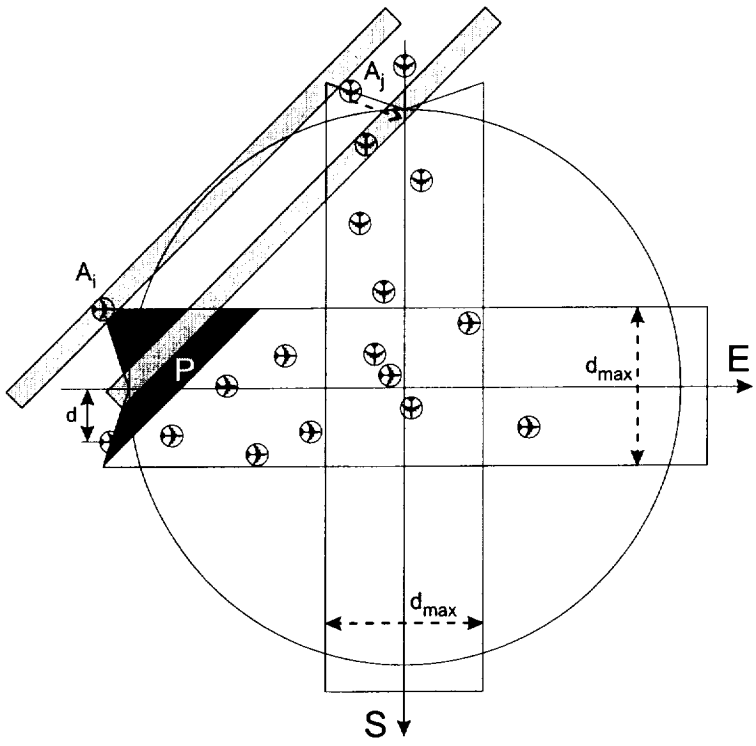

Figure 3-3: Existence of conflict resolution maneuver with the offset maneuver.

which is contradictory with the above assumption. Stated differently, there should be no aircraft other than A_i within the shaded area P (shaped like a skewed arrow tip) in Fig. 3-3.

Meanwhile, all southbound aircraft already inside the control volume have already performed their own maneuver leading to conflict-free trajectories, and are flying along straight southbound paths. Under the above hypothesis, their aisles intersect the protected circle of A_i for all possible offset maneuvers of A_i within the corridor. In particular, this is true when A_i performs a left offset maneuver of amplitude d_{max}, as shown in Fig. 3-3. Therefore, a southbound aircraft A_j (shown on the figure) is in conflict with A_i and must have deviated to the right by an amplitude d such that $d > d_{max} - D_{sep}\sqrt{2} = 0$.

However, because the area P is empty of any eastbound aircraft, the aircraft A_j would have been safe by maneuvering to the right by an amplitude strictly less than d. This implies that A_j's maneuver did not have minimum amplitude. It also contradicts the requirement that the maneuver of each aircraft must have minimum amplitude. Thus the amplitude of the aircraft deviation is bounded and its maximum value is:

$$d_{max} = \sqrt{2}D_{sep}. \tag{3.1}$$

This result applies to Figure 3-2 where $\sqrt{2}D_{sep} = 7.1$ nm, and explains the limit found in the heading distribution plot.

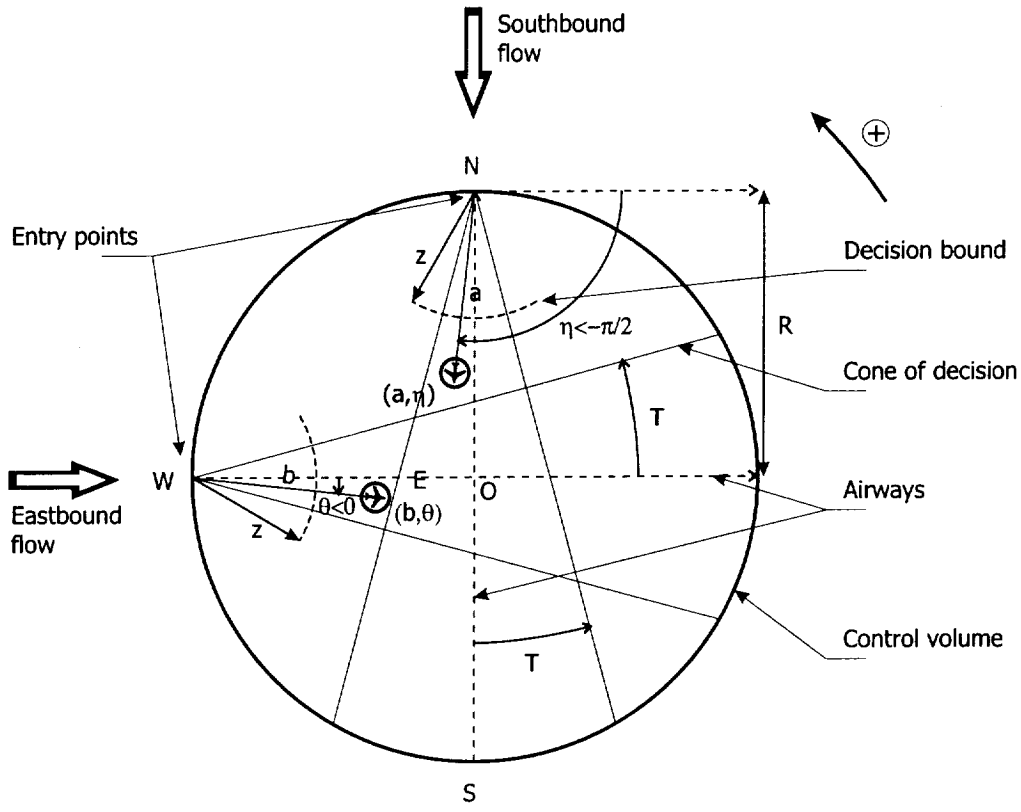

Figure 3-4: Airway intersection in a circular sector. All angles are measured using trigonometric conventions: East is 0 rad, North is $\pi/2$ rad, South is $-\pi/2$ rad and West is π rad.

3.3 Two flows using heading change

3.3.1 Model

Geometry

Fig. 3-4 shows the model under consideration in this section. Two orthogonal airways intersect at the origin (point O). Two flows of aircraft follow each airway: one flow is eastbound while the other is southbound. All aircraft are assumed to have the same speed v and be originally all aligned and separated along either one of the airways. As they enter a circular sector centered around O with radius D, they perform a corrective maneuver to avoid other aircraft already present in this sector.

Initially, aircraft are flying along eastbound or southbound airways. The southbound flow enters the sector at point N and its nominal exit point is S. Likewise, the entry point of the eastbound flow is W and its exit point is E. Again, a generic southbound aircraft is indexed as A_j, while an eastbound aircraft is indexed as A_i. Both flows intersect at point O.

Upon entering the sector, aircraft maneuver by finding the minimum heading change to avoid any conflict with aircraft already present in the sector (by assumption, no attention is paid either to aircraft that have not entered the sector yet or

have already left). This is the only maneuver aircraft can perform; after maneuvering, aircraft move along straight lines as defined by their original (and only) heading change. This conflict resolution scheme implements the First-Come First-Served priority stated in Section 2.3.3. A conflict is declared if the minimum miss distance between two aircraft is less than D_{sep}.

Coordinate system

In addition to the usual cartesian coordinate system (origin O, $\mathbf{x}$ pointing to the East, $\mathbf{y}$ pointing to the North), two systems of polar coordinates are used for southbound and eastbound aircraft, as shown in Fig. 3-4. The position of a southbound aircraft A_j in the sector is given by the polar coordinates (a, η), where a is the distance between N and the aircraft, and η is the directed angle between the vector $\mathbf{NA_j}$ and the eastbound direction. Likewise the position of eastbound aircraft is noted (b, θ).

Scaled variables

The radius of the sector is the reference length. The following non-dimensional variables are defined:

$$\delta = \frac{D_{sep}}{D}, \ \alpha = \frac{a}{D}, \ \beta = \frac{b}{D}, \tag{3.2}$$

as well as the scaled speed:

$$\nu = \frac{v}{D}. \tag{3.3}$$

3.3.2 Simulations

Simulations of the above system have been performed in Matlab. The radius D of the sector radius is assumed to be 100 nm. The speed of each aircraft is 400 kt, and D_{sep} is assumed to be 5 nm (thus $\delta = 0.05$). Aircraft enter the sector at regular or random time intervals.

Two illustrative simulations are shown in Figs. 3-5 and 3-6. Fig. 3-5 shows a simulation involving aircraft entering at regular time intervals with 250 aircraft in each flow. The aircraft are entering the sector spaced exactly by 5 nm. As might be expected, the resulting pattern obtained by simulation is periodic and bounded.

Fig. 3-6 shows the conflict resolution process resulting from a random aircraft arrival process: the spacings between two consecutive aircraft in the southbound or eastbound flows are uniformly distributed over the interval $[5, 10]$ nm. The simulation involved 250 aircraft in each flow. The population of heading change commands shown on the distribution plot remains bounded.

3.3.3 Stability proof

Motivated by these simulations, we now proceed with a proof that heading changes generated by conflict avoidance maneuvers remain bounded. Without loss of generality, the notion of *projected conflict zone* for an eastbound aircraft is first introduced,

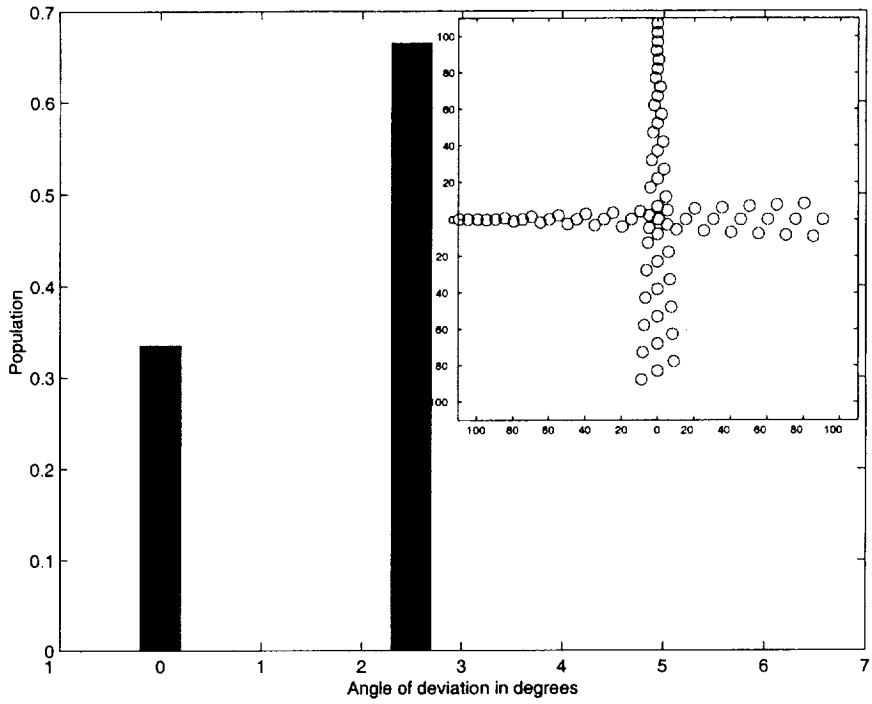

Figure 3-5: Insert: simulation with constant inter-arrival spacing (5 nm). Main plot: distribution of angular deviations.

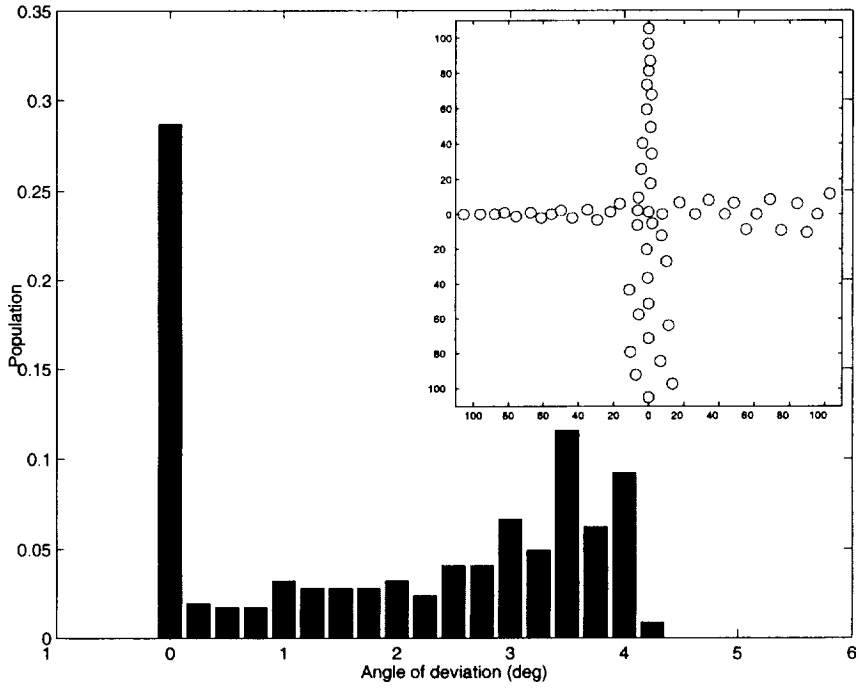

Figure 3-6: Insert: snapshot of simulation with random inter-arrival spacing (uniform distribution over $[5, 10]$ nm). Main plot: distribution of angular deviations.

followed by that of *eastbound protection zone* for an eastbound aircraft A_i. Armed with these notions, we conclude with a proof that aircraft angular deviations remain bounded.

Projected conflict zone of an eastbound aircraft

For a given aircraft A_i that has already maneuvered, consider the locus of the southbound aircraft positions resulting in a conflict with A_i. This locus is called *projected conflict zone* and is sketched in Fig. 3-7. It is this case equivalent with the "aisles" of the offset maneuver case (Section 3.2). It is worth noting that this locus is quite complex in shape and changes with the aircraft heading and its position. If the projected conflict zone intersects with any southbound aircraft, the corresponding heading for aircraft A_i is not conflict-free. An analytic expression for the projected conflict zone is now derived.

The starting point is the locus (α, η) of southbound aircraft A_j that would get into conflict with A_i. We first derive their positions and velocities as functions of α, β and ν, whose definitions are given by Eq. (3.2) and Eq. (3.3).

The positions of the aircraft A_i and potential intruder A_j are written in normalized cartesian coordinates:

$$\mathbf{WA_i} = \begin{pmatrix} \beta\cos\theta \\ \beta\sin\theta \end{pmatrix}, \quad \mathbf{NA_j} = \begin{pmatrix} \alpha\cos\eta \\ \alpha\sin\eta \end{pmatrix}.$$

Likewise the scaled velocities of these aircraft are expressed:

$$\mathbf{v_{A_i}} = \begin{pmatrix} \nu\cos\theta \\ \nu\sin\theta \end{pmatrix}, \ \mathbf{v_{A_j}} = \begin{pmatrix} \nu\cos\eta \\ \nu\sin\eta \end{pmatrix}.$$

Ref.[23] derives expressions for the normalized relative speed $\mathbf{c} = (c_x, c_y)^T$:

$$\mathbf{c} = \frac{\mathbf{v_{A_j}} - \mathbf{v_{A_i}}}{\|\mathbf{v_{A_j}} - \mathbf{v_{A_i}}\|}, \tag{3.4}$$

the relative position vector $\mathbf{r} = (r_x, r_y)^T$:

$$\mathbf{r} = \begin{pmatrix} -\alpha\cos\eta + \beta\cos\theta - 1 \\ -\alpha\sin\eta + \beta\sin\theta - 1 \end{pmatrix}, \tag{3.5}$$

and the minimum approach distance $\mathbf{m}$:

$$\mathbf{m} = \mathbf{c} \times (\mathbf{r} \times \mathbf{c}). \tag{3.6}$$

The above formulae lead to the minimum approach distance for A_i and A_j:

$$\begin{aligned} \mathbf{m}^2 &= (r_x c_y - r_y c_x)^2 \\ &= \frac{((-\alpha c_\eta + \beta c_\theta - 1)(s_\theta - s_\eta) + (\alpha s_\eta - \beta s_\theta + 1)(c_\theta - c_\eta))^2}{2 - 2c_\eta c_\theta - 2s_\eta s_\theta} \end{aligned}$$

where $\sin\theta$ and $\cos\theta$ have been replaced by the shorthands s_θ and c_θ, and likewise for η.

We now derive an expression to describe the boundary of the projected conflict zone for an incoming eastbound aircraft A_i. Rather than plotting this projected conflict zone when A_i enters the sector, we plot it when A_i has traveled the normalized distance $1/2$ in the sector (i.e. $R/2$ in the dimensional space), thereby considerably simplifying its graphical representation. We derive the $\alpha(\eta)$ that yield a minimum approach distance m of exactly the minimum separation distance δ: the desired zone is obtained by solving the equation $\mathbf{m}^2 = \delta^2$ in the variable α. The two roots of this equation, which are the locus as a function of $\alpha(\eta)$, are:

$$\rho(\eta) = \frac{1}{2} - \frac{(s_\theta s_\eta + s_\theta c_\eta + c_\theta s_\eta - c_\theta c_\eta + 1) - \delta\sqrt{2}\sqrt{1 + s_\theta s_\eta - c_\theta c_\eta}}{s_\theta + s_\eta}, \tag{3.7}$$

$$\sigma(\eta) = \frac{1}{2} - \frac{(s_\theta s_\eta + s_\theta c_\eta + c_\theta s_\eta - c_\theta c_\eta + 1) + \delta\sqrt{2}\sqrt{1 + s_\theta s_\eta - c_\theta c_\eta}}{s_\theta + s_\eta}. \tag{3.8}$$

These define the projected conflict zone of $A_i(\beta, \theta)$ in the southbound flow's coordinate system (see Fig. 3-7 left).

Note: the aisle has a different meaning in Section 3.2 than the projected conflict zone has here. The aisle of an eastbound aircraft in Fig. 3-3 must not intersect the safety zone of a southbound aircraft (see Section 2.1.4). Here, the projected conflict zone of an eastbound aircraft must not include the *position* of a southbound aircraft.

Intersection of the projected conflict zone of an eastbound aircraft with the set of heading angles available to a southbound aircraft

We call *decision bound* the two arcs centered at W or N, of radius $1/2$ and spanning the angular range $[-\chi, \chi]$. Let T be the maximum heading change allowed for aircraft of each flow. Equivalently: eastbound aircraft maneuver in $[-T, T]$ and southbound aircraft in $[-\pi/2 - T, -\pi/2 + T]$. Consider the angular range width χ, defined as the unusable heading range for a southbound aircraft on the southbound decision bound ($\alpha = 1/2$) due to the presence of an aircraft on the eastbound decision bound ($\beta = 1/2, \theta = T$). Fig. 3-7 illustrates this configuration.

Defining $\eta^\star$ such that $\sigma(\eta^\star) = 1/2$, χ is expressed as:

$$\chi = T + \eta^\star + \frac{\pi}{2}. \tag{3.9}$$

Geometric considerations show that:

$$\tan\chi = \frac{\delta\sqrt{2 - \delta^2}}{1 - \delta^2}. \tag{3.10}$$

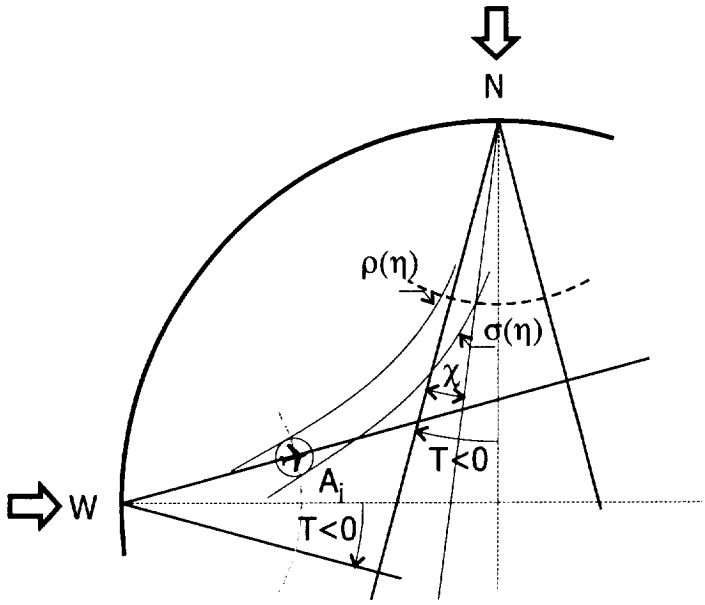

Figure 3-7: Edges of the projected conflict zone for A_i and definition of χ

Eastbound flow protection zone

We now introduce the notion of *protection zone*, which is the equivalent of the area P in Fig. 3-3 of Section 3.2.3. Consider the case whereby an eastbound aircraft A_{i+1} is about to enter the sector. Assume moreover that it is preceded by another eastbound aircraft A_i, which has already maneuvered so as to find a conflict-free trajectory. By definition, the projected conflict zone of A_i does not contain any southbound aircraft.

Can A_{i+1} take advantage of the fact that A_i is on a conflict-free trajectory to generate its own conflict-free trajectory? This would be the case if A_{i+1} could maneuver so as to include its own projected conflict zone within that of A_i, as shown in Fig. 3-8. It turns out there is a considerable range of positions of A_i for which the projected conflict zone of A_{i+1} is included in the projected conflict zone of A_i for a suitable heading change θ_n of A_{i+1}.

We define the *eastbound protection zone* as the locus of possible positions of A_i satisfying the following conditions: (i) the heading of A_i is within the range $[-\chi, \chi]$; (ii) there exists a heading change θ_n for which the projected conflict zone of A_i contains that of A_{i+1}.

The numerically computed figure of this protection zone for $\delta = 0.05$ is shown in Fig. 3-9.

An analytic computation of the eastbound protection zone for any value of δ would be preferable. It should be the object of future research efforts. The mathematical problem of interest for the proof appears in Appendix B.

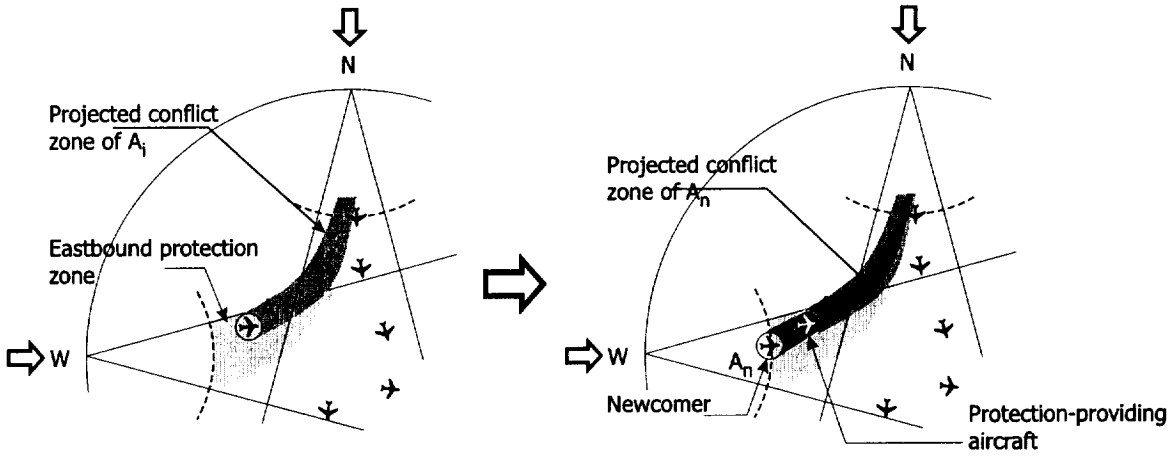

Figure 3-8: Eastbound protection zone. Left: an aircraft A_i has already maneuvered. Right: by maneuvering appropriately, A_n uses A_i's conflict-free solution.

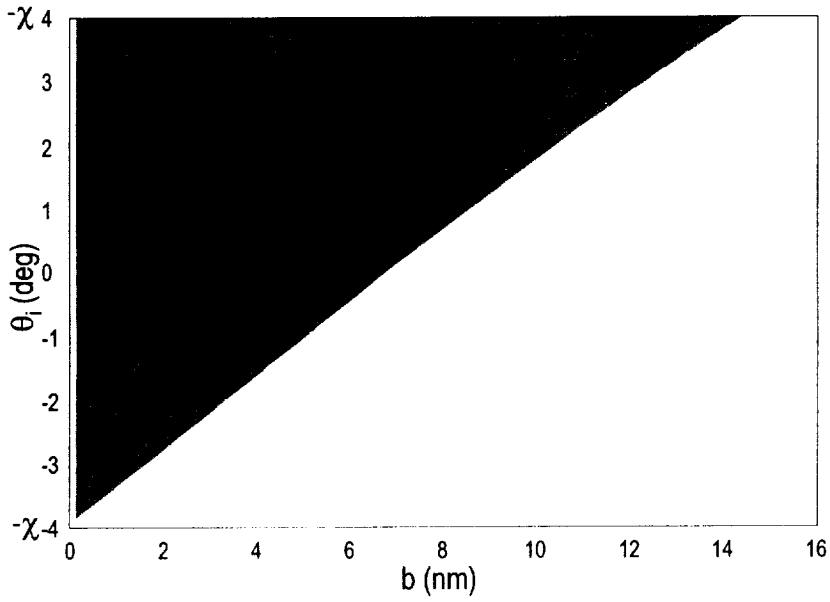

Figure 3-9: Plot of the eastbound flow protection zone for $\delta = 0.05$, where $\chi \simeq 4.1$ deg by Eq. (3.10).

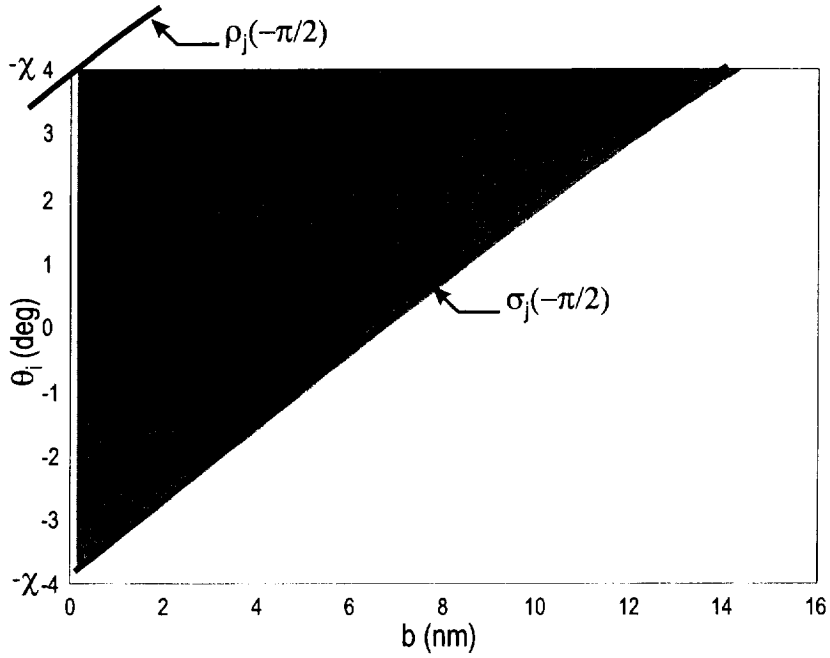

Figure 3-10: Plot of the eastbound protection zone overlaid with $\sigma_j(\theta)$ and $\rho_j(\theta)$, for $\delta = 0.05$.

Intersection of the projected conflict zone of a southbound aircraft with the eastbound protection zone

A southbound aircraft A_j choosing a heading $\eta = -\pi/2$ satisfies the following property: its projected conflict zone is completely contained in the eastbound protection zone.

Combining the numerical data from Section 3.3.3 with the expressions $\sigma_j(\theta)$ and $\rho_j(\theta)$ (the subscript j is added to make clear these functions concern the southbound flow) for the edges of the projected conflict zone of A_j, we numerically validated the above property for any $\delta < 0.2$ (see B). A result is shown for $\delta = 0.05$ in Fig. 3-10.

Proof and bound

Armed with these results, we can now complete the stability analysis for two intersecting flows of aircraft, when the aircraft perform heading change maneuvers. The following is an argument that stands very close to that used in Section 3.2.3. It is shown that an aircraft entering the sector, say the eastbound aircraft A_i, can always perform a heading change maneuver that results in a conflict-free trajectory, and this maneuver is bounded above.

We make the following hypothesis, and show a contradiction:

Hypothesis: There exists an aircraft A_i for which no conflict-free path can be found in the angular interval $[-T, T]$ around its original heading, with $T > \chi$, and

$$\tan\chi = \frac{\delta\sqrt{2-\delta^2}}{1-\delta^2}$$

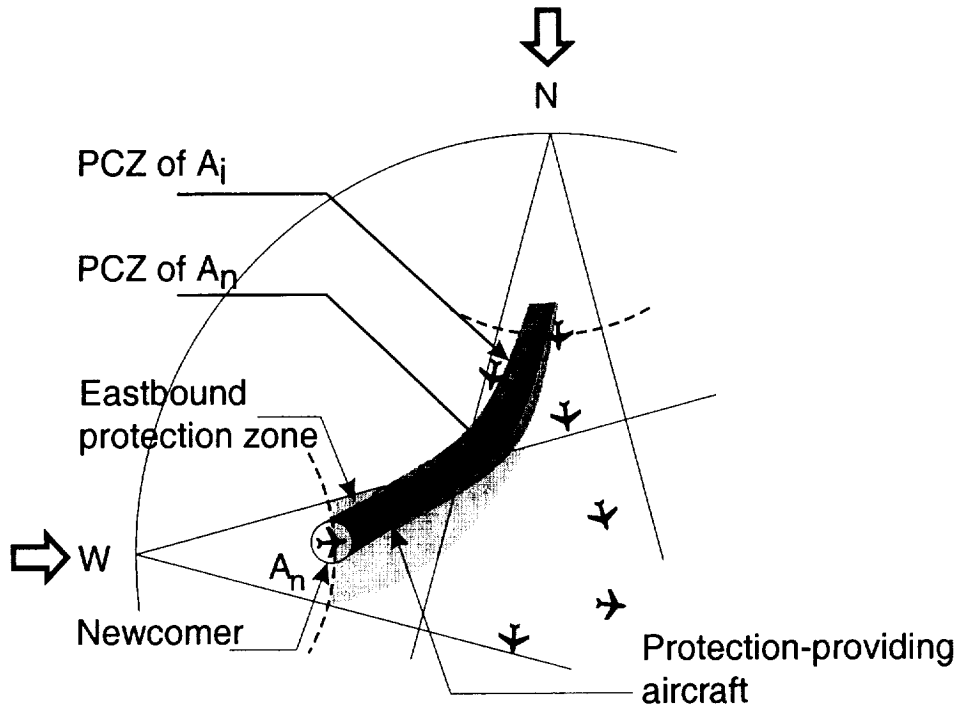

Figure 3-11: Eastbound protection zone and the projected conflict zone of an aircraft. Notes: loci shown here are not sketched to scale. "PCZ" stands for protected conflict zone.

If there were eastbound aircraft within the eastbound protection zone in front of A_i, their presence would provide a conflict-free path for A_i (by definition of the eastbound protection zone, see Section 3.3.3): by taking an appropriate heading, A_i would be able to move its projected conflict zone completely inside the projected conflict zone of an aircraft ahead, thus getting a conflict-free path solution. Fig. 3-11 shows a sketch of the location of these aircraft able to provide "help" to newcomers. Thus, there cannot be such aircraft within the eastbound protection zone because of the hypothesis.

At the same time, all southbound aircraft currently inside the sector have already performed their minimum heading change maneuver, and are flying along straight, conflict-free southbound paths. Our hypothesis implies that there exists a southbound aircraft on a conflict path with A_i for any heading change of A_i within the interval $[-T, T]$. In particular, when A_i deviates fully to the left (i.e. $\theta = +T$), it remains in conflict with at least one southbound aircraft A_j. This also implies that A_j must have deviated by $T - \chi > 0$ (χ does not depend on T, as shown above) to the left (i.e. its new heading is less than $-\pi/2 - T + \chi$) so that it is inside the projected conflict zone of A_i.

However, if A_j had not deviated ($\eta = -\pi/2$), it would have found a conflict-free path because its projected conflict zone is then free of conflict: it was shown above that its projected conflict zone is completely contained in the eastbound protection

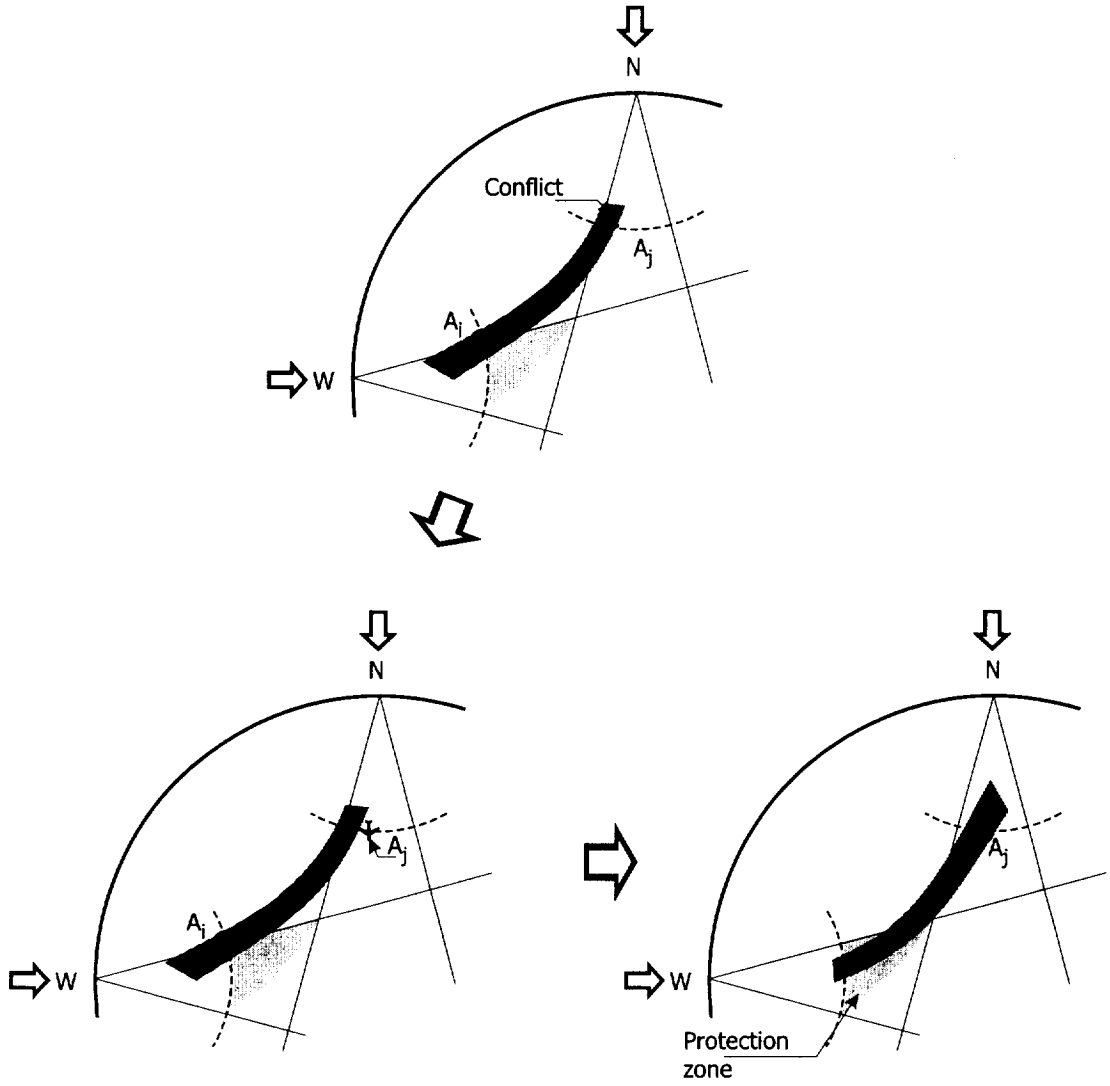

Figure 3-12: Illustration of the proof. Top: If the hypothesis is true, then there exists one southbound aircraft A_j that conflicts when A_i is fully to the left. Left: However, this conflict southbound aircraft could have not maneuvered and would still have found a conflict-free path because (Right) its projected conflict zone would have been inside the eastbound protection zone where there are no aircraft, by hypothesis.

zone, which is itself free of aircraft (see Fig. 3-12).

Therefore, there is a contradiction with the initial hypothesis, and the following is true: there always exists a solution (conflict-free path with heading change) within the interval $[-\chi, \chi]$, for all aircraft. By symmetry, the statement is true for both flows.

The next paragraph shows a simple construction where the deviation is exactly χ and χ is thus a tight bound on the maximum deviation.

We recall the expression Eq. (3.10) found above for χ:

$$\tan\chi = \frac{\delta\sqrt{2-\delta^2}}{1-\delta^2}$$

It is interesting to notice that Eq. (3.10) can be linearized for small δ resulting in $\chi = \delta\sqrt{2}$, yielding the result of Section 3.2.3 and [30] for the maximum lateral displacement in the area of conflict: $d_{max} = D_{sep}\sqrt{2}$.

One-on-one conflict

There exists a configuration where the heading change equals the value found in Eq. (3.10). This configuration is a one-on-one confrontation. Two aircraft, one from each flow, arrive in the sector at the same time. We can assume without loss of generality that the southbound aircraft maneuvers first. The angle of deviation needed for the eastbound aircraft to avoid the southbound one is χ.

3.4 Three flows using lateral displacement

This section considers the case of three intersecting flows of aircraft. The motivation for this extension is to build some understanding about the structure of intersecting flows of aircraft when coming from many different directions. Sequential, decentralized control laws do not generate stable closed-loop flow behaviors. A centralized, procedure-based, optimized control policy is proposed: spatial structuring of the airspace is identified that allows to support such an approach.

3.4.1 Model

To simplify the analysis, this section returns to the aircraft maneuvering model of lateral displacement originally considered in [29] and described in Section 2.1.2 (see Fig. 2-1-a). Such a model is justified in the case where the conflict area is well located in time and space. A heading change $\Delta\chi$ is then modeled as an instantaneous lateral jump of amplitude $D\Delta\chi$ where D is the "distance to conflict". Similarly, a velocity change Δv could be modeled as an instantaneous longitudinal jump of amplitude $\Delta v D/v$ where v is the nominal velocity of the aircraft.

The conflict geometry under study is that of three aircraft flows converging to a single point. The flows are symmetrically oriented with respect to the origin. Aircraft in each flow are assumed to follow the same initial trajectory and then enter a circular

control volume. Again, to avoid in-trail conflicts, the inter-aircraft spacing is no less than D_{sep}.

3.4.2 Simulations

Fig. 3-13 shows that a sequential conflict resolution scheme may lead to unstable flow behavior: three aircraft streams avoid conflicts arising due to interaction with the other flows, using lateral displacements in the way described in Section 3.2. Aircraft are allowed to perform only one conflict resolution maneuver when they enter the control volume, and consider other aircraft already within the control volume as moving obstacles they must avoid. Fig. 3-13 shows that the lateral deviations experienced by each flow become very large under such a control scheme. Further simulations (not shown in this figure) indicate aircraft deviations keep diverging. Therefore, a decentralized scheme is not appropriate for three flows.

3.4.3 Stabilization by centralized control

Many centralized approaches exist to solve conflicts that may not be solved via sequential approaches, including via on-line numerical optimization [29, 30, 35]. However, these approaches are not necessarily guaranteed to converge to an optimal or even feasible solution (indeed, the resulting optimization problems are often very complex). This creates a significant problem when system safety is involved such as in air transportation. We now show that centralized, optimization-based conflict resolution strategies are stabilizing for three intersecting flows by providing an explicit, feasible and bounded solution to that problem. While the procedure is described on three symmetrically arranged aircraft flows, we believe it can be extended to other encounter angles as well.

Meshing the space with projected conflict zones

The idea builds from Fig. 3-14. Aircraft from each flow project two "shadows" of width D_{sep} aligned along their relative velocity vector with respect to the other two aircraft flows. As described in Section 3.2, no aircraft from the other flows may be within these shadows without creating a conflict. The aircraft arrangement shown in Fig. 3-14 is able to cope with densely packed aircraft flows (where aircraft initially follow each other at minimum separation distance in each flow), while avoiding conflicts and generating only bounded aircraft deviations. Moreover this partition is valid for an arbitrary large number of aircraft. However, this flow resolution structure requires significant velocity control. A more desirable solution would try and avoid velocity control, and concentrate on offset maneuvers instead.

Fig. 3-14 may however be used as an inspiration to construct an airspace partition that may handle infinite intersecting flows via lateral deviations only. The idea is to generate an airspace partition using appropriately constructed aisles (aligned along relative velocity vectors) and resulting *spots* where aircraft in each flow may

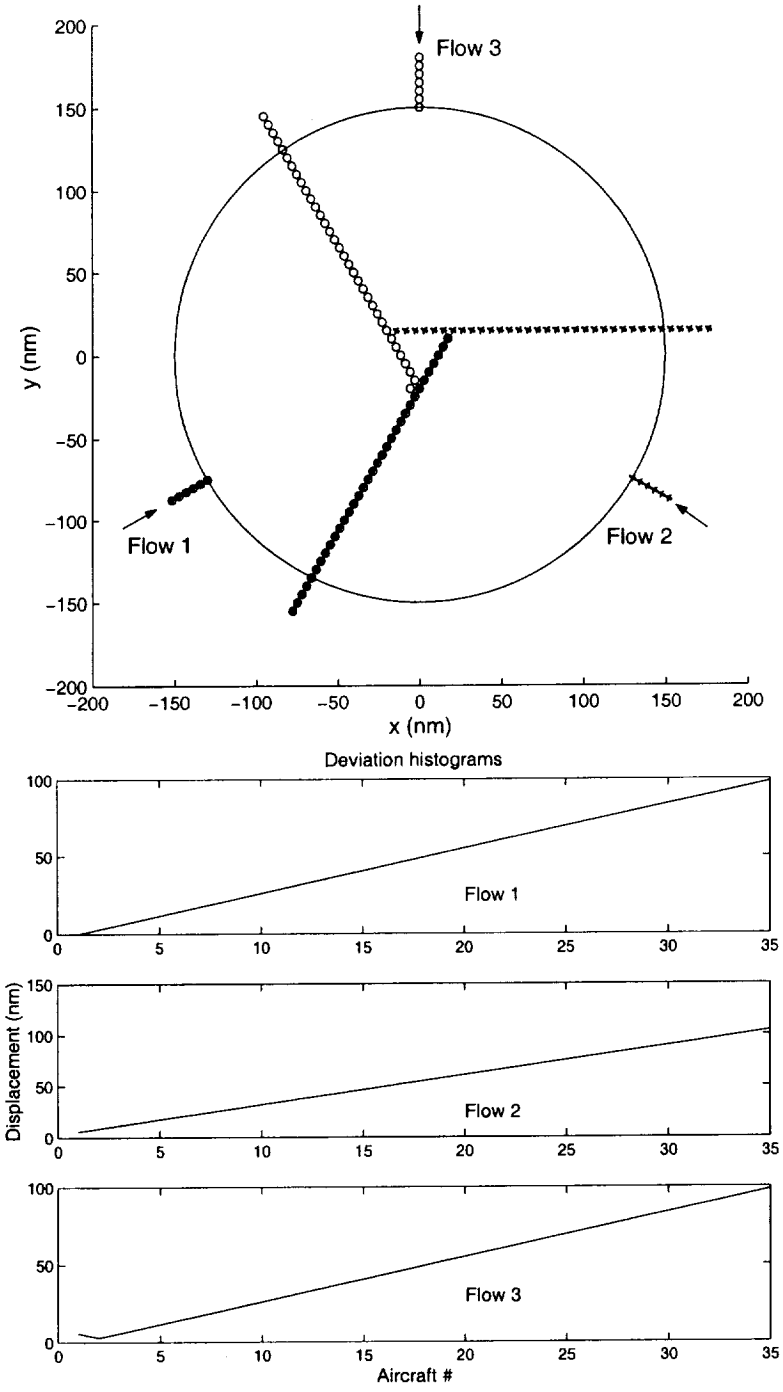

Figure 3-13: Divergence of 3 flows under decentralized, sequential resolution strategy. The initial separation distance is 5 nm. Top: airspace simulation. Bottom: amplitude of maneuver as a function of time of entry

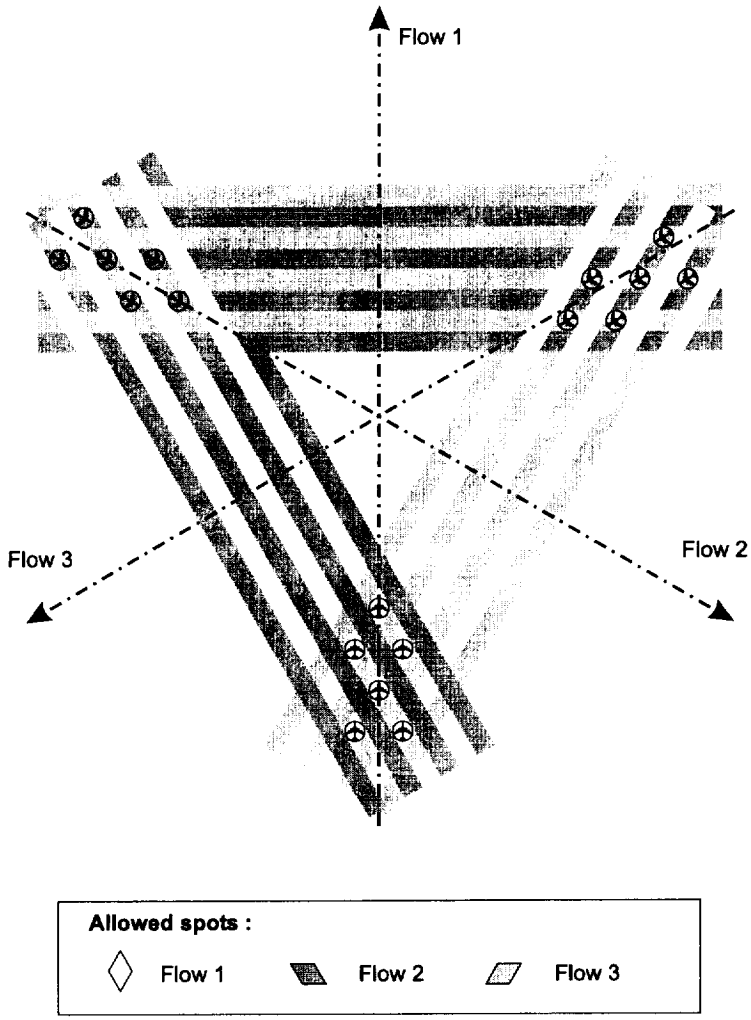

Figure 3-14: A way to partition the airspace for three 120 deg oriented aircraft flows.

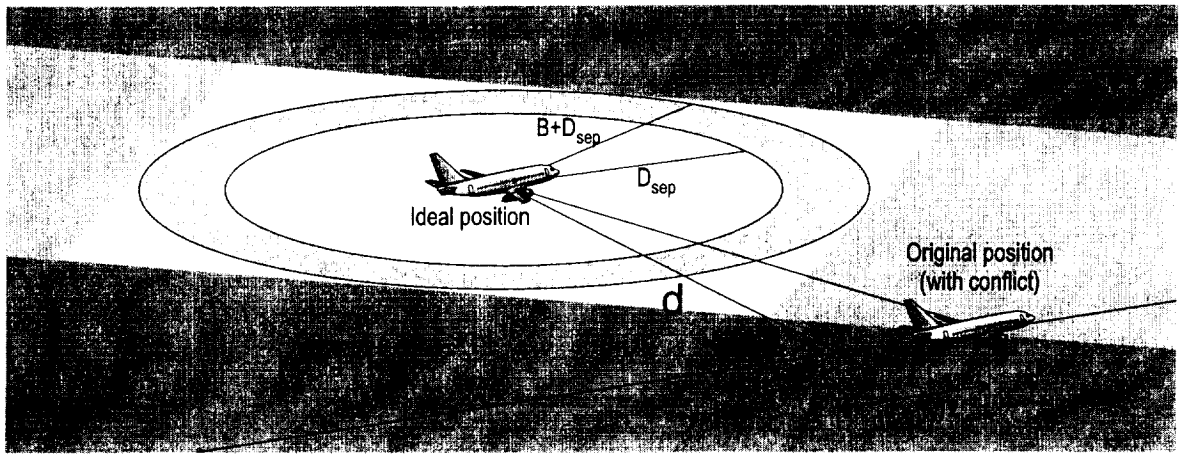

Figure 3-15: By performing a lateral displacement, an aircraft can be translated to a safe spot (blank airspace). A buffer B can be added to account for uncertainties and lack of maneuvering precision.

locate themselves to avoid aircraft in the other flows (Fig. 3-15). Such a concept was proposed in a different context in [21].

Robustness to arrival process

One available design variable when constructing this structure is the width of each aisle. However, as shown in Fig. 3-16, choosing the same aisle width for each flow does not result in any improvements, because for some initial aircraft locations along their nominal path, there exist no lateral deviation leading to a safe "spot" via lateral deviations only (these locations are shown with black lines on the figure).

Feasible solutions are obtained if the airspace is structured with different aisle width patterns for each of the three aircraft flow pairs. The structure shown in Fig. 3-17 can handle any aircraft flow as described at the beginning of this section; as such it provides a bounded, feasible initial flow configuration that may be used for example as a starting point for an on-line optimization procedure. This solution has been optimized to minimize the maximal lateral displacement using a randomized search algorithm. It is then compared with solutions obtained with mathematical programming software for finite sets of aircraft belonging to three flows.

For the three flows, we outlined the spots where aircraft could be positioned. As noted, the size of each aisle to safety distance ratio (h/D_{sep}) is now different for each flow pair interaction, and the pattern of aisle, periodic. As can be inferred from the way our structure has been constructed, the region where the positioning occurs can be partitioned with equilateral triangles whose edge length is $4D_{sep}/\sqrt{3}$, as shown for flow 1 in Fig. 3-18. This airspace decomposition allows aircraft from any flows to perform lateral maneuvers and find a conflict-free location, as proven thereafter.

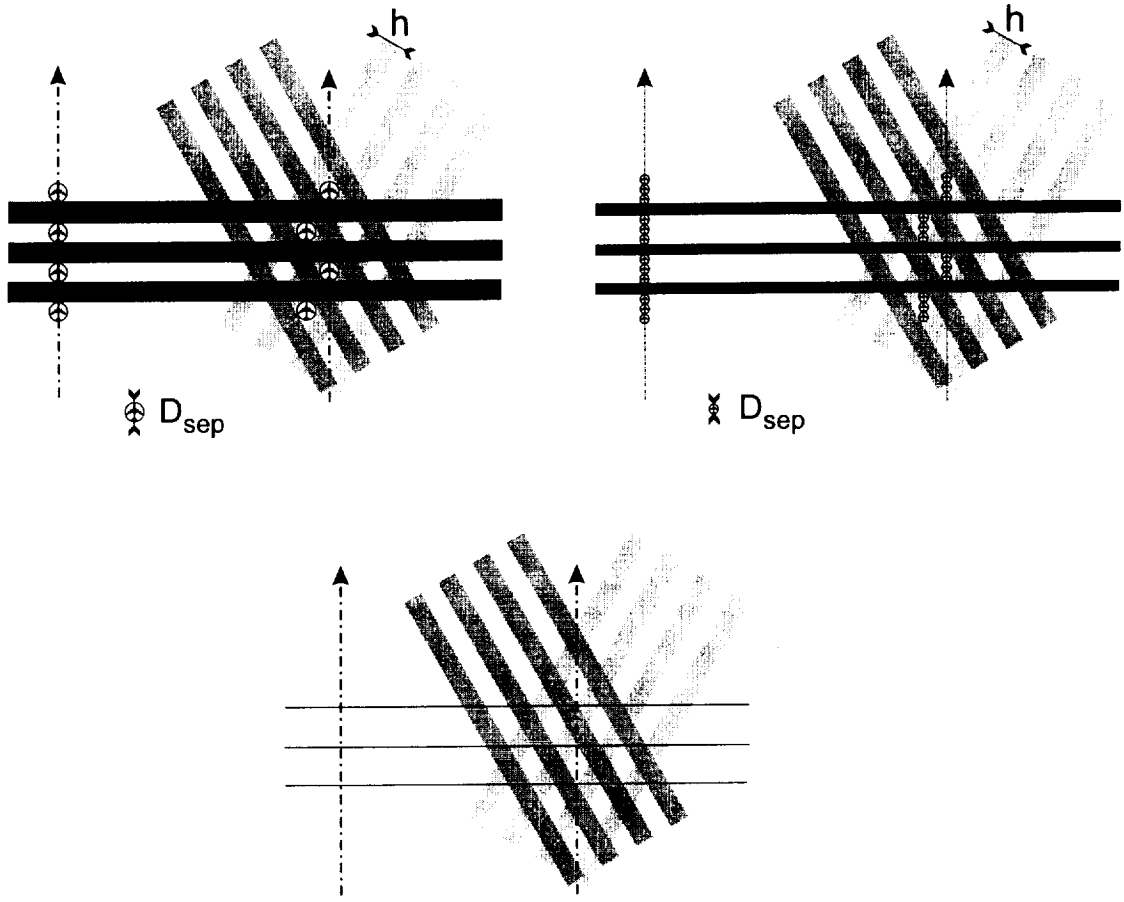

Figure 3-16: Uniformly changing aisle width does not help some aircraft to find a "safe spot". Top left: $h/D_{sep} = 1$. Top right: $h/D_{sep} = 2$. Bottom: $h/D_{sep} \to \infty$.

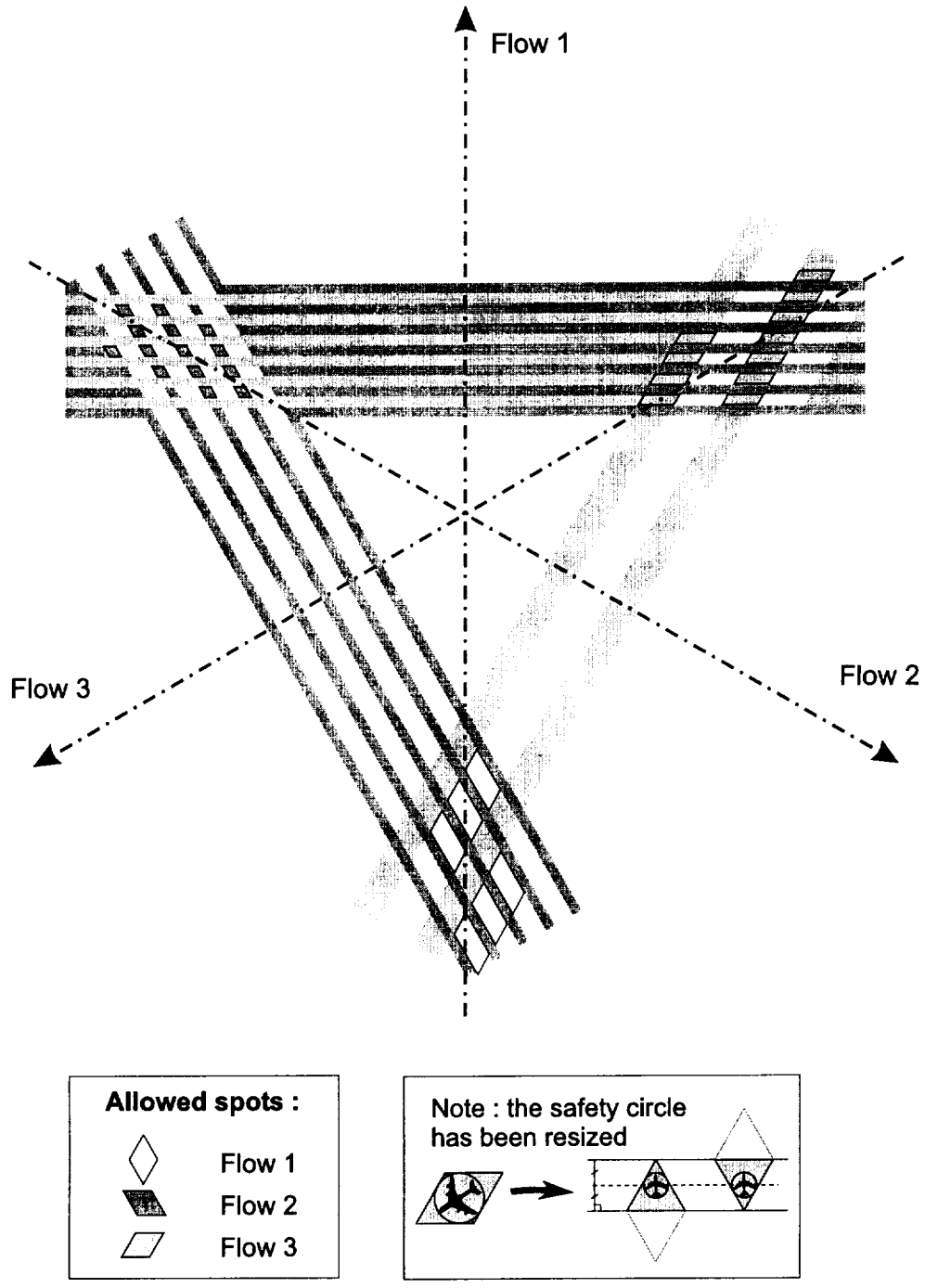

Figure 3-17: A way to structure airspace for three 120 deg oriented aircraft flows, so that the constraint on the flow that appeared in Fig. 3-16 is released. This structure has been optimized to minimize the maximal lateral displacement.

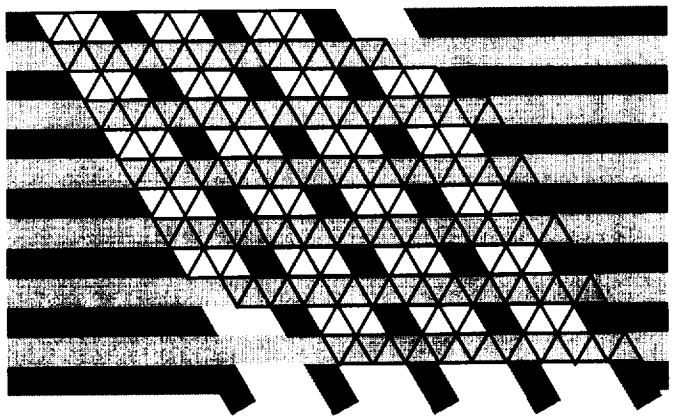

Figure 3-18: Partition of the region of positioning for flow 2 with equilateral triangles. Once such a partition has been identified, it is verified that any aircraft along the original flight path axis is able to reach a *protected* zone (dark triangles) via lateral displacement only.

Optimization of the geometry and performance bound

Consider Fig. 3-19. We represent the allowed spots as a function of the abscissa for flow 1 with the aisle structure in the background. Other spot locations may also be feasible, as sometimes a displacement to one side of the original track is equivalent in cost (distance from the axis) to a displacement to the other side. The plot is periodic, due to the periodicity of the crossing patterns. For flow 1 (Fig. 3-19), a whole period is shown, which corresponds to a length of $24D_{sep}$. The spot locations are systematically computed by Matlab for the three flows and are shown in Fig. 3-20. It is noted that the period for flow 2 is $40D_{sep}$, and for flow 3, $60D_{sep}$. By inspection of Fig. 3-20, the maximum deviation experienced occurs in flows 2 and 3, for a value of:

$$d_{max} = 6.4D_{sep}. \tag{3.11}$$

This gives a maximal overall lateral displacement of 32.0 nm as well as an upper bound on the maximum lateral deviation that may be performed by aircraft. This is far from being a realistic value and cannot possibly be applied "as is" for practical flow management purposes. However, it may be of value to get some understanding of the way conflict resolution processes work.

Comparison with mixed integer programming optimization

The conservatism of the solution proposed in the previous section may be evaluated using numerical optimization procedures on particular, finite aircraft flow instances.

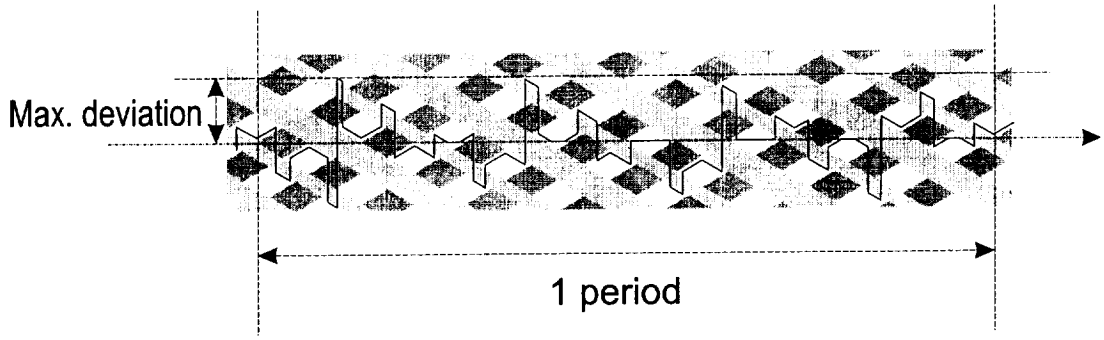

Figure 3-19: Determination of safe optimal spots with a given structure. Non conflicting spots are blank. At each abscissa, the closest safe spot from the original path is determined. The result is the solid line, exhibiting periodicity. The maximal deviation is immediately derived.

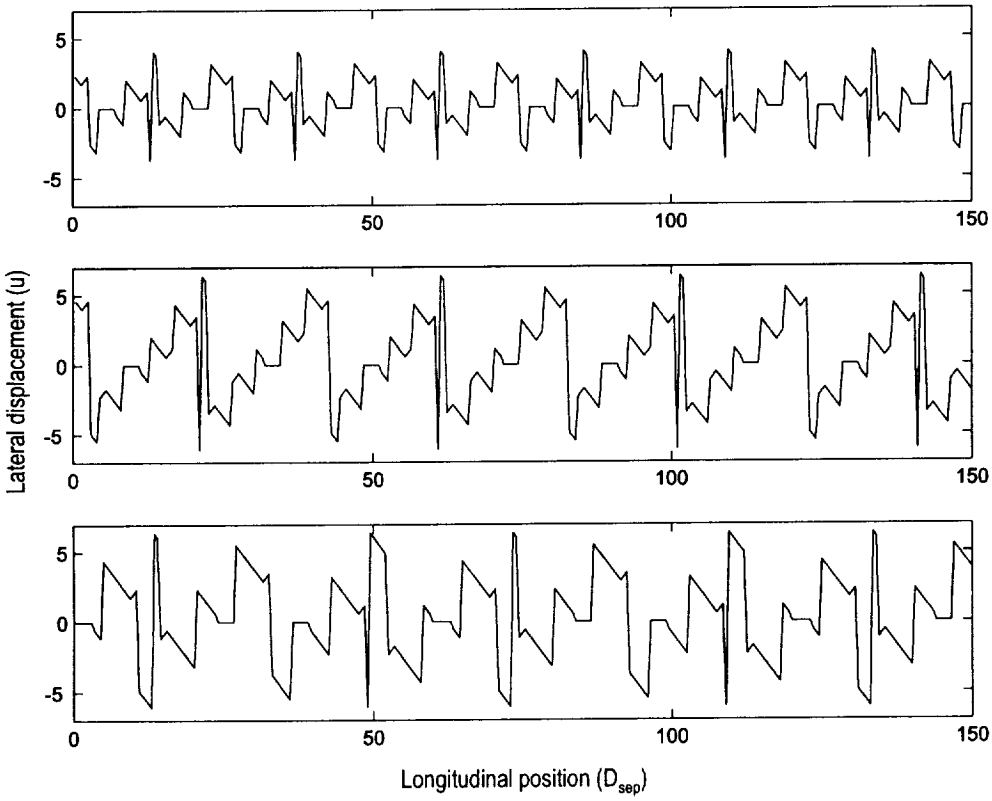

Figure 3-20: Result of the systematic calculation of best safe spots under Matlab for the structure shown in Fig. 3-17. Here, the unit u is $2D_{sep}/\sqrt{3}$. The results for flows 1 to 3 appear from top to bottom.

We considered three densely packed flows (initial aircraft separation within a flow is 5 nm) of twenty aircraft in each flow, and used a centralized solution procedure based on mixed integer programming. It is similar to that described and applied to two intersecting aircraft flows in our earlier work [29].

As may be seen in Fig. 3-21 (bottom), the largest displacement experienced by the aircraft is 23.1 nm. This solution is found using CPLEX, a linear programming optimization software [22]. This numerical test provides a lower bound on the aircraft lateral deviation, which is about 30 % less than that provided by the airspace structure provided earlier (Fig. 3-21, top). This gives an estimate of the performance of a configuration built by procedure (using our structure) compared with that of an optimized configuration (using CPLEX).

Application to an en-route situation

Fig. 3-22 shows an illustration of the procedure-based control scheme. A real-world intersection of airways (Durango VOR[1]) is shown in Fig. 3-22-a. In Fig. 3-22-b, a number of aircraft are shown approaching the beacon. Some of these are on a conflict path with each other. The structure given by our procedure-based control scheme is overlaid in Fig. 3-22-c. To avoid all conflicts, aircraft need to be brought to the spots shown in Fig. 3-22.d. The choice of maneuver is free: specifically, offset maneuvers are possible as they are almost equivalent to lateral displacement. In this case, safe spots should be found by searching on a line inclined at an angle $\pm(\pi/2 + \chi/2)$ with respect to the direction of the low. (see also Section 3.2)

3.5 Summary

Table 3.1 summarizes the three models analyzed in this chapter. Results from [28] are given for comparison purposes.

[1]VHF Omnidirectional Radio Range Beacon used for in-flight navigation.

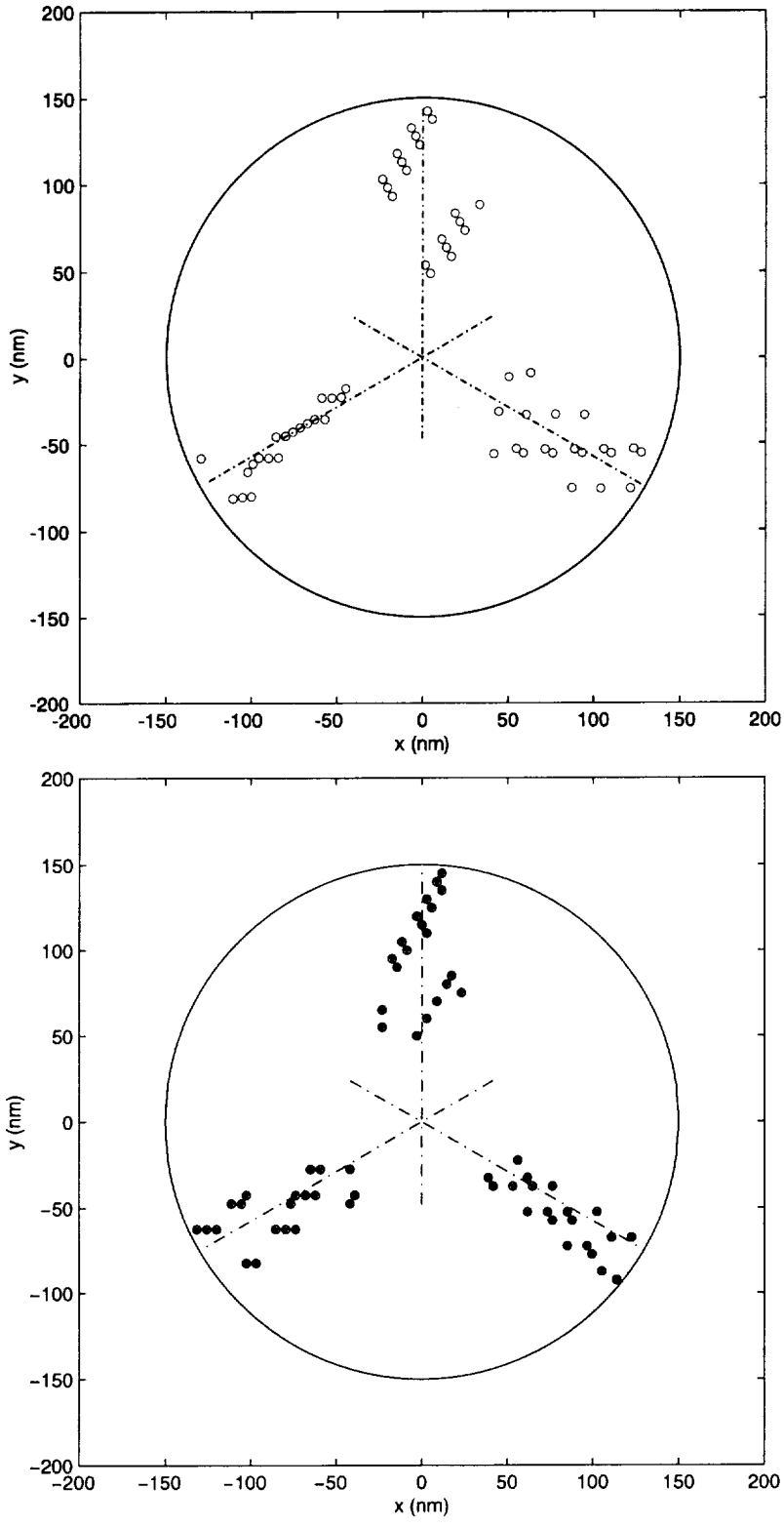

Figure 3-21: Top: Conflict resolution for 3 streams of 20 aircraft obtained by applying the structure shown in Fig. 3-17, maximum deviation is 32 nm. Bottom: Conflict resolution for the same configuration via mixed integer linear programming, maximum deviation is 23.1 nm

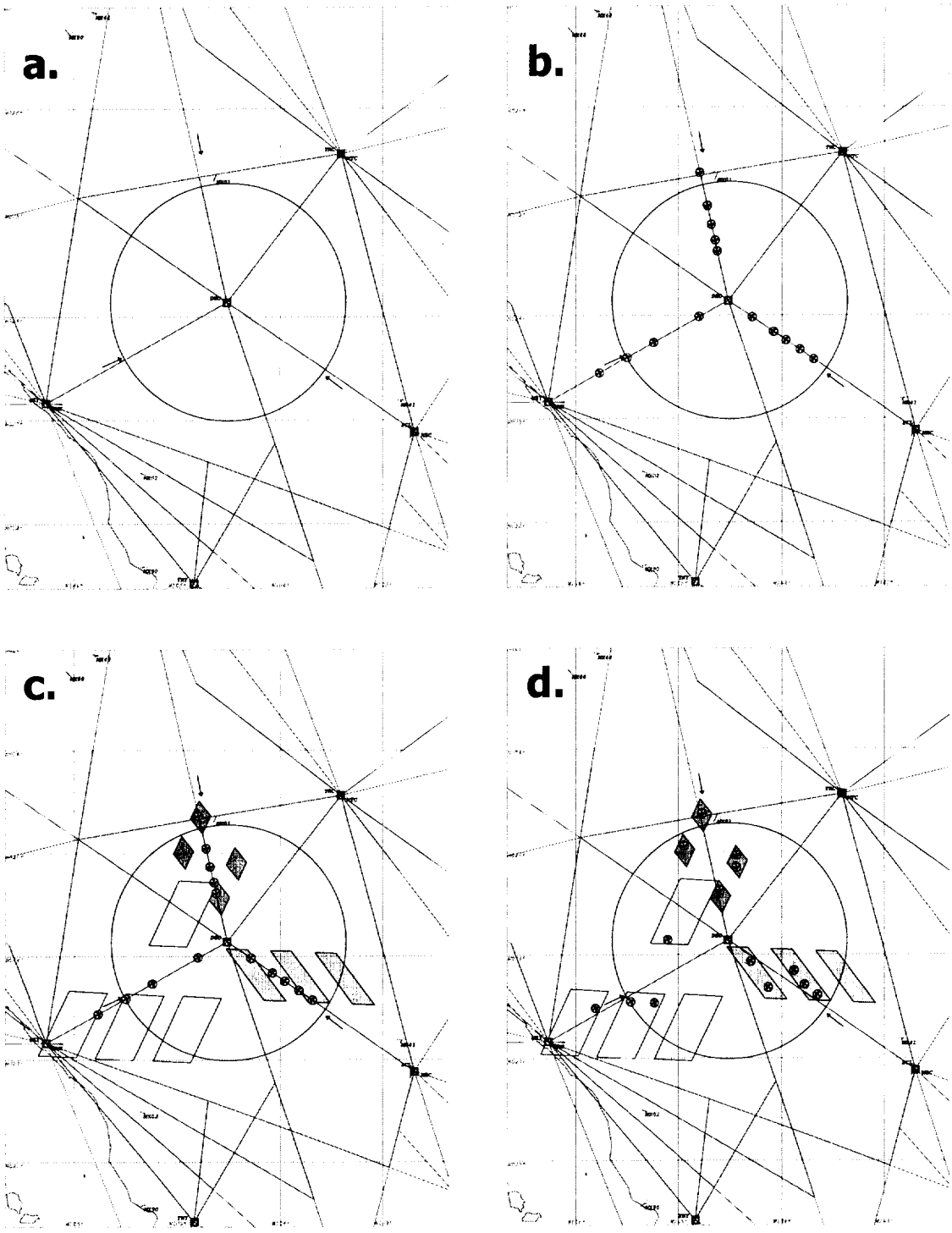

Figure 3-22: Illustration of our procedure-based, centralized control scheme for three flows intersecting over the Durango VOR, Mexico. Chart imported from Microsoft Flight Simulator.

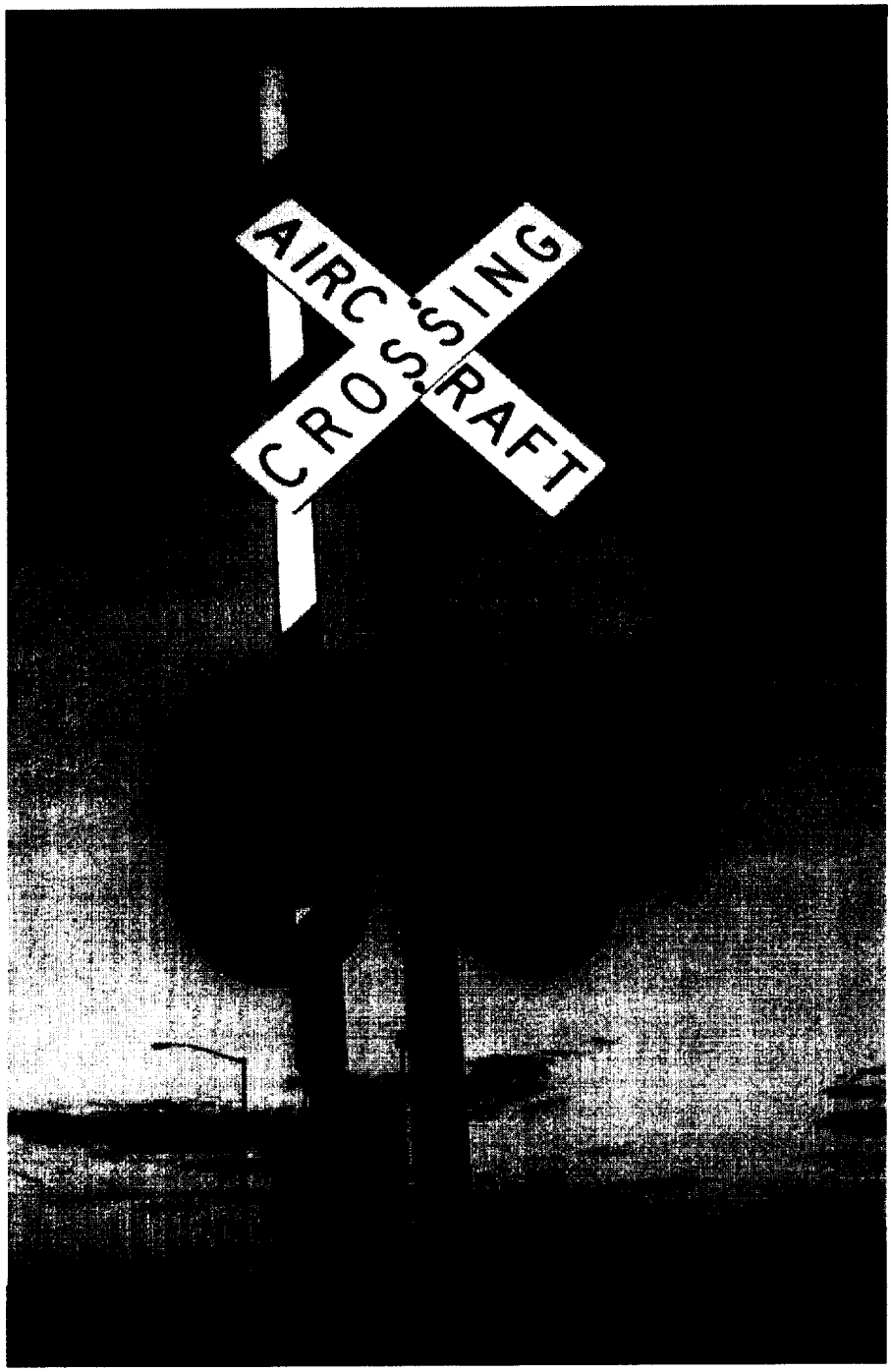

Figure 3-23: A procedure-based aircraft conflict avoidance system at Anchorage International Airport (Alaska)...

Type	Flows	Category	Performance	Stability	Reference
Lat. disp.	2	Decentr.	$d_{max} = D_{sep}\sqrt{2}$	By proof	[28]
Offset	2	Decentr.	$d_{max} = D_{sep}\sqrt{2}$	By proof	[Section 3.2]
Hdg. chg.	2	Decentr.	$\tan\chi = \frac{\delta\sqrt{2-\delta^2}}{1-\delta^2}$	By proof	[Section 3.3]
Lat. disp.	3	Centr.	$d_{max} = 6.4D_{sep}$	Offline construction	[Section 3.4]
Lat. disp.	3	Centr.	Flow dependent	Online computation convergence	[28]

Table 3.1: Summary of conflict models

Chapter 4

Control of a linear flow under separation and scheduling constraints

4.1 Background

This chapter investigates the problem of propagation of delays in the NAS. The limited capacity of a runway in bad weather conditions is often the origin of rate restrictions in the en-route airspace. Aircraft going to that particular runway are impacted sometimes very early in their flight as restrictions tend to spread easily in the system (see Section 1.1.2). Fig. 1-3 illustrates a problem that occurred when restrictions for aircraft inbound to Newark airport impacted traffic hundreds of miles away in a short amount of time (see [39]).

To delay the propagation of restrictions to upstream sectors, real-life controllers use a number of different tools (see [40]). One tool is *speed control*: by slowing down an aircraft, it is possible to increase the distance from the preceding aircraft, and thus decrease the sector's apparent output rate of aircraft. This works for a limited period of time since the aircraft cannot fly below a certain minimum speed. Another tool is *path stretching*, whereby the controller increases the distance flown by an aircraft in his sector to delay the exit. Path stretching is also limited in time because of geometric constraints of the sector.

Aircraft arrivals scheduling and sequencing represent an increasingly challenging task, sometimes addressed by automation tools at the ATC facility. Ref. [14] set the basis for most of the research in Air Traffic Management. Delay propagation in the NAS is the object of a few studies, such as [4]. Ref. [7] treats the problem of conflict resolution under scheduling constraints. We choose to analyze scheduling issues at the sector level to derive macroscopic trends. Some of the issues mentioned thereafter also appear in the management of other types of transportation. (see [34, 41] for road traffic applications)

This chapter investigates the behavior of one sector that uses the control schemes mentioned above to meter its aircraft. Variables of interest are sector length D and

width w, speed range, and rate restrictions.

Our metrics are the capacity of the sector and the responsiveness to an output rate change. This provides a performance index for the control schemes we consider. We complete the definition of capacity found in Section 2.4.2 as follows: it is the number of aircraft that have come in at a rate λ and have come out at the restricted output rate μ_r after speed control. Responsiveness is the time between a change of the output rate restriction μ_r and the change of the actual output rate μ as seen by an observer at the exit of the sector.

Section 4.2 introduces the models used for the sector and the aircraft. Section 4.3 presents the control laws to be used to schedule aircraft, and simulations are performed in Section 4.4. Section 4.5 analyzes and derives results of capacity and performance of the global control scheme.

This chapter presents results that appeared in [10].

4.2 System definition

This section describes the models used for the analysis: sector geometry, aircraft kinematics, and aircraft flow behavior.

4.2.1 Sector geometry

The en-route sector of interest is modeled by a rectangle, and trajectories are restricted to be two-dimensional (see Section 2.1.3). In the study of speed control, this rectangular geometry can be further simplified into a one-dimensional sector: Fig. 4-1 shows that sectors close to major airports match this one-dimensional model. In the real-world, a lot of sectors also have minor crossing traffic requesting separation: this is not taken into account in our study. (see [7] for an analysis on this matter)

Our sector is a rectangle of length D and width w, with aircraft arriving at $x = 0$ (entry point I) and leaving at $x = D$ (exit point O). Fig. 4-1 shows that most sectors have a length a lot larger than their width. This length D is typically 150 nm in the National Airspace System and the width w is 40 nm. Points I and O represent the *fixes* where flights are handed over from one sector to the next (Fig. 4-1).

4.2.2 Aircraft

Aircraft are modeled as massless points that perfectly follow speed commands. No dynamics are modeled, and speed changes occur instantaneously. Each aircraft A_i is associated with a state-vector position-speed (x_i, v_i). Aircraft fly within a certain speed range due to buffeting speed limitation on the lower end and maximum Mach number on the upper end: $v_i \in [v_{min}, v_{max}]$.

Important times in the aircraft journey through the sector are the entry and exit times, denoted t_i and s_i, respectively.

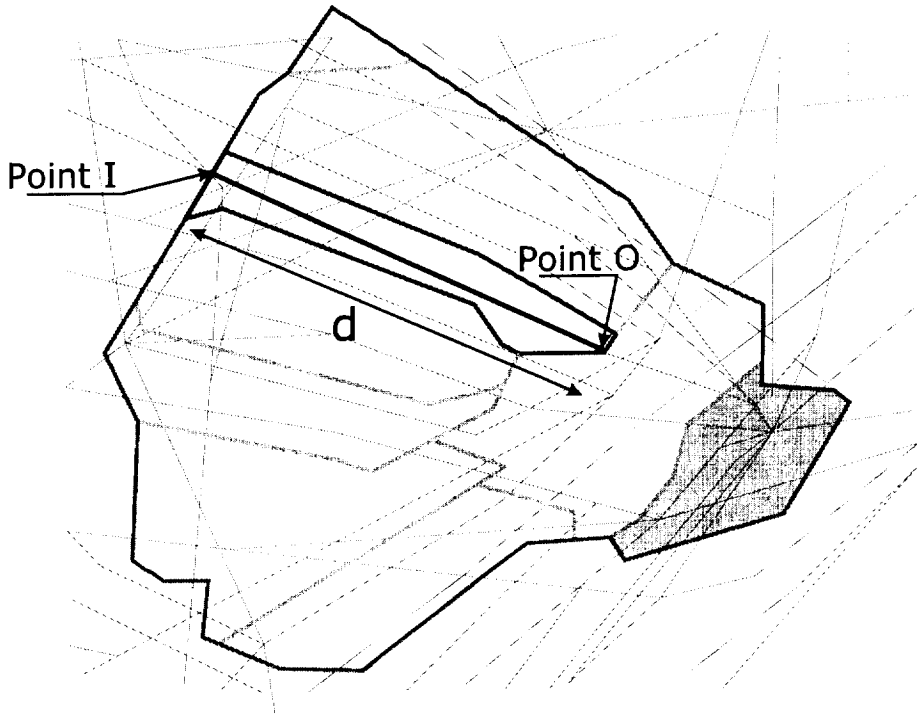

Figure 4-1: Layout of the New York Center Sector. All three major New York airports are located in the shaded area. One sector has been singled out to show how our model mimics the sectors with some realism.

4.2.3 Flow

The aircraft flow enters the sector through point I (where the aircraft are handed over from the upstream sector) and exits at point O (where the aircraft are handed over to the downstream sector). The input rate is λ and the output rate is μ. The input rate λ corresponds, in the real world, to the output rate μ of an upstream sector. If we index the sectors with respect to their streamwise position, we thus have $\lambda^{k+1} = \mu^k$ for all k.

We consider one single sector, for which μ is dictated from outside, while λ can be controlled (by refusing incoming aircraft). This model may lead to the upstream propagation of rate restriction throughout sectors. Because a restriction on μ cannot usually be respected instantaneously, μ_r denotes the desired output rate (desired by the downstream sector). μ is the achieved output rate, which ideally should equal μ_r.

Given an input flow λ, aircraft arrival times are modeled in two ways:

- Deterministic model: aircraft interarrival times τ are constant when λ is constant and equal to $\tau = 1/\lambda$.
- Randomized model: aircraft interarrival times are normally distributed according to $N[1/\lambda, \varsigma^2]$ where ς is the standard time deviation of the distribution.

It should be noted that it is impossible to keep an input rate λ higher than μ_r for an extended time. Drawing a parallel with the principle of mass conservation, we

have "aircraft conservation" in the sector: in steady state, there must be as many aircraft entering as aircraft leaving. We assume this sector is an en-route sector, and thus has no airports to act as "sinks" of aircraft.

4.3 Control laws

This section analyzes the various control schemes from basic kinematics. In Section 4.3.1, these laws are inquired from a "black box" perspective, regardless of the type of control. Section 4.3.2 describes the back-propagation process at the level of the individual sector.

Section 4.3.3 investigates the implementation of the schedule from Section 4.3.1 with speed control. Two variations of speed control are investigated in our study. As both are based on the same principle, only the first is extensively described. The second is a simple and straightforward modification of the first. Finally, Section 4.3.4 analyzes the implementation of the desired schedule with path stretching.

We implement a First-In, First-Out control scheme, so that aircraft are not allowed to overtake one another.

4.3.1 Scheduling

The problem of buffering an aircraft flow in a sector can be seen as a scheduling task. It consists in scheduling the aircraft exit times to match an output rate limit, although the input rate has another value. Constraints are of different nature: distance, time, rates, and speed constraints are imposed simultaneously. Frequent conversions between those types of constraints thus appear in the derivations.

An aircraft enters the sector at t_i and exits at s_i. The time it spends in the sector is r_i, where $t_i + r_i = s_i$. The apparent longitudinal speed is $v_i = D/r_i$.

Let us first derive the desired (scheduled) time of exit s_i. This is subject to three types of constraints, ordered by priority:

- Aircraft physical capacity: the two aircraft operational speed constraints (v_{min} and v_{max}), Eq. (4.1) and Eq. (4.2);
- Regulatory constraint: the separation constraint (minimum separation of D_{sep}), Eq. (4.3);
- Traffic management constraint: output rate μ_r, Eq. (4.4).

Following the same order, we have:

$$s_i \leq t_i + \frac{D}{v_{min}} \tag{4.1}$$

$$s_i \geq t_i + \frac{D}{v_{max}} \tag{4.2}$$

$$s_i \geq s_{i-1} + \frac{D_{sep}}{v_{i-1}} \tag{4.3}$$

$$s_i = s_{i-1} + \frac{1}{\mu_r}. \tag{4.4}$$

Thus, the scheduled time of exit s_i is:

$$\min\left(t_i + \frac{D}{v_{min}}, \max\left(t_i + \frac{D}{v_{max}}, s_{i-1} + \frac{D_{sep}}{v_{i-1}}, s_{i-1} + \frac{1}{\mu_r}\right)\right). \tag{4.5}$$

A special note should be made here for the separation constraint. The scheduled time of arrival derived from the separation constraint Eq. (4.3) only guarantees separation at exit. However, separation has to be maintained throughout the sector. Eq. (4.3) is sufficient to guarantee this separation, given that aircraft enter the sector already separated. Let us denote ϵ the distance between two consecutive aircraft. If both aircraft keep their respective speed constant, then ϵ varies linearly with time. If separation is guaranteed both when the speed command is given (by assumption) and when the aircraft exit Eq. (4.3), then it is assured by continuity anywhere inbetween. Thus Eq. (4.3) is sufficient to assure separation at any point of the flight within the sector.

Since each optimal exit time depends on the exit time of the preceding aircraft, s_i needs to be determined recursively. For speed control, the speed command is then derived directly from s_i with $v_i = D/(s_i - t_i)$.

4.3.2 Input rate control

When the sector is unable to deal with an output restriction, it may either decide to violate the output restriction or request a lower input rate from the upstream sector. The latter option is considered here.

Various ways to request a lower input rate are possible. "λ" could be requested to be well below, exactly equal to, or slightly above (but then for a limited time) the imposed output rate μ_r. We choose to decrease this input rate - that is, the output of the upstream sector - to the output restriction when minimum speed is reached. Before that, no restrictions exist.

This strategy back-propagates the restriction as late in time as possible. This is a relatively tougher restriction than if the restriction is back-propagated right from the start.

4.3.3 Speed control

We now look specifically at the speed control scheme, under two of its variations:

- Entry control, where aircraft are controlled only once - at their entry - and keep the commanded speed setting until they exit;

- Extended control, where aircraft speeds are continuously controlled in the first $100\gamma\%$ of the sector. They keep the last setting in the last $100(1-\gamma)\%$ of the sector.

Entry control

In the *entry control* law, the control system commands incoming aircraft speed on entry only. This speed setting is not be modified until the aircraft exits.

We consider the four constraints stated above by priority:

- Speed must remain in the operational range of the aircraft: the actual v_i is given in Eq. (4.9).
- Separation must be maintained throughout the sector: this requirement can be verified by only enforcing the separation constraint at the exit with a speed command v^s: Eq. (4.7).
- An ideal exit time enforces the desired output rate μ_r. The speed is adjusted in Eq. (4.6) to v^r so that maximum efficiency is achieved, meaning that all aircraft pairs are exactly a time $1/\mu_r$ apart at the output.
- Of the last two constraints, the most important is separation: the speed to be commanded to the aircraft must never be higher than that computed in Eq. (4.7), yielding v^m in Eq. (4.8).

All these requirements translate into the following constraints:

$$v^r = \frac{D}{\frac{D-x_{i-1}}{v_{i-1}} + \frac{1}{\mu_r}}, \tag{4.6}$$

$$v^s = v_{i-1}\frac{D}{D + D_{sep} - x_{i-1}}, \tag{4.7}$$

$$v^m = \min(v^r, v^s), \tag{4.8}$$

$$v_i = \text{sat}\,{}^{v_{max}}_{v_{min}}(v^m). \tag{4.9}$$

where the saturation function is defined as:

$$\begin{aligned} \text{sat}\,{}^{b}_{a}(x) &= a \text{ for } x \leq a & (4.10)\\ &= x \text{ for } a < x < b & (4.11)\\ &= b \text{ for } x \geq b. & (4.12) \end{aligned}$$

v_i is the speed command effectively passed on to the aircraft. A system diagram appears in Fig. 4-2 (top), where measured parameters are shown.

Extended control

In this second strategy of speed control, aircraft are submitted to the controller's command while they are flying over the first $100\gamma\%$ of the sector. The output rate restriction μ_r is only allowed to be piece-wise constant: the speed commands change

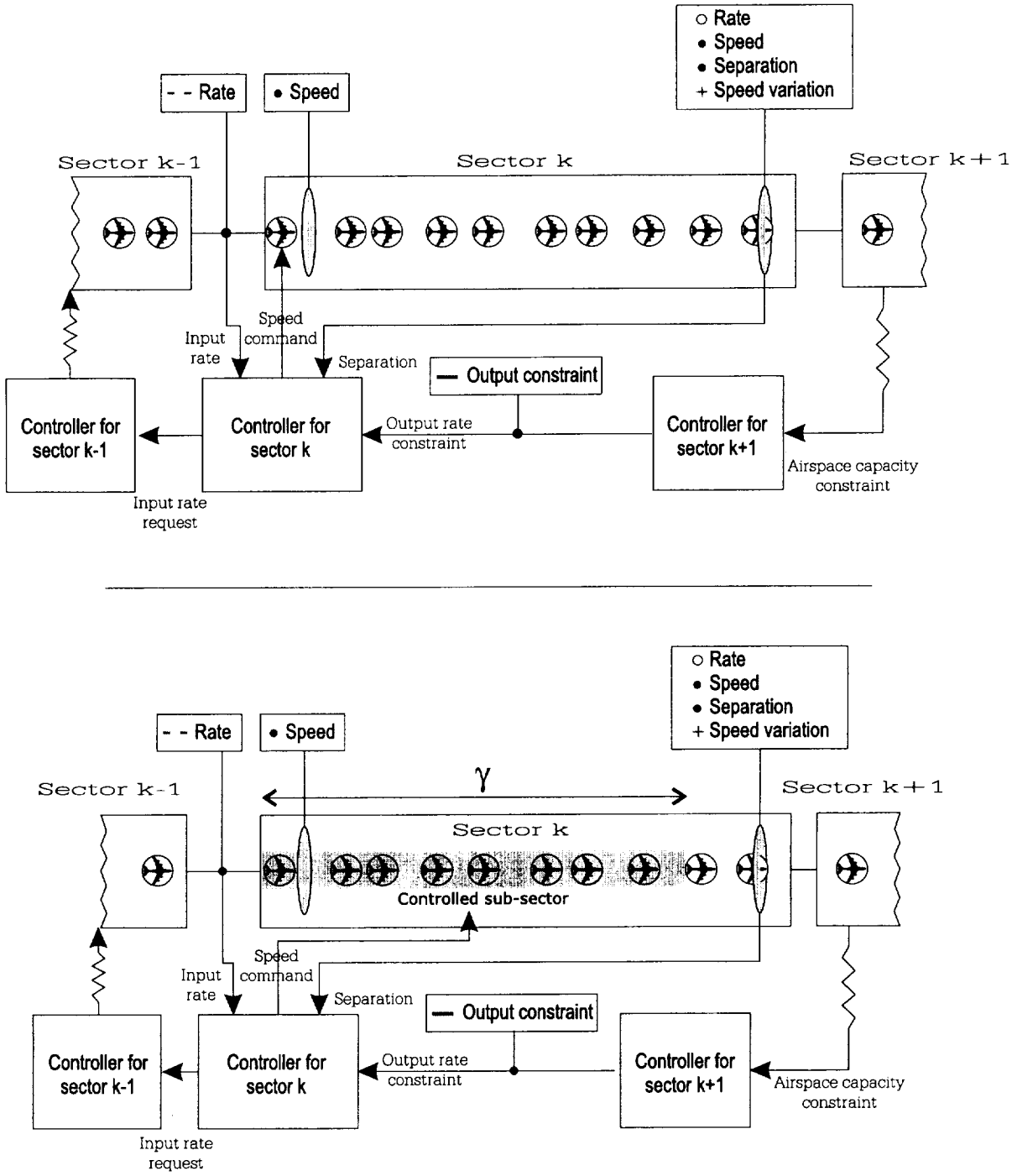

Figure 4-2: Diagram of the system. Measured parameters are represented with color markers consistent with those shown on plots. Top: Entry control. Bottom: Setup of the extended control law, which includes the possibility to control a portion γ of the sector.

only during the step changes of μ_r. The same requirements as in the previous paragraph apply, leading to the following system of equations:

$$v^r = \frac{D - x_i}{\frac{D-x_{i-1}}{v_{i-1}} + \frac{1}{\mu_r}}, \tag{4.13}$$

$$v^s = v_{i-1}\frac{D - x_i}{D + D_{sep} - x_{i-1}}, \tag{4.14}$$

$$v^m = \min(v^r, v^s), \tag{4.15}$$

$$v_i = \text{sat}_{v_{min}}^{v_{max}}(v^m). \tag{4.16}$$

If $x_i \in [0, \gamma D]$ then v_i is the speed command given to aircraft A_i when μ_r changes. If $x_i \in]\gamma D, D]$ then the speed setting is the last command given to aircraft A_i in $[0, \gamma D]$.

As the information relative to the output rate restriction is influencing the speed of aircraft further into the sector, the responsiveness of the sector to a change in μ_r is expected to be better than for *entry control.*

Fig. 4-2 (bottom) gives an overview of the extended law.

4.3.4 Path stretching

We now address the scheduling problem stated in Section 4.3.1 using *path stretching.* This approach follows the example of today's air traffic controllers, who usually extend the path of aircraft to slow them down.

Principle

Path stretching consists of deviating the aircraft by an angle χ_1 for a time ζ_i^1, and taking the returning angle χ_2 for a time $\zeta_i^2 = t_i - s_i - \zeta_i^1$. Our path stretching maneuver is restricted to two legs. More legs could be considered, which would lead to more control authority at the expense of analytical simplicity. Path stretching is symmetrical if $\zeta_i^1 = \zeta_i^2$ (and $\chi_1 = -\chi_2$). The heading changes are assumed to be instantaneous, as by Section 2.1.2. (see Fig. 4-3). For all cases, the following constraints exist (the aircraft exits at one only point):

$$\begin{aligned} \zeta_i^1 \sin\chi_1 &= \zeta_i^2 \sin\chi_2 \\ D &= v(\zeta_i^1 \cos\chi_1 + \zeta_i^2 \cos\chi_2). \end{aligned}$$

Performance gain with path stretching

A straightforward analysis shows that path stretching induces an apparent (projected on the straight trajectory) speed modification of:

$$\frac{\Delta v}{v} = \frac{\tau_1 \cos\chi_1 + \tau_2 \cos\chi_2}{\tau_1 + \tau_2} - 1, \tag{4.17}$$

where τ_1 and τ_2 are the times spent on each of the two legs of path stretching. To limit maneuver amplitude, only a certain range of χ's should be used.

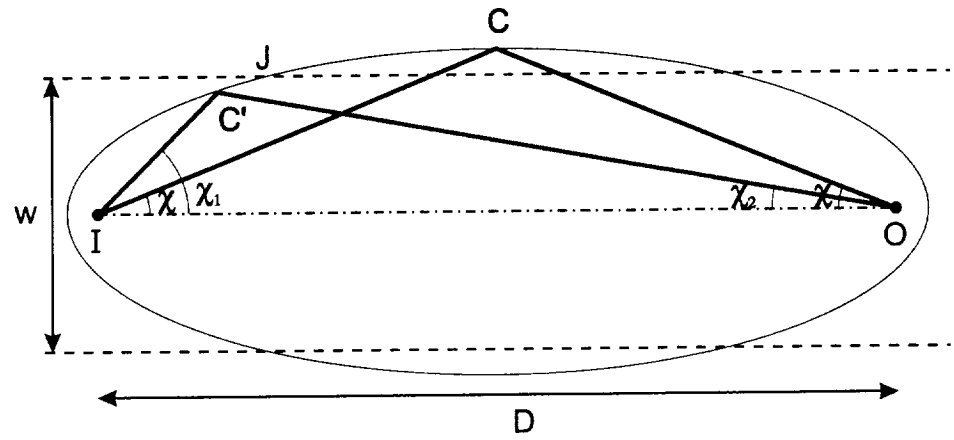

Figure 4-3: Path stretching: notations and corner point locus

Symmetrical path stretching

We first consider the case of symmetrical path stretching ($\zeta_i^1 = \zeta_i^2$, thus $\chi_1 = \chi_2 = \chi$). Here, the largest lateral deviation from the original path occurs at $t_i + \zeta_i^1$, i.e. at the corner point C in the middle of the trajectory between the entrance and the exit (see Fig. 4-3). Given w, the width of the sector, and D, its length, the maximum allowable deviation is:

$$\tan \chi_{max} = \frac{w}{D}. \tag{4.18}$$

Eq. (4.17) simplifies to:

$$\frac{\Delta v}{v} = \cos \chi - 1 \tag{4.19}$$

and

$$\frac{\Delta v}{v} = \frac{D - \sqrt{D^2 + w^2}}{\sqrt{D^2 + w^2}}. \tag{4.20}$$

Typical values of D (150 nm) and w (40 nm) give $\Delta v/v \approx -3.4\%$.

Asymmetrical path stretching

Contrary to the preceding section, we now consider the case where $\chi_1 \neq \chi_2$. From Eq. (4.17), the locus of corner points of trajectories with identical $\Delta v/v$ is found to be an ellipse. Fig. 4-3 shows that the use of asymmetrical path stretching helps achieve the same $\Delta v/v$ with less lateral deviation (the blue trajectory in Fig. 4-3 has its corner point C beyond the width limit of the sector, while the red trajectory, of the same length, has its corner point C' within the limits). We choose the minimal χ_1 that achieves the requested $\Delta v/v$.

Fig. 4-4 (right part of the curve) shows the angle χ as a function of $\Delta v/v$ for a given D and w (typical values used in the previous section). Efficiency of a control scheme is measured by the inverse of the slope of the curve, representing the incremental angular deviation needed to slow down the aircraft by an incremental amount of $\Delta v/v$. The asymmetrical path stretching scheme is thus less efficient than its symmetrical counterpart.

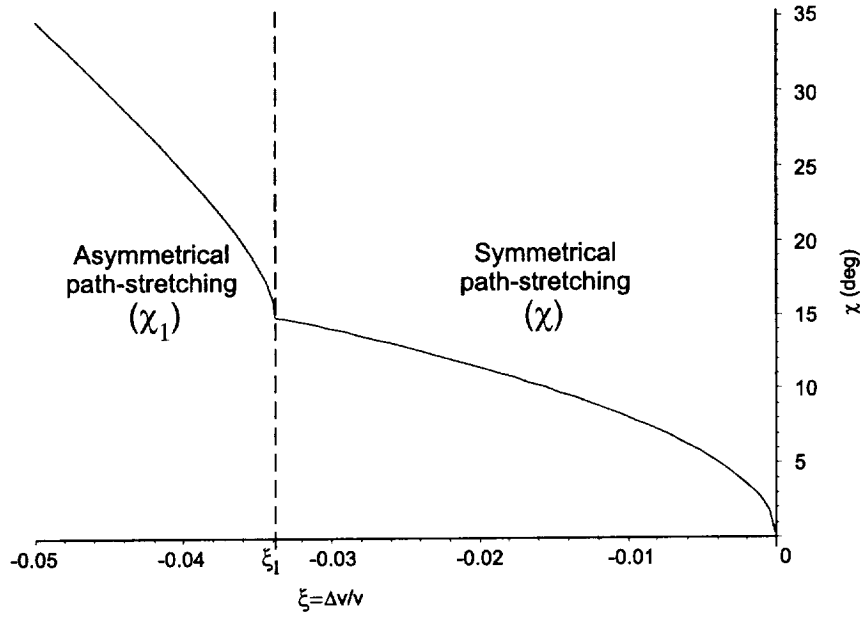

Figure 4-4: Deviation angle χ (or χ_1) as a function of the apparent decrease in (projected) speed $\Delta v/v = \xi$, for a sector of length $D = 150$ nm and width $w = 40$ nm. The function is continuous and consists of two parts, noticeable by the discontinuity of the slope at $\Delta v/v = \xi_l \approx -3.4\%$: the left part is when symmetrical path stretching is used, and the right part is when the upper limit on width (w) is reached and asymmetrical path stretching is enforced.

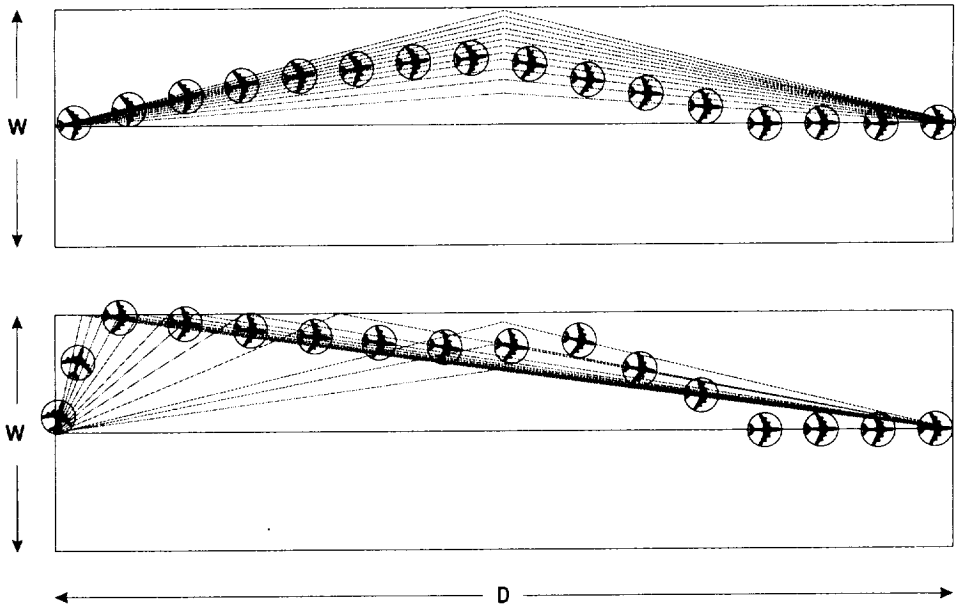

Figure 4-5: Snapshot of a sector under path stretching flow control. Sector length is $D = 150$ nm and width $w = 40$ nm. Trajectories are shown in dimmed lines. Top: Symmetrical path stretching. Bottom: Asymmetrical path stretching.

General result for path stretching

Fig. 4-4 shows the general result regarding path stretching. The function $\chi(\xi)$, with $\xi = \Delta v/v$, is the following:

- for $\xi < \xi_l$:

$$-\arctan \frac{w}{-D + \sqrt{\frac{(D^2+w^2)\xi^2+2(D^2+w^2)\xi+w^2}{(\xi+1)^2\xi(\xi+2)}}} \tag{4.21}$$

- for $\xi > \xi_l$:

$$\arccos(1+\xi) \tag{4.22}$$

with $\xi_l = \frac{D}{\sqrt{w^2+D^2}} - 1$. This result does not take into account separation, which is investigated in the next section.

Path stretching and separation

Because path stretching uses a second dimension by moving the airplanes on a plane, separation becomes a harder issue than in the speed control case, where timing constraints guarantee separation. Fig. 4-5 shows snapshots of a sector using path stretching for flow control; both symmetrical and asymmetrical cases are shown.

The variation of the distance between two aircraft in line, A_1 and A_2, is investigated ($t_2 > t_1$, i.e. A_1 is the first aircraft):

$$\mathbf{x_i}(t) = (v(t-t_i)\cos\chi_i, v(t-t_i)\sin\chi_i). \tag{4.23}$$

Denoting $\Delta t = t_{i+1} - t_i$, and noticing that the entry separation between two aircraft is:

$$v\Delta t = D_{sep} + B \tag{4.24}$$

where B is the extra buffer between aircraft at entry, we derive the distance $\epsilon(t)$:

$$\begin{aligned}\epsilon(t) = &(vt(\cos\chi_2 - \cos\chi_1) - (D_{sep} + B)\cos\chi_2)^2 \\ &+(vt(\sin\chi_2 - \sin\chi_1) - (D_{sep} + B)\sin\chi_2)^2.\end{aligned} \tag{4.25}$$

ϵ is an increasing function of time when $\chi_2 > \chi_1$, which is the case when a restriction exists (see Fig. 4-4, when ξ is decreasing, χ is increasing) so that there is no loss of separation on the first leg of the trajectory. For the return leg, the distance between the two aircraft decreases. However, they are separated a priori by the choice of ξ - thus of χ - which takes into account separation at the exit. Since they are separated at the corner point, and are separated at the exit, then by monotonicity they are separated throughout their first leg. Thus, when a restriction exists, no loss of separation occurs, regardless of the initial separation (larger than D_{sep} by assumption).

It is different when the restriction has been lifted, and the recovery process is under way. The minimum distance may then be violated. To solve this problem, the following policy is implemented: every other aircraft scheduled during the recovery process is sent on the lower part of the sector[1], in a zone that has not been used before. Therefore, we ensure a virtual separation at entry equal to $2D_{sep}$. The following proves that this separation is sufficient to avoid any separation problem.

Using this policy, we have $B = D_{sep}$. We find the minimum of ϵ:

$$\epsilon_{min} = \min_{t>0} \epsilon(t) = D_{sep}\sqrt{2(1 + \cos\chi_1\cos\chi_2 + \sin\chi_1\sin\chi_2)}, \tag{4.26}$$

which is always larger than D_{sep} as long as $(\chi_1, \chi_2) \in [0, \pi/2]^2$. This proves our previous claim on separation for the first leg. With arguments analogous to those used previously, separation is also guaranteed on the second leg.

Analogy with speed control

Preceding sections show that path stretching gives results similar to speed control from the scheduling point of view. Specifically, as the path stretching command is only given once, and is not modified while the aircraft is in the sector, it is analogous to entry control.

In the case of speed control, scheduling is respected as long as the lower speed limit is not reached. With path stretching, scheduling is respected as long as geometrical limits are not reached. These limits are derived in Section 4.5.3.

Simulations of some restriction scenarios follow. They have been computed using only speed control. The performance results are analogous to those obtained with path stretching.

[1]This policy can be used all the time, we only *need* it during the recovery process.

4.4 Simulations

Simulations of the system using speed control are run under Matlab. In all examples below, the sector of interest is 150 nm long, consistent with today's National Airspace System design. Airspeed ranges from 400 kt to 500 kt (see Section 2.1.2). Appendix A provides a summary of all simulations parameters shown below. To derive simulations for path stretching, this range could be adjusted and derived from geometrical considerations.

A number of parameters are monitored as functions of time. Fig. 4-2 (top) shows a concise view of the system, including the points where parameters are measured. The following section details the plotted values.

4.4.1 Simulation parameters

Simulation results are shown with three different plots (see Fig. 4-6 below for illustration). The top plot shows the speed given to the aircraft at the entrance of the sector (one blue dot per aircraft) and the speed at the exit of the sector (purple circles). One data is not a simple translation in time of the other, because an aircraft flying at 400 kt takes more time to pass through the sector than an aircraft flying at 500 kt. One way to read this plot is to see the two lines as representing the range of speeds of the aircraft within the sector. For instance, at $t = 2$ hr in Fig. 4-6, aircraft in the sector have speeds ranging from 415 kt to 465 kt, approximately.

The middle plot shows a number of different rates of aircraft (i.e. the number of aircraft going through certain points over an hour): the dotted green line represents the input rate λ from the upstream sector (sector $k-1$ as labeled in Fig. 4-2), the solid red line the restriction μ_r on the output flow as requested by the downstream sector (sector $k+1$). The blue dots represent the actual output rate μ. These dots turn to stars if the rate is in violation of the output constraint. However, because in this model we "flush" the first few aircraft, some blue dots appear as being above the red line: they represent the "flushed" aircraft.

The bottom plot shows two different things: first, with blue dots, the separation of aircraft at the exit is shown. This separation, in nautical miles (nm) should never be below 5 nm. If the separation is greater than or equal to 5 nm at the exit, Section 4.3.3 shows that the separation between aircraft is also above the safety minimum during the whole time within the sector. Finally, a graph consisting of green crosses shows the difference in speed of two consecutive aircraft.

4.4.2 Sector saturation

Deterministic arrivals - Entry control

In this first simulation (Fig. 4-6), we test the endurance of the system when an output restriction lower than the input rate lasts for a time long enough to witness a saturation of the system.

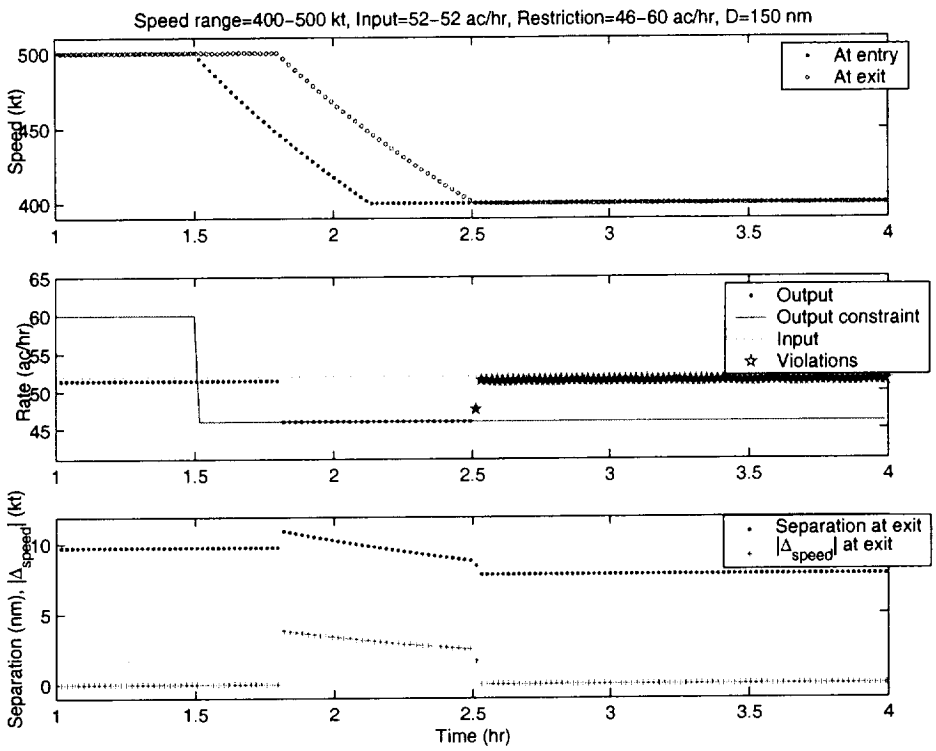

Figure 4-6: Simulation with deterministic scheduled arrivals. A restriction is imposed on the output rate at $t = 1.5$ hr.

The situation is initially at steady-state with 52 aircraft arriving per hour ($\lambda = 52$) at a speed of $v = 500$ kt, thus creating a spacing of $v/\lambda = 9.6$ nm. The output restriction is set to $\mu_r = 60$, thus above the input rate λ (i.e. no restriction is imposed). There is no speed command given to the incoming aircraft.

At $t = 1.5$ hr, the output restriction goes below the input rate at $\mu_r = 46$, triggering the need for speed control of incoming aircraft. Arriving aircraft are slowed down and any new aircraft goes slower than those preceding. This control only impacts the output rate after the time needed for the first impacted aircraft to reach the end of the sector, approximately $t = D/v = 18$ min (our measure of responsiveness). From there on, the output rate matches the output rate constraint until the speed command reaches an unacceptably low level ($v_{min} = 400$ kt). When this level is reached, the new incoming aircraft are only given the command to slow down to v_{min}, in order to maintain spacing. The output μ rate returns to λ (all new aircraft are given the exact same speed when entering, thus their output time spacing remains their input time spacing), and the output restriction is violated.

Deterministic arrivals - Entry and input rate control

One option to avoid violating the restriction is to back-propagate it to the upstream sector and impose a lower input rate at some point in time (see Fig. 4-7): this mimics what is done in the real ATM world. Section 4.3.2 describes the control scheme

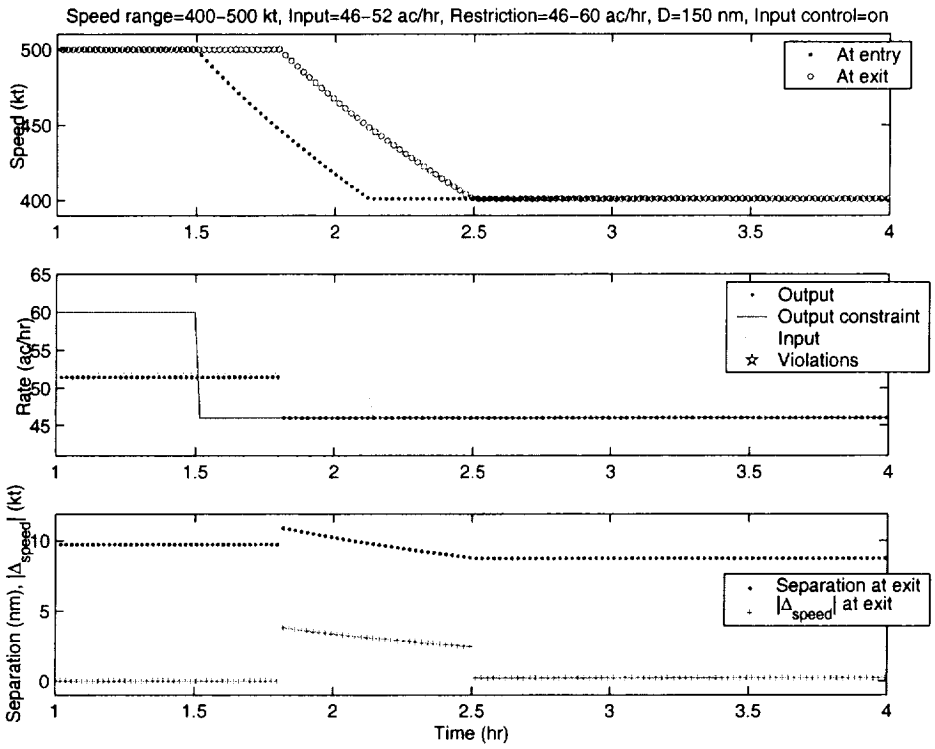

Figure 4-7: Simulation with deterministic scheduled arrivals. A restriction is imposed on the output at $t = 1.5$ hr. Input control is active and lowers the input rate at t$\simeq$ 2.2 hr.

implemented and shown in Fig. 4-7.

Because the input rate exactly matches the output rate, speed control is unnecessary and impossible, thus prohibiting the speed of the flow to build up again. To see the speed command increase, one needs some extra time spacing, provided either by a lower input rate or a higher output rate (the latter is possible when the restriction is lifted).

Randomized arrivals - Entry control

Fig. 4-8 presents a simulation analogous to that of Fig. 4-6, except the arrival process is now randomized. The random variable here is the time between two successive arrivals. This inter-arrival time is normally distributed with a mean equal to $1/\lambda$, with λ appearing on the plot as a dotted green line, and a standard deviation $\varsigma = 5$ s. Approximately 95% of all inter-arrival times occur in $[1/\lambda - 2\varsigma; 1/\lambda + 2\varsigma]$.

The capacity - defined as the number of aircraft passing through the sector and able to match the desired output constraint - is not much impacted by the randomness of the arrivals. Multiple runs of simulations with randomized arrivals have shown that the average capacity remains constant for different values of ς, as long as the randomness does not imply a violation of the minimum separation constraint at the entry.

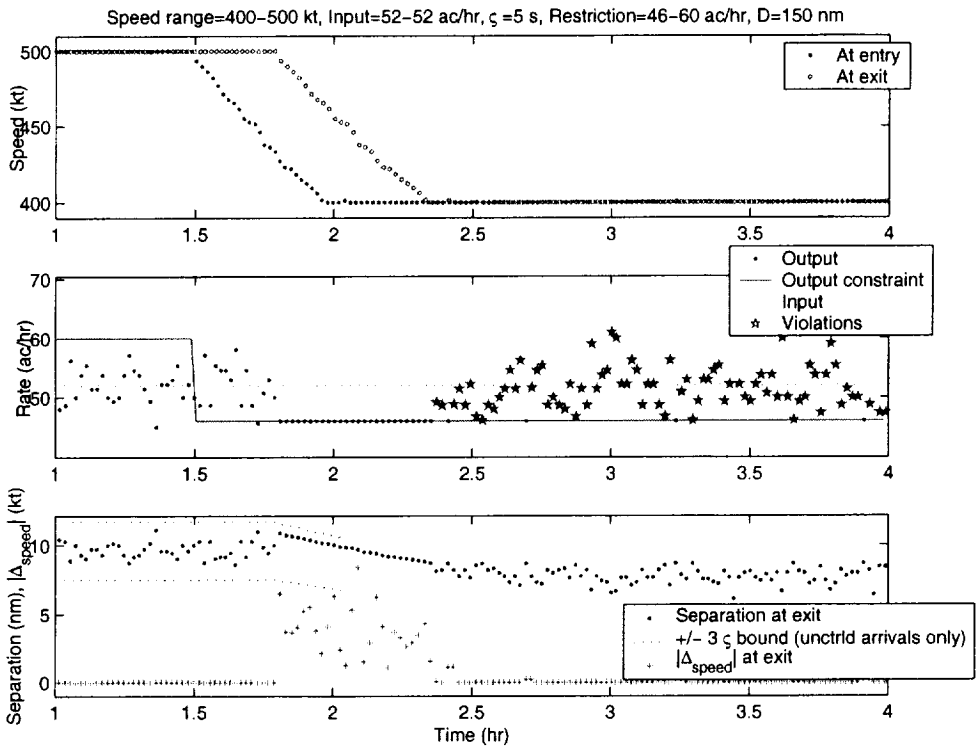

Figure 4-8: Simulation with randomized arrivals. A restriction is imposed on the output at $t = 1.5$ hr.

Deterministic arrivals - Extended control

In the operational environment, an output restriction might be imposed by the downstream sector with short notice. The goal is then to match the desired output rate in the shortest time. To improve the responsiveness of the system (equal to $t = D/v$ in the entry control scheme), we consider controlling the first $100\gamma\%$ of the sector (Fig. 4-2 bottom). It is impossible to control 100% of the sector because this might imply dramatic speed changes close to exit. Furthermore, the assumption of instantaneous speed change does not hold in such a case.

Fig. 4-9 shows a simulation using this particular algorithm, with $100\gamma = 80\%$ of the sector controlled. The responsiveness is improved. Straightforward analysis tells us that the 20% of the sector not under control translates into a delay of $t = (1-\gamma)D/v$ (or approximately 4 min) before the restriction is met. This is better than the result obtained with entry control (18 min).

The speed evolution with time is different. The speed curve at exit from $t \simeq 1.6$ hr to $t \simeq 1.8$ hr has a particular shape (compare Fig. 4-9 with Fig. 4-6). It reflects the speed commands given to the aircraft already in the sector when the restriction is imposed. Once those aircraft are flushed, the usual variation returns.

An interesting property appears when modifying the parameter γ. The capacity of the sector remains unchanged for a wide range of γ. We assume here that the speed commands given to aircraft within the sector at the issuance of the restriction

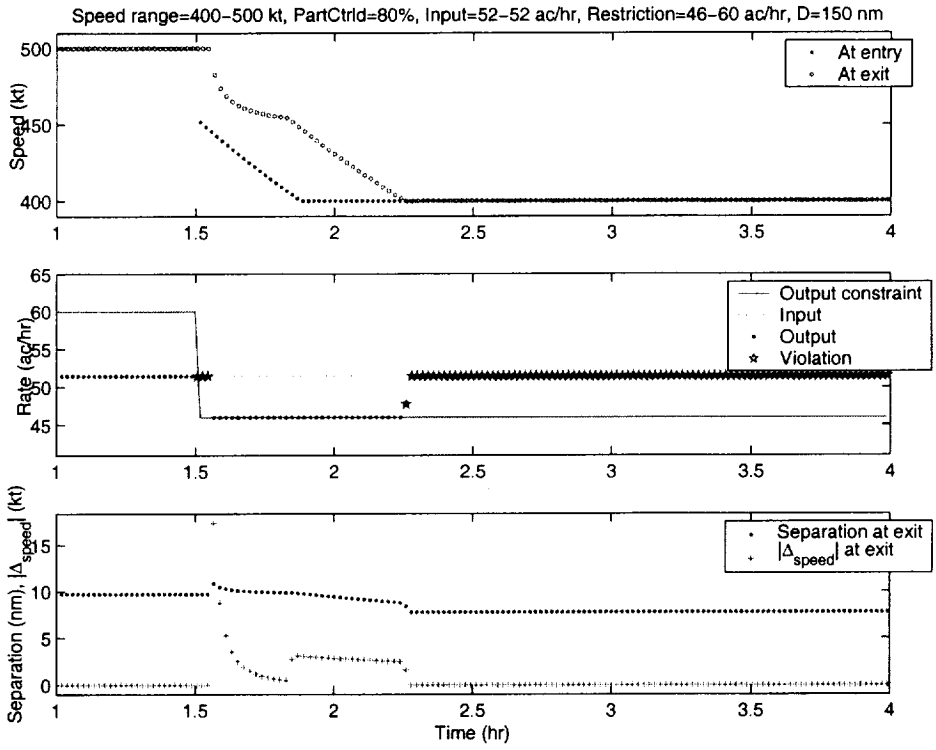

Figure 4-9: Simulation with 80% of the sector controlled. A restriction is imposed on the output at $t = 1.5$ hr.

is in the acceptable range of speed (i.e., greater than v_{min}). Controlling a greater portion of the sector only improves responsiveness. This is of great interest from an Air Traffic Management perspective. An analysis is given in Section 4.5.2.

4.4.3 Temporary restriction

After a restriction has been present for some time, and this restriction has been lifted to a value higher than the input rate, speed commands should be driven back to their original value (here $v = 500$ kt). However, two parameters influence this recovery process: the minimum separation distance between aircraft must be respected as well as the new output rate (Section 4.3.3).

In the following simulations two modes of recovery are identified: one where the output restriction is the limiting factor, and another where the minimum separation distance is.

Fig. 4-10 shows a simulation where the output rate drives this recovery: the speed command is high enough, so that aircraft are time-spaced at the output at the lowest value admissible for the given output rate (here: μ_r=60). Separation remains above the 5 nm limit, and thus does not constitute a hard bound.

Fig. 4-11 shows a simulation where speed commands are given so that the 5 nm spacing is respected throughout the sector. If speed commands were given only based on the possible output rate, this separation would have been violated. Thus, the

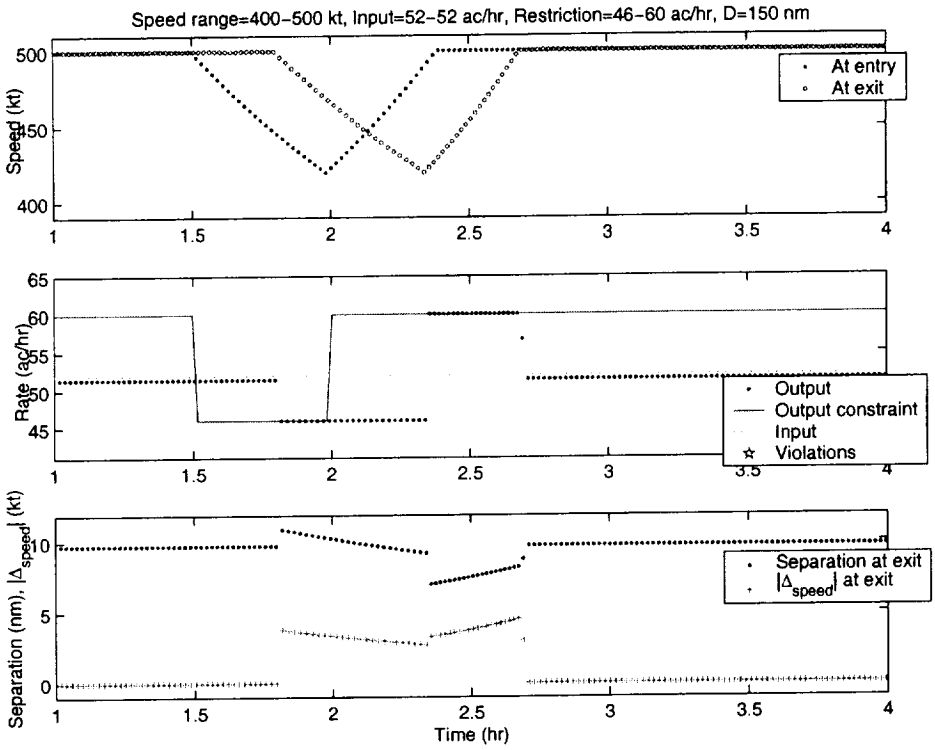

Figure 4-10: Simulation with deterministic scheduled arrivals. A restriction is imposed on the output at $t = 1.5$ hr and returns to 60 ac/hr at $t = 2$ hr.

actual output rate is lower than the maximum allowed.

4.4.4 Finite acceleration

Contrary to the rest of this thesis, we now consider aircraft with a finite acceleration capacity. This simulation will not lead to an analysis and is only meant to provide a ground for comparison with massless aircraft models. We build on the simulation found in Fig. 4-9 that addresses extended control of the sector. The exact same parameters are used, except the acceleration and deceleration that are set at ± 0.4 kt/s. This is an acceptable figure found in Air Traffic Control manuals [31, 13].

For such a value, differences between the purely kinematic and this enhanced model are barely observable (see Fig. 4-12). Noticeably: no loss of separation occur, and the capacity is cut by 10% aircraft (3 out of 32). This decrease of capacity is a direct consequence of the limited acceleration: for an equivalent aircraft in both models, the commanded speed needs to be lower to counterbalance the distance accrued while flying faster than desired during the deceleration phase. Thus, an aircraft takes more of the "speed reserve" and this reserve is exhausted earlier than in the purely kinematic case, yielding a lower capacity.

The restrictions imposed here are not very tough (reduction of only 12% of the capacity), and do not require dramatic speed changes. Further simulations should be run to better understand this problem.

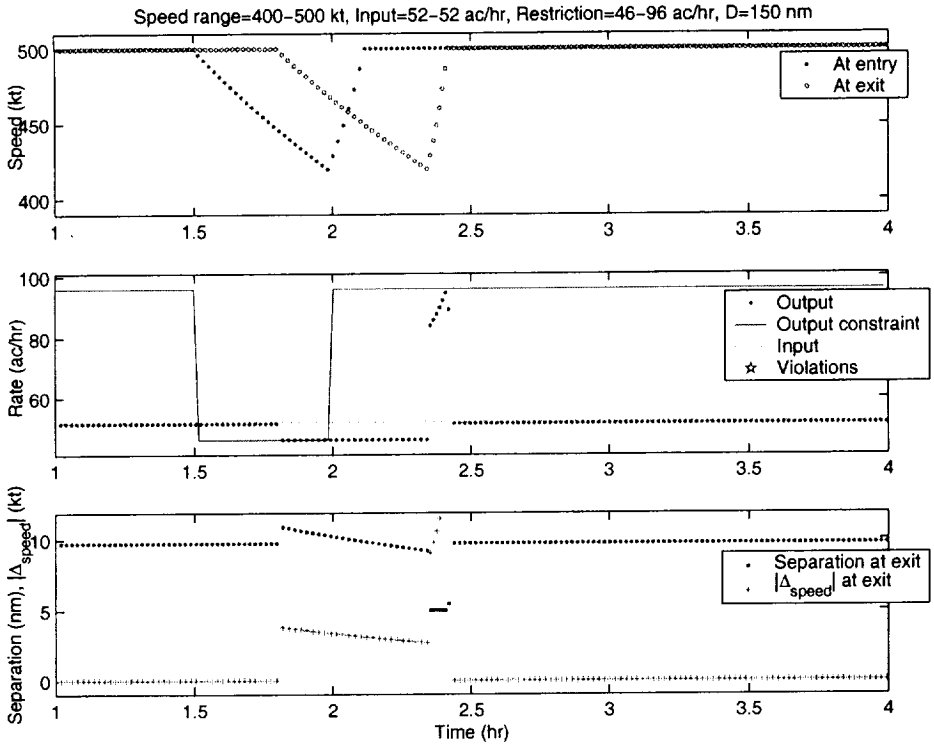

Figure 4-11: Simulation with deterministic scheduled arrivals. A restriction is imposed on the output at $t = 1.5$ hr and returns to 96 ac/hr at $t = 2$ hr.

4.5 Capacity analysis

We defined and simulated three control schemes: speed control in its two variants (entry control and extended control), and path stretching. In this last section, we derive the theoretical capacity of these schemes. We conclude our study with the capacity obtained when speed control and path stretching are successively used.

4.5.1 Entry control

Capacity computation can be achieved in two different ways in the case of speed control. One is to use Eq. (4.6) recursively to compute the speed of the n^{th} aircraft when a restriction μ_r is enforced, with a flow initially flying at v_f. Once v_n is known, capacity is computed by solving $v_n = v_{min}$ for n. Closed-form results are not available, due to the recursive nature of the calculation.

Another way to proceed is to see aircraft as vehicles with scheduled times of entry and exit. Knowing those two times, speed is easily derived knowing the length of the sector. We restrict our analysis to entry control only under deterministic arrivals and extend the result to the extended control case in Section 4.5.2.

The metering constraint μ_r is set at time t. Thus, for all aircraft A_i such that $t_i > t$, the exit time s_i is set so that $s_i - s_{i-1} = 1/\mu_r$. We assume $t = t_0^+$, i.e. the constraint is set when aircraft A_0 enters. The speed command given to A_0 has not

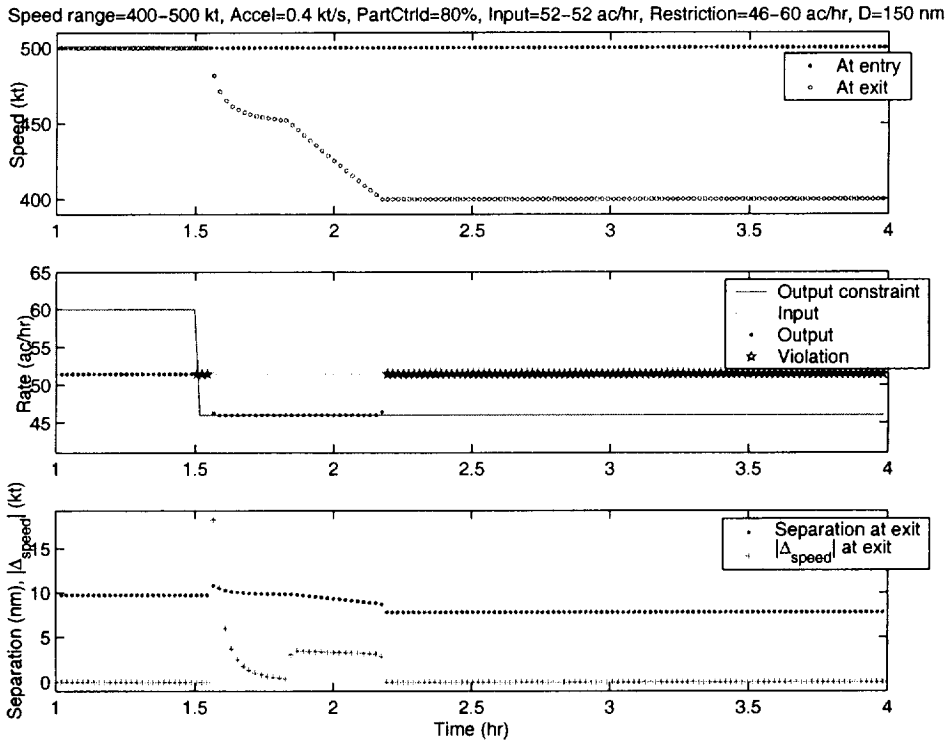

Figure 4-12: Simulation with an enhanced aircraft model. The acceleration is limited to 0.4 kt/s. This plot should be compared with Fig. 4-9 as the same simulation parameters are used: deterministic scheduled arrivals, control over 80% of the sector, restriction imposed on the output at $t = 1.5$ hr and lifted.

taken into account the restriction μ_r. Thus:

$$\begin{aligned} s_0 &= t + \frac{D}{v_0} \\ &= S \\ s_1 &= t + \frac{D}{v_1} \\ &= \frac{1}{\mu_r} + S \\ s_n &= \frac{n}{\mu_r} + S. \end{aligned} \tag{4.27}$$

Also:

$$t_n = \frac{n}{\lambda} + t. \tag{4.28}$$

Combining Eq. (4.27) and Eq. (4.28):

$$v_n = \frac{D}{n\left(\frac{1}{\mu_r} - \frac{1}{\lambda}\right) + \frac{D}{v_f}}. \tag{4.29}$$

Equating Eq. (4.29) with v_{min}, we can solve for n_{VC}, the capacity of the sector obtained with speed control:

$$n_{VC} = \frac{D\left(1 - \frac{v_{min}}{v_f}\right)}{v_{min}\left(\frac{1}{\mu_r} - \frac{1}{\lambda}\right)} \tag{4.30}$$

As expected, the capacity of the sector depends on the length D, the flow speed v_f, the minimum speed v_{min}, and the input and output restriction rates.

4.5.2 Extended control

Section 4.4.2 showed that extended control has the same capacity regardless of γ.

Fig. 4-13 shows a visual proof of that property. The red trajectories are created by aircraft controlled under entry control only. The restriction is issued at t. From there on, entering aircraft are assigned times of exit, separated in accordance with μ_r. Accordingly, speed commands that are expected to respect these schedules are given. This lasts until the minimum speed is reached - the minimum speed is geometrically visualized by a green triangle on the picture.

Black trajectories represent aircraft controlled under the extended law (control over $100\gamma\%$ of the sector). We notice that the trajectories and scheduled times of exit are identical. Only the time of issuance of the restriction t' appears later than for the previous case, which means it is closer to the time when the metering is enforced (already noticed with the faster response). Trajectories are identical except for those which intercept the line representing time t' (i.e. the aircraft already in the sector at time t'). These trajectories have "kinks" in them, resulting from the change of speed given to them at this time. They have the same scheduled times (with another

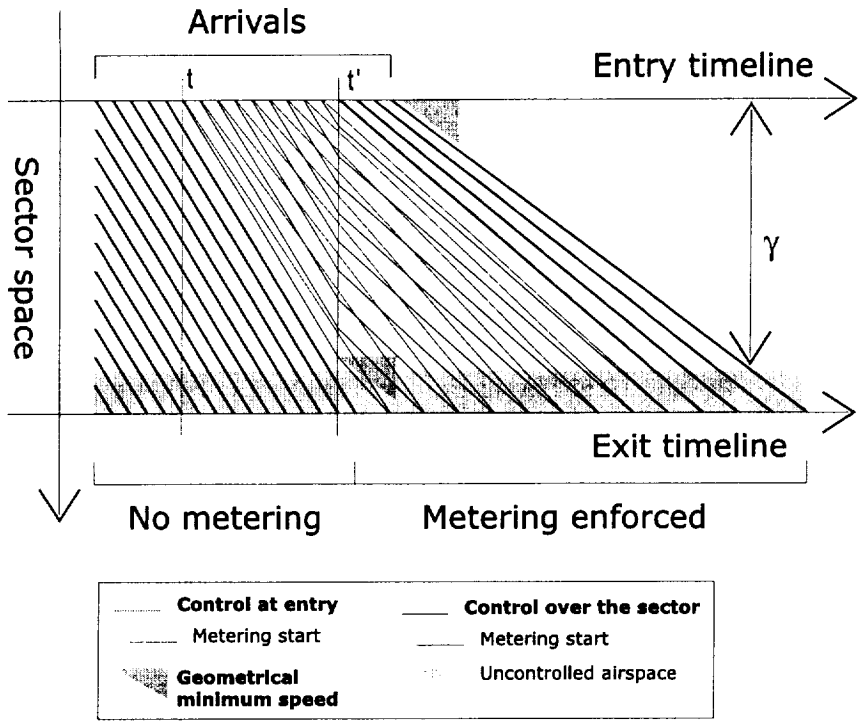

Figure 4-13: Geometrical approach to understand why capacity does not change with the controlled proportion of a sector γ. Shown in black and red, solid lines are the time-space trajectories of aircraft either under single entry control or control over γ of the sector.

time reference, though), and as such do not interfere differently with the trajectories of the aircraft still out of the sector at t'. The evolution after the first aircraft have been flushed away from the sector is identical in both cases, and maximum capacity is reached at the same time, when v_{min} (represented by the triangle) is reached. Thus, both control laws yield the same capacity.

We recall the capacity Eq. (4.30), which still applies for the extended control case:

$$n_{VC} = \frac{D\left(1 - \frac{v_{min}}{v_f}\right)}{v_{min}\left(\frac{1}{\mu_r} - \frac{1}{\lambda}\right)}.$$

4.5.3 Path stretching

The gain in capacity due to path stretching can be computed in a way similar to the previous cases. Theoretically, the maximum length of a two-leg path in the sector with prescribed entry and exit points is $l_{max} = \sqrt{D^2 + w^2}$, where w and D are the width and length of the sector. The minimum length is evidently the straight line, $l_{max} = D$. Given that this trajectory is flown at speed v_f, the apparent speed v^{app} of an aircraft under path stretching control varies in the range:

$$v^{app} \in [v^{app}_{min} = v_f \frac{D}{\sqrt{w^2 + D^2}}, v^{app}_{max} = v_f] \tag{4.31}$$

We can now use Eq. (4.29), and by equating v_n with v_{min}^{app}, we get a capacity for path stretching:

$$n_{PS} = \frac{\sqrt{w^2 + D^2} - D}{v_f \left(\frac{1}{\mu_r} - \frac{1}{\lambda}\right)} \tag{4.32}$$

A noticeable fact about the latter expression is its dependence on $1/v_f$. From a practical perspective, it means that the path stretching "tool" is more efficient with a lower entry speed. It is then logical to think about sequencing both control schemes (speed control and path stretching) to obtain an enhanced capacity.

4.5.4 Sequence of control policies

In this last section, we adopt the following procedure:

- No restriction is initially applied to the sector's outgoing rate.
- When a restriction occurs, entry speed control is enforced. Airplanes start decreasing their speed according to their positions in the flow.
- Airspeed control authority is lost after n_{VC} aircraft. The n_{VC}^{th} aircraft has speed greater than or equal to v_{min}. To transition smoothly to path stretching (at the beginning of which aircraft do not deviate much from the straight line), aircraft under path stretching control are given a speed of v_{min}, avoiding any separation problem.
- Path stretching control authority is lost after n_{PS}.
- If the restriction is lifted before this happens, the recovery process first involves sending every other aircraft on the other side of the sector (see Section 4.3.4). When the apparent speed of the aircraft returns to v_{min}, entry speed control takes over path stretching until a return to normal is effective.

Using this two-scheme procedure, we obtain a sector capacity of:

$$n_{total} = \frac{\sqrt{w^2 + D^2} - D\frac{v_{min}}{v_f}}{v_{min}\left(\frac{1}{\mu_r} - \frac{1}{\lambda}\right)}. \tag{4.33}$$

Chapter 5

Conclusions

This work considers two aspects of en-route airspace operations, in an idealized fashion. Although aircraft are modeled without dynamics, the maneuvers under consideration lead to nice yet meaningful results of stability or performance of control policies.

Intersecting flows of aircraft are the object of Chapter 3. Section 3.2 complements the initial works of Mao [28, 29, 30] on two intersecting aircraft flows and extends his results to the new, more realistic offset maneuver model. Section 3.3 is an analysis of the same model where aircraft use pure heading changes to perform conflict avoidance. In Section 3.4, the problem of divergence of three intersecting flows with decentralized conflict avoidance algorithms is addressed with a centralized, procedure-based control concept. Comparison with flow-dependent control strategies requiring online computations shows competitive performance. Future work on this side of the project should concentrate on extending results of Section 3.3 to aircraft flows intersecting at various angles and with different speeds in each flow.

Aircraft flow buffering and delay back-propagation in the air traffic system are modeled in Chapter 4. Simple considerations show how adequate control of a sector facing input/output imbalance can alleviate the overload of the airspace network by avoiding unnecessary transmission of delays. Compact performance indices bring insight as to what capacity to expect in various models. A natural and necessary extension to that part of the work would be to add the impact of an intersecting flow.

This step would allow the coupling of conflict avoidance and traffic scheduling constraints. It is a natural way to address the recurring question of airspace sector capacity and help in the redesign of the air traffic control system.

Appendix A

Simulations

Figure	Model	D (nm)	Aircraft	Arrival	Maxi
3-2	Offset, 2 flows	100	500	Uniform: [5, 15] nm	7.1 nm
3-5	Hdg. chg., 2 flows	100	200	Constant (5 nm)	2.8 deg
3-6	Hdg. chg., 2 flows	100	200	Uniform: [5, 10] nm	4.5 deg
3-13	Lat. disp., 3 flows	150	105	Constant (5 nm)	100 nm
3-21-top	Lat. disp., 3 flows	150	60	Constant (5 nm)	32 nm
3-21-bottom	Lat. disp., 3 flows	150	60	Constant (5 nm)	23.1 nm

Fig.	Arrival	Speed range	Input	Output	Duration	Control	Dynamics
4-6	Regular	[400,500] kt	52 ac/hr	[46,60] ac/hr	2.5 hr	Entry	Massless
4-7	Regular	[400,500] kt	Ctrld	[46,60] ac/hr	2.5 hr	Entry	Massless
4-8	Normal ($\varsigma = 5$ s)	[400,500] kt	52 ac/hr	[46,60] ac/hr	2.5 hr	Entry	Massless
4-9	Regular	[400,500] kt	52 ac/hr	[46,60] ac/hr	2.5 hr	Extended (80%)	Massless
4-10	Regular	[400,500] kt	52 ac/hr	[46,60] ac/hr	0.5 hr	Entry	Massless
4-11	Regular	[400,500] kt	52 ac/hr	[46,96] ac/hr	0.5 hr	Entry	Massless
4-12	Regular	[400,500] kt	52 ac/hr	[46,60] ac/hr	2.5 hr	Entry	$\pm$0.4 kt/s

Table A.1: Summary of simulations parameters. Top: Intersecting flows of aircraft. (Chapter 3) Bottom: Aircraft buffering. (Chapter 4)

Appendix B

Complementary problem

Section 3.3.3 introduced the eastbound protection zone. This area is used in the stability proof of Section 3.3 to show that it would have contained the projected conflict zone of the southbound aircraft A_j if A_j had not deviated at all (i.e. $\eta = -\pi/2$). For the sake of the argument, the condition to prove here is slightly different: if A_j had only deviated by $\chi/2$ (i.e. $\eta = -\pi/2 - \chi/2$), prove that A_j's projected conflict zone would have been in the eastbound protection zone. This subtlety has been omitted in the stability proof for clarity of exposure. It does not change the proof in any way because the contradiction remains: "A_j could have deviated less".

The mathematical problem is exposed below. Explanations for each steps are given afterwards.

Given

$$0 \leq \delta \leq \frac{1}{2} \tag{B.1}$$

and

$$\chi = \arctan \frac{\delta\sqrt{2-\delta^2}}{1-\delta^2} \tag{B.2}$$

we want to prove that for all

$$\theta \in \left[-\frac{\chi}{2}, \chi\right] \tag{B.3}$$

there exists a

$$\theta_n(\theta) \in [-\chi, \chi] \tag{B.4}$$

such that for all

$$\eta \in \left[-\frac{\pi}{2} - \chi, -\frac{\pi}{2} + \chi\right] \tag{B.5}$$

we have:

$$\Delta_1 \geq 0 \text{ and } \Delta_2 \geq 0 \tag{B.6}$$

with

$$\begin{aligned} \Delta_1 \;=\; & -(\sin(\theta_n)\sin(\eta) + \sin(\theta_n)\cos(\eta) + \cos(\theta_n)\sin(\eta) - \cos(\eta)\cos(\theta_n) + 1 \\ & -\delta\sqrt{2}\sqrt{1 + \sin(\theta_n)\sin(\eta) - \cos(\eta)\cos(\theta_n)})/(\sin(\theta_n) + \sin(\eta)) + (-1 \\ & +\cos(\tfrac{\chi}{2})\sin(\theta) + \cos(\tfrac{\chi}{2})\cos(\theta) - \sin(\tfrac{\chi}{2})\cos(\theta) + \sin(\tfrac{\chi}{2})\sin(\theta) \end{aligned} \tag{B.7}$$

$$+\sqrt{2}\sqrt{-\delta^2\left(\cos(\frac{\chi}{2})\sin(\theta)-\sin(\frac{\chi}{2})\cos(\theta)-1\right)}/(-\cos(\frac{\chi}{2})+\sin(\theta))$$
$$+(\sin(\eta)\sin(\theta)+\sin(\theta)\cos(\eta)+\cos(\theta)\sin(\eta)-\cos(\eta)\cos(\theta)+1$$
$$-\delta\sqrt{2}\sqrt{1+\sin(\eta)\sin(\theta)-\cos(\eta)\cos(\theta)})/(\sin(\theta)+\sin(\eta))$$

and

$$\begin{aligned}\Delta_2 = & -(-1+\cos(\frac{\chi}{2})\sin(\theta)+\cos(\frac{\chi}{2})\cos(\theta)-\sin(\frac{\chi}{2})\cos(\theta)+\sin(\frac{\chi}{2})\sin(\theta) \\ & +\sqrt{2}\sqrt{-\delta^2\left(\cos(\frac{\chi}{2})\sin(\theta)-\sin(\frac{\chi}{2})\cos(\theta)-1\right)}/(-\cos(\frac{\chi}{2})+\sin(\theta)) \\ & -(\sin(\eta)\sin(\theta)+\sin(\theta)\cos(\eta)+\cos(\theta)\sin(\eta)-\cos(\eta)\cos(\theta)+1 \\ & +\delta\sqrt{2}\sqrt{1+\sin(\eta)\sin(\theta)-\cos(\eta)\cos(\theta)})/(\sin(\theta)+\sin(\eta)) \\ & +(\sin(\theta_n)\sin(\eta)+\sin(\theta_n)\cos(\eta)+\cos(\theta_n)\sin(\eta)-\cos(\eta)\cos(\theta_n)+1 \\ & +\delta\sqrt{2}\sqrt{1+\sin(\theta_n)\sin(\eta)-\cos(\eta)\cos(\theta_n)})/(\sin(\theta_n)+\sin(\eta)).\end{aligned} \tag{B.8}$$

Eq. (B.1) states that the control volume has to be sufficiently large to enable conflict avoidance maneuver. In practice, δ is usually in the order of 0.2 or less. Eq. (B.2) recalls the result of Eq. (3.10). A_j has maneuvered so that $\eta = -\pi/2 - \chi/2$: its projected conflict zone intersects the eastbound decision bound for $\theta \in [-\chi/2, \chi]$, yielding Eq. (B.3). Let us consider the "southern edge" of A_j's projected conflict zone (i.e. σ, see Fig. 3-7). We want to show the following lemma.

Lemma: any eastbound aircraft A_i sitting on this southern edge provides a conflict free solution for a newcoming eastbound aircraft A_n sitting on the eastbound decision bound with angle θ_n.

Equivalently, this shows that the southern edge is in the eastbound protection zone. Eq. (B.4), Eq. (B.5), and Eq. (B.6) provide the verification of the lemma. Eq. (B.8) and Eq. (B.9) are both positive if the projected conflict zone of A_n is inside that of A_i.

One difficulty of this mathematical problem arises from the absence of expression for θ_n (Eq. (B.4) only says: "there exists a θ_n"). By curve-fitting, an expression has been found for θ_n and gives a correct θ_n for $\delta < 0.2$. Given the geometric parameter δ and the position of A_i described by θ, θ_n is expressed by:

$$\theta_n = \bar{\theta}\mathbf{M}\bar{\delta}^{\mathbf{T}}, \tag{B.9}$$

where

$$\bar{\theta} = \begin{pmatrix} 1 & \theta & \theta^2 & \theta^3 \end{pmatrix}, \tag{B.10}$$

$$\bar{\delta} = \begin{pmatrix} 1 & \delta & \delta^2 & \delta^3 & \delta^4 \end{pmatrix}, \tag{B.11}$$

$$\mathbf{M} = \begin{pmatrix} -1.731\cdot 10^{-5} & -0.7062 & -0.5177 & -0.8154 & +0.1876 \\ -1.942\cdot 10^{-5} & +1.342\cdot 10^{-3} & -1.019 & -3.399 & +0.6398 \\ +2.824\cdot 10^{-5} & -3.818\cdot 10^{-4} & -1.396\cdot 10^{-2} & -2.905 & -6.633 \\ -1.101\cdot 10^{-4} & +9.107\cdot 10^{-3} & -0.2543 & +2.903 & -17.00 \end{pmatrix}. \tag{B.12}$$

Appendix C

Nomenclature

A_i	=	Eastbound or generic aircraft
A_j	=	Southbound aircraft
A_n	=	Newcoming aircraft
a	=	Radial coordinate of a southbound aircraft
B	=	Additional buffer distance between aircraft
b	=	Radial coordinate of an eastbound aircraft
C	=	Corner point
$\mathbf{c}$	=	Normalized relative speed
D	=	Distance to point with constraints (radius or length sector)
d	=	Lateral displacement amplitude
d_{max}	=	Maximal lateral displacement amplitude
D_{sep}	=	Minimum separation distance between aircraft
E	=	East point
h	=	Aisle width
I	=	Entry point
i	=	Index
J	=	Point on the lateral limit of the sector
j	=	Index
k	=	Index
M	=	Matrix of polynomial coefficients
$\mathbf{m}$	=	Miss distance vector
N	=	North point
n	=	Index
O	=	Intersection or exit point
P	=	Protection zone
$r_.$	=	Time in sector
S	=	South point
$s_.$	=	Exit time
$t_.$	=	Entry time
v	=	Speed

Continued...

W	=	West point
w	=	Sector width
x	=	Cartesian coordinate
y	=	Cartesian coordinate
α	=	Scaled a
β	=	Scaled b
γ	=	Portion of sector under control
δ	=	Scaled D_{sep}
ϵ	=	Distance between two aircraft
$\zeta_{1,2}$	=	Time on a path-stretching leg
η	=	Angular coordinate of a southbound aircraft
θ	=	Angular coordinate of an eastbound aircraft
λ	=	Input rate
μ	=	Output rate
μ_r	=	Desired output rate
ν	=	Scaled v
ξ	=	$\Delta v/v$
ρ	=	Northern edge of the projected conflict zone
σ	=	Southern edge of the projected conflict zone
ς	=	Standard deviation of interarrival times
τ	=	Interarrival time
χ	=	Heading change

Bibliography

[1] Concept definition for Distributed Air/Ground Traffic Management (DAG-TM). Technical report, Advanced Air Transportation Technologies (AATT) Project, September 1999.

[2] Operational evaluation report on ADS-B. Final report, Operational evaluation coordination group, 1999.

[3] J. Andrews. A relative motion analysis of horizontal avoidance. Technical report, MIT, Lincoln Lab, 1978.

[4] A. Bayen, P. Grieder, and C. Tomlin. A control theoretic predictive model for sector-based air traffic flow. *AIAA Guidance, Navigation and Control Conference*, (AIAA-2002-5011), August 2002.

[5] K. Bilimoria. A geometric optimization approach to air conflict resolution. *Proceedings of the AIAA Guidance Navigation and Control Conference and Exhibit, Denver, CO*, (AIAA-2000-4265), August 2000.

[6] K. D. Bilimoria, K. S. Sheth, H. Q. Lee, and S. R. Grabbe. Performance evaluation of airborne separation assurance for free flight. *AIAA Guidance, Navigation and Control Conference*, (AIAA-2000-4269), 2000. Denver, CO.

[7] K.D. Bilimoria and H.Q. Lee. Aircraft conflict resolution with an arrival time constraint. *AIAA Guidance, Navigation and Control Conference*, (AIAA-2002-4444), August 2002.

[8] S. Devasia, M. Heymann, and G. Meyer. Automation procedures for air traffic management: a token-based approach. *Proceedings of the American Control Conference, Anchorage, AK*, May 2002.

[9] S. Devasia and G. Meyer. Automated conflict resolution procedures for air traffic management. *Proc. IEEE Conf. Decision and Control*, Dec. 1999.

[10] D. Dugail, E. Feron, and K. Bilimoria. Conflict-free conformance to en-route flow-rate constraints. *to appear in the AIAA GNC Conference Proceedings, Monterey, CA*, (AIAA-2002-5013), August 2002.

[11] D. Dugail, E. Feron, and K. Bilimoria. Stability of intersecting aircraft flows using heading change maneuver for conflict avoidance. *Proceedings of the American Control Conference, Anchorage, AK*, May 2002.

[12] D. Dugail, Z.-H. Mao, and E. Feron. Stability of intersecting aircraft flows under centralized and decentralized conflict avoidance rules. *Proceedings of the AIAA Conf. on Guidance, Navigation and Control*, 2001.

[13] P. Dumaître. *Contrôle de la circulation aérienne et technique d'utilisation: le contrôleur et les performances-avions en approche.* Ecole Nationale de l'Aviation Civile, 2 edition, 1993.

[14] H. Erzberger and W. Nedell. Design of an automated system for management of arrival traffic. Technical Memorandum TM-102201, NASA, June 1989.

[15] E. Frazzoli, Z.-H. Mao, J.-H. Oh, and E. Feron. Resolution of conflicts involving many aircraft via semidefinite programming. *To appear in AIAA Journal of Guidance, Control and Dynamics*, 2000.

[16] G. Granger, N. Durand, and J.-M. Alliot. Optimal resolution of en-route conflicts. *4th USA/Europe Air Traffic Management RD Seminar*, December 2001.

[17] J. Histon, C. Aigoin, D. Dalahaye, R. J. Hansman, and S. Puechmorel. Introducing structural considerations into complexity metrics. *4th Air Traffic Management R&D Seminar*, December 2001.

[18] J. Histon and R. J. Hansman. Identification of potential air traffic complexity factors through field observations at Boston ATC facilities. Presentation at the JUP quarterly review, January 2001.

[19] J. Hu, M. Prandini, and S. Sastry. Optimal coordinated motions of multiple agents moving on a plane. *SIAM Journal on Control and Optimization*, 2001. Submitted.

[20] I. Hwang and C. Tomlin. Protocol-based conflict resolution for finite information horizon. *Proceedings of the American Control Conference, Anchorage, AK*, May 2002.

[21] H. Idris and R.W. Simpson. New approach to the planning and control of air traffic in the terminal area. *AIAA Conf. on Guidance, Control and Dynamics, Boston, MA*, 1998.

[22] ILOG. *ILOG CPLEX user's guide.* 1999.

[23] J. Krozel and M. Peters. Strategic conflict detection and resolution for free flight. *Proc. IEEE Conf. Decision and Control, San Diego, CA*, December 1997.

[24] J. Krozel, M. Peters, and K. Bilimoria. A decentralized control strategy for distributed air/ground traffic separation. *AIAA Conf. Guidance, Navigation, and Control*, August 2000.

[25] J. Krozel, M. Peters, K. D. Bilimoria, C. Lee, and J. S. B. Mitchell. Syetem performance characteristics of centralized and decentralized air traffic separation strategies. *4th Air Traffic Management R&D Seminar*, December 2001.

[26] J.K. Kuchar and L.C. Yang. A review of conflict detection and resolution modeling methods. *IEEE Transactions on Intelligent Transportation Systems*, 1(4), 2000.

[27] K. C. Lin, A. Sisti, and L. Chow. Study on crowded two-dimensional airspace-self-organized criticality. *AIAA Journal of Aircraft*, 35(2):301–306, March-April 1998.

[28] Z.-H. Mao. Stability and performance of intersecting aircraft flows under decentralized conflict resolution. Master's thesis, MIT, 2000.

[29] Z.-H. Mao, E. Feron, and K. Bilimoria. Stability of intersecting aircraft flows under decentralized conflict avoidance rules. *AIAA Conf. Guidance, Navigation and Control*, August 2000.

[30] Z.-H. Mao, E. Feron, and K. Bilimoria. Stability and performance of intersecting aircraft flows under decentralized conflict avoidance rules. *IEEE Trans. Intelligent Transportation Systems*, 2(2):101–109, 2001.

[31] M. Martin. *Opérations aériennes*, volume 1-2. Ecole Nationale de l'Aviation Civile, 4 edition, 1990.

[32] F. Médioni. *Méthodes d'optimisation pour l'évitement aérien: systèmes centralisés, systèmes embarqués.* PhD thesis, Ecole Polytechnique, 1998.

[33] P. Mishra and G. Pappas. Flying hot potatoes. *Proceedings of the American Control Conference, Anchorage, AK*, May 2002.

[34] K. Nagel, M. Rickert, P. Simon, and M. Pieck. The dynamics of iterated transportation simulations. *TRIannual Symposium on Transportation ANalysis (TRISTAN-III) in San Juan, Puerto Rico*, 1998.

[35] W.P. Niedringhaus. Stream option manager: automated integration of aircraft separation, merging, stream management, and other air traffic control functions. *IEEE Trans. Systems, Man, and Cybernetics*, 25(9):1269–1280, 1995.

[36] L. Pallottino, A. Bicchi, and S. Pancanti. Safety of a decentralized scheme for free-flight ATMS using mixed integer linear programming. In *American Control Conference*, May 2002. Accepted.

[37] L. Pallottino, E. Feron, and A. Bicchi. Conflict resolution problems for air traffic management systems solved with mixed integer programming. *IEEE Transaction on Intelligent Transportation Systems*, 3(1):3–11, March 2002.

[38] R.W. Simpson. *Course Notes for 16.72: Air Traffic Control.* MIT, 1993.

[39] A. Sinha and D. Boone. The anatomy of delays: Complexity and interconnectivity of nas traffic flow. Presentation, The MITRE Corp., February 2001.

[40] T. Weidner and S. Green. Modeling air traffic management automation metering conformance benefits. *AIAA Progress in Astronautics and Aeronautics Series: Air Transportation Systems Engineering*, 193, 2001.

[41] Q. Yang. *A Simulation Laboratory for Evaluation of Dynamic Traffic Management Systems.* PhD thesis, MIT, 1997.

Stability of intersecting aircraft flows using heading change maneuvers for conflict avoidance

Zhi-Hong Mao * David Dugail † Eric Feron ‡ Karl Bilimoria §

December 20, 2002

Abstract

This paper considers two intersecting flows of aircraft that must avoid each other. Considering avoidance maneuvers modeled by instantaneous heading changes, this paper introduces sufficient conditions for a "domino effect" not to occur, whereby one aircraft's conflict avoidance action fails to generate cascaded, diverging conflict avoidance actions. The mathematics involved with the heading change model are considerably more complex than using simpler, previous maneuver models. However, this additional effort is largely compensated by the improved realism of the maneuver model, as well as new insights in the inherent robustness of conflict avoidance maneuver schemes against real or perceived acceptable separation standards. The analytical results are compared with simulations.

1 Introduction

The increase of air traffic over the past decades has resulted in increased air traffic controller workload and more frequent airborne delays. However, better navigation, communication and computing technology has made it possible to conceive new concepts of traffic operations, such as Free Flight, which bear the hope for more efficient handling of airborne traffic.

The development and subsequent implementation of any new air traffic management concept of operations requires one to study in-depth the mechanisms by which airplanes are able to maintain separation from other airplanes at any time and in a predictable fashion. Several recent efforts have aimed at proposing solutions to automate aircraft separation by issuing required trajectories to airborne aircraft, either through centralized

*Harvard-MIT Division of Health Sciences and Technology, Massachusetts Institute of Technology, Cambridge, MA 02139. maozh@mit.edu

†Department of Aeronautics and Astronautics, Massachusetts Institute of Technology, Cambridge, MA 02139. dugail@alum.mit.edu

‡Room 33-213, Laboratory for Information and Decision Systems, Department of Aeronautics and Astronautics, Massachusetts Institute of Technology, Cambridge, MA 02139. feron@mit.edu Author to whom all correspondence should be addressed

§NASA Ames Research Center, Moffett Field, CA 94035. kbilimoria@mail.arc.nasa.gov

decision-making schemes or decentralized mechanisms. These papers often propose sensible and technologically advanced schemes (relying in particular on on-line optimization algorithms) [4, 5, 7, 9, 14].

Other efforts have focused more on analyzing existing control schemes, with the hope of extracting essential features of control mechanisms that are able to guarantee aircraft separation under usual traffic flow patterns [3, 6, 12, 13]. This paper follows this approach, by analyzing a specific conflict resolution scheme under a class of aircraft traffic flow patterns. The aim of this paper is to demonstrate that, under certain conditions, such conflict resolution schemes are *stable*, that is, they do not induce arbitrarily large avoidance maneuvers. In [11], a conflict resolution scheme involving *instantaneous offset maneuvers* and *sequential decision making* was applied to two crossing flows of aircraft and the stability of the resulting closed-loop system was analyzed. It was shown that this scenario resulted in a *stable* behavior, assuming aircraft all have the same velocity. In our context, stability means that aircraft conflict avoidance maneuvers remain bounded.

This paper extends the results of [11] by considering instantaneous heading changes as conflict resolution maneuvers. Indeed, the instantaneous offset maneuver scheme of [11] is not physically realistic, although we believe it provides significant insight. On the contrary, heading change maneuvers stand much closer to reality in terms of flyability and in terms of implementability using current air traffic control procedures.

The introduction of heading change maneuvers instead of instantaneous offset maneuvers does not change many of our conclusions: We show in this paper that under mild technical conditions closed-loop stability of two intersecting flows of aircraft under decentralized, sequential conflict resolution schemes. This result comes, however, at the cost of considerably more complex mathematical manipulations, provided in this paper. In addition, we provide several new insights about the relative theoretical merits of conflict resolution using heading changes vs. offset maneuvers. In particular, we show that heading change maneuvers are often inherently more robust to traffic uncertainties and perceived safe separation minima when several aircraft are involved.

2 System description

The scenario under consideration is shown in Fig. 1. Two flows of aircraft, oriented at a given angle $\theta \in (0, \pi)$ relative to each other, feed aircraft into a circular sector (control volume) with radius R along two airways that intersect at the center O of the conflict area. All aircraft are assumed to have the same speed v and are assumed to be originally all aligned and separated along either one of the airways. As they enter the sector, they perform a corrective maneuver aimed at avoiding other aircraft already present in this sector.

To simplify the analysis of aircraft flows and to derive analytical results, we conducted our work in two dimensions. This framework is justified in the real-world by various considerations, such as

- Airspace representation to the controller is on a radar screen, thus in two dimensions.

- The vertical en-route structure should be modified as a last resort solution only.
- Inefficiencies arise from fuel burn used to perform altitude changes.
- Passenger comfort is disrupted when the aircraft performs climbs or descents.

Aircraft trajectories are assumed to be piecewise linear; thus we assume heading changes are instantaneous. Flows 1 and 2 enter the sector at points E_1 and E_2, respectively. Upon entering the sector, aircraft maneuver by finding the minimum heading change to avoid any conflict with aircraft already present in the sector; by assumption, no attention is paid either to aircraft that have not entered the sector yet or have already left. We assume a heading change is the only maneuver an aircraft can perform; thus after maneuvering, aircraft move along straight lines as defined by their original (and only) heading change, and become moving obstacles for aircraft entering the sector after them. This conflict resolution scheme can therefore be interpreted as a First-Come First-Serve conflict resolution scheme.

The idea of working with a fixed sector matches with the present mode of operation of the air traffic control system, and this idea has been used for mathematical analyses in [2]. The sequential control scheme of First-Come First-Serve (in which the aircraft conflict resolution decision is made at the entry point of a sector) also matches loosely with the current air traffic control practice within a sector: Controllers pay great attention to incoming aircraft and their impact on the sector when the aircraft get close to the boundary of the sector; controllers often establish communications with an aircraft before the aircraft physically enters the sector - in such a way, control can be issued in time; additionally, control is often transferred to a downstream controller before the aircraft has reached the exit boundary of the sector [6]. A reliable implementation of such sequential conflict resolution is described in [1].

A conflict is declared if the miss distance between two aircraft is less than a given separation distance D_{sep}. This separation distance currently arises from radar resolution limits and is chosen to be $D_{\text{sep}} = 5$ nm (nautical miles). Assume a 2.5 nm-radius safety zone is attached to each aircraft (note that the size of the aircraft drawn in all figures is considerably exaggerated): The 5 nm separation standard is thus violated if two of these circular zones intersect.

In addition to the usual Cartesian coordinate system, two systems of polar coordinates are used for the two aircraft flows, as shown in Fig. 1. The position of an aircraft from flow 1 in the sector is given by the polar coordinates (s, ϕ), where s is the distance between E_1 (the entry point of Flow 1 into the sector) and the aircraft, and ϕ is the heading change angle. $\phi > 0$ corresponds to a clockwise heading change, i.e., a turning to the right of the aircraft, while $\phi < 0$ represents a counterclockwise heading change or a turning to the left of the aircraft. Likewise the polar coordinates of aircraft from flow 2 are noted (r, η).

3 Simulations

Simulations of the above system have been performed using Matlab. The purpose of these simulations is to obtain a qualitative idea of the behaviors that do emerge from

the proposed conflict resolution scheme under different conditions. Examples of both stable and unstable aircraft flows have been found. A general theoretical analysis will be developed in the next section.

For comparison purposes, the encounter angle of the crossing aircraft flows is set to be the same for all simulations: $\theta = \frac{\pi}{2}$. The speed of each aircraft is 400 kt, and $D_{\mathbf{sep}}$ is assumed to be 5 nm. Aircraft enter the sector at regular or random time intervals. For better appreciation of the aircraft flow patterns, different symbols are used to represent aircraft from different flows in the simulation plots: Simple circles are used for southbound aircraft, and circles with aircraft figures in them are used for eastbound aircraft.

Two illustrative simulations for $R = 80$ nm are shown in Fig. 2. Fig. 2 (top) shows a simulation involving aircraft entering at regular time intervals with 250 aircraft in each flow. The aircraft are entering the sector spaced exactly by 5 nm. The resulting pattern obtained by simulation is periodic and bounded. Fig. 2 (bottom) shows the conflict resolution process resulting from a random aircraft arrival process: The spacings between two consecutive aircraft in the southbound or eastbound flows are uniformly distributed over the interval $[5, 10]$ nm. The simulation involved 250 aircraft in each flow. The population of heading change commands shown on the distribution plot remains bounded although the maximum angular deviation is larger.

The next simulation shows an example where the sequential conflict resolution with heading change maneuvers fails to maintain stability. Fig. 3 (top) presents a snapshot of the traffic flow taken during the conflict resolution process. The sector radius is $R = 20$ nm, and the aircraft in a flow are uniformly spaced by 5 nm. The resulting pattern of aircraft flow does not show clear periodicity as compared to Fig. 2 (top). It is also shown in Fig. 3 (top) that some maneuvered southbound aircraft are not able to avoid conflicts with the eastbound aircraft. Interestingly, however, under the same initial conditions, large but bounded offset maneuvers can successfully handle the traffic (see the bottom picture of Fig. 3). An offset maneuver is modeled as an idealized maneuver of instantaneous lateral position change of an aircraft (for more details see [10, 11]). Compared with offset maneuvers, our simulations indicate that heading change maneuvers can encounter more difficulties during conflict resolution for some extreme conditions such as R being too small or θ being either too small or too big.

The last simulation shows heading change maneuvers can also be more robust to traffic uncertainties and variations of perceived safe separation minima from aircraft to aircraft. This is illustrated by a simulation in which the separation minimum $D_{\mathbf{sep}}$ varies from one aircraft to the next as follows: $D_{\mathbf{sep}}(k) = D_{\mathbf{sep},0} + \epsilon(1 - \frac{1}{k})$, where ϵ is a small positive number and k indicates the kth aircraft entering the sector. In the simulation, R and ϵ are set to be 40 nm and 0.5 nm, respectively. Fig. 4 presents the results of conflict resolution for two compact aircraft flows using both offset maneuvers (top picture) and heading change maneuvers (bottom picture). The top picture shows obvious divergence of aircraft offsets, while the bottom picture shows periodic and bounded aircraft heading changes. We will return to this question in the next section.

4 Stability of intersecting flows of aircraft under heading change maneuvers

Motivated by these simulations, we now proceed with providing sufficient conditions for heading changes generated by conflict avoidance maneuvers to remain bounded.

Coming up with these sufficient conditions requires significant mathematical efforts, which justify the development of a few intermediate results. We first derive conditions on the polar coordinates for two aircraft in two different flows not to conflict with each other. We then point our attention to the notion of "projected conflict zone" and "protected safety zone", which delineate conditions under which one aircraft in a given flow may be able to take advantage of the path followed by a previous aircraft in the same flow to automatically generate a conflict-free path. Armed with these concepts, we then provide sufficient conditions for the existence of bounded conflict-free heading change maneuvers for all aircraft and at any time.

4.1 Conditions for a pair of aircraft to follow conflict-free trajectories

Consider two aircraft flows (1 and 2), oriented at an angle θ relative to each other, entering a circular sector centered around O with radius R. The situation is depicted in Fig. 5.

The conditions for a pair of aircraft to follow conflict-free trajectories are summarized in the proposition below:

Proposition 1: Consider a pair of aircraft from flow 1 and flow 2 with polar coordinates (s, ϕ) and (r, η), respectively, and assume that $\theta + \eta - \phi$ is not equal to 0 nor π. Then in order for the two aircraft to follow conflict-free trajectories, their polar coordinates must satisfy either

$$r \leq R_{\text{inner}} \equiv \frac{2R \sin\frac{\theta}{2} \sin\frac{\eta+\phi}{2} - D_{\text{sep}}}{\cos\frac{\theta+\eta-\phi}{2}} + s \tag{1}$$

$$\text{or} \quad r \geq R_{\text{outer}} \equiv \frac{2R \sin\frac{\theta}{2} \sin\frac{\eta+\phi}{2} + D_{\text{sep}}}{\cos\frac{\theta+\eta-\phi}{2}} + s. \tag{2}$$

Proof: The proof is based on the geometric relations shown in Fig. 5. We imagine that the aircraft from flow 1 (we call it aircraft 1) projects a linear, slab-shaped "shadow" of width D_{sep}, centered around the aircraft and aligned with the relative velocity vector $\mathbf{v}_2 - \mathbf{v}_1$, where $\mathbf{v}_1$ and $\mathbf{v}_2$ represent the velocity vectors of the two aircraft, respectively. This shadow is oriented at the angle

$$\beta = \frac{\pi}{2} - \frac{\theta + \eta - \phi}{2} \tag{3}$$

relative to the velocity vectors $\mathbf{v}_1$ or $\mathbf{v}_2$. Consider a safety zone of radius $D_{\text{sep}}/2$ centered around each aircraft. For the aircraft from flow 2 (we call it aircraft 2) to avoid any conflict, its circular safety zone must not intersect the "shadow" projected from the aircraft 1.

As shown in Fig. 5, E_1 and E_2 represent the points from which the two aircraft enter the sector. Let $d(X,Y)$ denote the distance between points X and Y, e.g., $d(E_1,O) = d(E_2,O) = R$. Then

$$d(E_1,E_2) = 2R\sin\frac{\theta}{2}. \tag{4}$$

Let θ' be the angle between the new flying directions of the two aircraft after completing their maneuver, and let O' be the intersecting point of their new trajectories. We can derive

$$\theta' = \theta + \eta - \phi. \tag{5}$$

Let U denote the position of aircraft 1. Point C in Fig. 5 is the position of aircraft 2 for which a collision will occur: The circular safety zone of aircraft 2 is fully covered by the projected shadow of aircraft 1, implying that the miss distance between aircraft 1 and 2 would be zero. Obviously $d(O',U) = d(O',C)$. Points B and F are two positions at which the safety zone of aircraft 2 is tangent to the projected shadow of aircraft 1. We can derive

$$d(B,C) = d(F,C) = \frac{D_{\text{sep}}}{\cos\frac{\theta'}{2}} = \frac{D_{\text{sep}}}{\cos\frac{\theta+\eta-\phi}{2}}. \tag{6}$$

From the previous argument, we know that, in order for aircraft 2 to avoid conflicting with aircraft 1, r should satisfy either

$$r \le R_{\text{inner}} \equiv d(E_2,B) \tag{7}$$

$$\text{or} \quad r \ge R_{\text{outer}} \equiv d(E_2,F). \tag{8}$$

Note that

$$R_{\text{inner}} = d(E_2,C) - d(B,C) \ \text{ and } \ R_{\text{outer}} = d(E_2,C) + d(F,C). \tag{9}$$

We now derive the expression for $d(E_2,C)$. Draw a line passing through E_1 parallel to the line UC. Assume that this line intersects line E_2O' at C'. Since $d(O',U)$ is equal to $d(O',C)$ and UC is parallel with E_2C', we have $d(C',C) = d(E_1,U) = s$ and further

$$d(E_2,C) = d(E_2,C') + s.$$

We need to find out the expression for $d(E_2,C')$. Denote α the angle between E_1E_2 and E_1C'. It is easily seen that

$$\alpha = \frac{\eta+\phi}{2}. \tag{10}$$

Then using standard triangle geometry relations, we have

$$\frac{d(E_2,C')}{\sin\alpha} = \frac{d(E_1,E_2)}{\sin\beta}.$$

According to (3), (4), and (10), we have

$$d(E_2,C') = \frac{2R\sin\frac{\theta}{2}\sin\frac{\eta+\phi}{2}}{\cos\frac{\theta+\eta-\phi}{2}}.$$

So we get

$$d(E_2, C) = d(E_2, C') + s = \frac{2R \sin\frac{\theta}{2} \sin\frac{\eta+\phi}{2}}{\cos\frac{\theta+\eta-\phi}{2}} + s. \tag{11}$$

Bringing (7), (8), (9), and (11) together completes the proof. **Q.E.D.**

Note that Proposition 1 excludes the two following special cases: $\theta + \eta - \phi = 0$ and $\theta + \eta - \phi = \pi$. The case of $\theta + \eta - \phi = 0$ corresponds to a situation where the two aircraft are flying along parallel trajectories. In this case there is no conflict between the two aircraft for any r and s, provided that there is no initial conflict between them. The case of $\theta + \eta - \phi = \pi$ corresponds to a scenario in which the two aircraft are heading toward each other along a straight line - therefore a conflict can not be avoided.

4.2 Projected conflict zone

For a given aircraft that has already maneuvered, we define its *projected conflict zone* as the locus of possible aircraft positions of the other flow resulting into a conflict. This projected conflict zone is sketched in Fig. 6. It is worth noting that this locus changes with the aircraft heading and its position.

Based on Proposition 1, we can write an analytic expression for the projected conflict zone of an aircraft. Without loss of generality, consider an aircraft from flow 1 with polar coordinates (s, ϕ). Its projected conflict zone is then the following set of positions of aircraft from flow 2:

$$\{(r, \eta) \mid R_{\text{inner}}(s, \phi, \eta) < r < R_{\text{outer}}(s, \phi, \eta), -\chi \leq \eta \leq \chi\}, \tag{12}$$

where

$$R_{\text{inner}}(s, \phi, \eta) = \frac{2R \sin\frac{\theta}{2} \sin\frac{\eta+\phi}{2} - D_{\text{sep}}}{\cos\frac{\theta+\eta-\phi}{2}} + s, \tag{13}$$

$$R_{\text{outer}}(s, \phi, \eta) = \frac{2R \sin\frac{\theta}{2} \sin\frac{\eta+\phi}{2} + D_{\text{sep}}}{\cos\frac{\theta+\eta-\phi}{2}} + s, \tag{14}$$

and χ is the decision bound, i.e., a still unknown upper bound for the magnitude of heading changes of all aircraft.

The maximum allowed heading change for aircraft is restricted by several factors, such as the size and shape of a sector, the spatial distribution of airways, and physical ranges of aircraft performance. In the simplified air traffic model discussed in this paper, the magnitude of aircraft heading changes is constrained by the aircraft flow geometry and aircraft conflict resolution rules. Under the model assumptions, an aircraft considers possible conflicts with aircraft within the sector only, and this aircraft performs only one maneuver. For such reason, the heading change of an aircraft must be kept from causing a possible collision with another aircraft at a location where the latter aircraft has not yet entered the sector and has not yet gotten the chance to make a maneuver to avoid

the conflict (refer to the top picture of Fig. 7). Therefore, the magnitude of any heading change should be no greater than

$$\frac{\pi}{2} - \frac{\theta}{2} - \arcsin \frac{D_{\text{sep}}}{2R \sin \frac{\theta}{2}}. \tag{15}$$

In addition, the maximum heading change should also be less than

$$\frac{\theta}{2}. \tag{16}$$

Otherwise, the conflict resolution could possibly result in parallel flows, which are not able to cross each other (see the bottom picture of Fig. 7).

For the above range of aircraft heading changes, R_{inner} and R_{outer} have the following properties, which we will use later in the proofs of Proposition 3 and the theorem.

Proposition 2: Assume that $|\phi|$ and $|\eta|$ are bounded above by (15) and (16). Then both $R_{\text{inner}}(s, \phi, \eta)$ and $R_{\text{outer}}(s, \phi, \eta)$ are strictly monotone increasing functions of ϕ and η.

Proof: The proof consists of four parts.

Part 1: "R_{inner} is a strictly monotone increasing function of ϕ." To prove this, we show $\frac{\partial R_{\text{inner}}}{\partial \phi} > 0$.

$$\begin{aligned}
\frac{\partial R_{\text{inner}}}{\partial \phi} &= \frac{\partial (2R \sin \frac{\theta}{2} \sin \frac{\eta+\phi}{2} - D_{\text{sep}})}{\partial \phi} \frac{1}{\cos \frac{\theta+\eta-\phi}{2}} + \\
&\quad (2R \sin \frac{\theta}{2} \sin \frac{\eta+\phi}{2} - D_{\text{sep}}) \frac{\partial (\frac{1}{\cos \frac{\theta+\eta-\phi}{2}})}{\partial \phi} + \frac{\partial s}{\partial \phi} \\
&= \frac{R \sin \frac{\theta}{2} \cos \frac{\eta+\phi}{2}}{\cos \frac{\theta+\eta-\phi}{2}} - \frac{R \sin \frac{\theta}{2} \sin \frac{\eta+\phi}{2} - \frac{1}{2} D_{\text{sep}}}{(\cos \frac{\theta+\eta-\phi}{2})^2} \sin \frac{\theta+\eta-\phi}{2} \\
&= \frac{R \sin \frac{\theta}{2} (\cos \frac{\eta+\phi}{2} \cos \frac{\theta+\eta-\phi}{2} - \sin \frac{\eta+\phi}{2} \sin \frac{\theta+\eta-\phi}{2})}{(\cos \frac{\theta+\eta-\phi}{2})^2} + \frac{\frac{1}{2} D_{\text{sep}} \sin \frac{\theta+\eta-\phi}{2}}{(\cos \frac{\theta+\eta-\phi}{2})^2} \\
&= \frac{R \sin \frac{\theta}{2} \cos (\frac{\eta+\phi}{2} + \frac{\theta+\eta-\phi}{2})}{(\cos \frac{\theta+\eta-\phi}{2})^2} + \frac{\frac{1}{2} D_{\text{sep}} \sin \frac{\theta+\eta-\phi}{2}}{(\cos \frac{\theta+\eta-\phi}{2})^2} \\
&= \frac{R \sin \frac{\theta}{2} \cos (\frac{\theta}{2} + \eta) + \frac{1}{2} D_{\text{sep}} \sin \frac{\theta+\eta-\phi}{2}}{(\cos \frac{\theta+\eta-\phi}{2})^2}.
\end{aligned} \tag{17}$$

It is implied from (15) and (16) that $-\frac{\theta}{2} < \phi < \frac{\theta}{2}$, $-\frac{\theta}{2} < \eta < \frac{\theta}{2}$, $-\frac{\pi}{2} + \frac{\theta}{2} < \phi < \frac{\pi}{2} - \frac{\theta}{2}$, and $-\frac{\pi}{2} + \frac{\theta}{2} < \eta < \frac{\pi}{2} - \frac{\theta}{2}$. And due to $\theta \in (0, \pi)$, we have $0 < \frac{\theta+\eta-\phi}{2} < \frac{\pi}{2}$ and $0 < \frac{\theta}{2} + \eta < \frac{\pi}{2}$. Therefore, $\sin \frac{\theta}{2} > 0$, $\cos (\frac{\theta}{2} + \eta) > 0$, $\sin \frac{\theta+\eta-\phi}{2} > 0$, and $\cos \frac{\theta+\eta-\phi}{2} > 0$. So we have $\frac{\partial R_{\text{inner}}}{\partial \phi} > 0$, according to (17).

Part 2: "R_{outer} is a strictly monotone increasing function of ϕ." To prove this, we show $\frac{\partial R_{\text{outer}}}{\partial \phi} > 0$. Like in Part 1, we may derive

$$\frac{\partial R_{\text{outer}}}{\partial \phi} = \frac{R \sin\frac{\theta}{2} \cos(\frac{\theta}{2}+\eta) - \frac{1}{2} D_{\text{sep}} \sin\frac{\theta+\eta-\phi}{2}}{(\cos\frac{\theta+\eta-\phi}{2})^2}. \tag{18}$$

Next we show $\cos(\frac{\theta}{2}+\eta) - \frac{D_{\text{sep}}}{2R\sin\frac{\theta}{2}} \sin\frac{\theta+\eta-\phi}{2} > 0$. Note that

$$\begin{aligned}
\eta \le \frac{\pi}{2} - \frac{\theta}{2} - \arcsin\frac{D_{\text{sep}}}{2R\sin\frac{\theta}{2}} \quad &\Rightarrow \\
\frac{\pi}{2} - \frac{\theta}{2} - \eta \ge \arcsin\frac{D_{\text{sep}}}{2R\sin\frac{\theta}{2}} \quad &\Rightarrow \\
\sin(\frac{\pi}{2} - \frac{\theta}{2} - \eta) \ge \frac{D_{\text{sep}}}{2R\sin\frac{\theta}{2}} \quad &\Rightarrow \\
\cos(\frac{\theta}{2}+\eta) \ge \frac{D_{\text{sep}}}{2R\sin\frac{\theta}{2}} \quad &\Rightarrow \\
\cos(\frac{\theta}{2}+\eta) > \frac{D_{\text{sep}}}{2R\sin\frac{\theta}{2}} \sin\frac{\theta+\eta-\phi}{2}.&
\end{aligned}$$

Therefore, $\cos(\frac{\theta}{2}+\eta) - \frac{D_{\text{sep}}}{2R\sin\frac{\theta}{2}} \sin\frac{\theta+\eta-\phi}{2} > 0$ and thus $\frac{\partial R_{\text{outer}}}{\partial \phi} > 0$.

Part 3: "R_{outer} is a strictly monotone increasing function of η." It can be tested that both $\frac{1}{\cos\frac{\theta+\eta-\phi}{2}}$ and $2R\sin\frac{\theta}{2}\sin\frac{\eta+\phi}{2} + D_{\text{sep}}$ are greater than 0 and are strictly monotone increasing functions of η, which allows us to conclude.

Part 4: "R_{inner} is a strictly monotone increasing function of η." To prove this, we show $\frac{\partial R_{\text{inner}}}{\partial \eta} > 0$. Like in Part 1, we may derive

$$\frac{\partial R_{\text{inner}}}{\partial \eta} = \frac{R \sin\frac{\theta}{2} \cos(\frac{\theta}{2}-\phi) - \frac{1}{2} D_{\text{sep}} \sin\frac{\theta+\eta-\phi}{2}}{(\cos\frac{\theta+\eta-\phi}{2})^2}. \tag{19}$$

Like in Part 2, we show $\cos(\frac{\theta}{2}-\phi) - \frac{D_{\text{sep}}}{2R\sin\frac{\theta}{2}} \sin\frac{\theta+\eta-\phi}{2} > 0$. Note that

$$\begin{aligned}
-\phi \le \frac{\pi}{2} - \frac{\theta}{2} - \arcsin\frac{D_{\text{sep}}}{2R\sin\frac{\theta}{2}} \quad &\Rightarrow \\
\frac{\pi}{2} - \frac{\theta}{2} + \phi \ge \arcsin\frac{D_{\text{sep}}}{2R\sin\frac{\theta}{2}} \quad &\Rightarrow \\
\sin(\frac{\pi}{2} - \frac{\theta}{2} + \phi) \ge \frac{D_{\text{sep}}}{2R\sin\frac{\theta}{2}} \quad &\Rightarrow \\
\cos(\frac{\theta}{2} - \phi) \ge \frac{D_{\text{sep}}}{2R\sin\frac{\theta}{2}} \quad &\Rightarrow \\
\cos(\frac{\theta}{2} - \phi) > \frac{D_{\text{sep}}}{2R\sin\frac{\theta}{2}} \sin\frac{\theta+\eta-\phi}{2}.&
\end{aligned}$$

Therefore, $\cos(\frac{\theta}{2} - \phi) - \frac{D_{sep}}{2R\sin\frac{\theta}{2}} \sin\frac{\theta+\eta-\phi}{2} > 0$ and thus $\frac{\partial R_{\text{inner}}}{\partial \eta} > 0$. **Q.E.D.**

4.3 Protected safety zone

Equipped with the concept of projected conflict zone, we now introduce the concept of *protected safety zone*. Assume that an aircraft A_f from flow 1 enters the sector following aircraft A_p (also from flow 1), which has already maneuvered so as to find a conflict-free trajectory. By definition, the projected conflict zone of A_p does not contain any aircraft from flow 2. We then ask the question: Can A_f take advantage of the fact that A_p is on a conflict-free trajectory to generate A_f's own conflict-free trajectory? This would be the case if A_f could maneuver so as to include its own projected conflict zone within that of A_p, as illustrated in Fig. 6. It turns out that under certain conditions on the problem parameters (sector size and minimum separation distance standard) there is a range of heading changes of A_f for which the projected conflict zone of A_f is indeed *included* in the projected conflict zone of A_p. We will define this range of heading changes of A_f as the *protected safety zone* of A_f with respect to A_p.

We now write an analytic expression for the protected safety zone. Let the pre-maneuver candidate polar coordinates of aircraft A_f be (s_f, ϕ) and the post-maneuver coordinates of A_p be (s_p, ϕ_p).

From the above definition, the protected safety zone of A_f with respect to A_p, denoted $\Phi_f(s_p, \phi_p, \chi)$ or Φ_f as shorthand, is the set of all headings ϕ satisfying

$$\begin{aligned} & R_{\text{inner}}(s_f, \phi, \eta) \geq R_{\text{inner}}(s_p, \phi_p, \eta) \\ \text{and} \quad & R_{\text{outer}}(s_f, \phi, \eta) \leq R_{\text{outer}}(s_p, \phi_p, \eta) \\ \text{for all} \quad & -\chi \leq \eta \leq \chi. \end{aligned} \tag{20}$$

In the following proposition, we present several properties of the protected safety zone.

Proposition 3: (1) ϕ is a conflict-free heading change for aircraft A_f if $\phi \in \Phi_f(s_p, \phi_p, \chi)$; (2) the post-maneuver heading $|\phi_f|$ of aircraft A_f is bounded above by $|\phi|$ for any $\phi \in \Phi_f(s_p, \phi_p, \chi)$; (3) $\Phi_f(s_p, \phi_p, \chi)$ is a closed interval; and (4) $\Phi_f(s_p, \phi_p, \chi_1)$ is a subset of $\Phi_f(s_p, \phi_p, \chi_2)$ for any $\chi_1 > \chi_2 > 0$.

Proof: The first part of Proposition 3 follows directly from the definition of projected safety zone and Proposition 1. Note that ϕ_f, the optimal heading change of aircraft A_f, need not necessarily belong to Φ_f, since other options exist for an aircraft than that of "following" a previous aircraft. The second part of Proposition 3 is a consequence of the optimality assumption on modeled aircraft maneuvers.

Consider now the third part. Φ_f is obviously a closed interval when Φ_f is empty or Φ_f has only one element. Then consider the case when Φ_f has more than one element. Let $\phi_1, \phi_2 \in \Phi_f(s_p, \phi_p, \chi)$ and $\phi_1 < \phi_2$. If ϕ belongs to $\Phi_f(s_p, \phi_p, \chi)$ for any $\phi \in (\phi_1, \phi_2)$, then $\Phi_f(s_p, \phi_p, \chi)$ is a convex set, and thus an interval. Since both R_{inner} and R_{outer} are strictly monotone increasing functions of ϕ (according to Proposition 2), we have $R_{\text{inner}}(s_f, \phi, \eta) > R_{\text{inner}}(s_f, \phi_1, \eta) \geq R_{\text{inner}}(s_p, \phi_p, \eta)$ and $R_{\text{outer}}(s_f, \phi, \eta) <$

$R_{\text{outer}}(s_f, \phi_2, \eta) \leq R_{\text{outer}}(s_p, \phi_p, \eta)$ for all $\eta \in [-\chi, \chi]$. Therefore, $\phi \in \Phi_f(s_p, \phi_p, \chi)$ and thus Φ_f is an interval. Further, it can be tested that the limit point of any converging sequence $\{\phi_i, i = 1, 2, ...\} \subset \Phi_f$ also belongs to Φ_f (due to the continuity of R_{inner} and R_{outer}). This implies that Φ_f is a closed set. Hence, we prove that Φ_f is a closed interval.

Considering the fourth part, it can be easily tested that ϕ belongs to $\Phi_f(s_p, \phi_p, \chi_2)$ whenever $\phi \in \Phi_f(s_p, \phi_p, \chi_1)$. Therefore, $\Phi_f(s_p, \phi_p, \chi_1)$ must be a subset of $\Phi_f(s_p, \phi_p, \chi_2)$. **Q.E.D.**

The size of the protected safety zone, i.e., the interval length of Φ_f, can be viewed as an index of robustness. Numerical investigations show that the protected safety zone is very often an interval with nonempty interior, and that its size depends upon various parameters such as $s_p - s_f$, ϕ_p, χ, θ, and R. Fig. 8 illustrates how the size of protected safety zone changes with those parameters. It can be seen that the size of the protected safety zone varies as a very non-trivial function of those parameters.

The bigger the protected safety zone Φ_f is, the larger range of safe heading angles there will be for A_f to take advantage of the presence of A_p, and therefore the more reliable it is for A_f to "hide" safely behind A_p regardless of traffic uncertainties such as perturbations of some flight parameters. One example has been presented in the previous simulation (Fig. 4), where heading change maneuvers are shown to be more robust than offset maneuvers in the sense that they can successfully handle perturbations of perceived safe separation minima. Note that in the offset model, the aircraft protected safety zone always consists of a single element.

Proposition 3 implies that a feasible solution to the optimization problem

$$\min |\phi| \text{ subject to (20)} \tag{21}$$

provides an upper bound for $|\phi_f|$. However, (21) is usually very difficult to solve due to the infinite-dimensional nature of (20). Besides figuring out a solution to (21), we may instead examine the following equation in ϕ, the solution of which is very often a feasible solution to (20) (this can be rigorously tested via a computational method, as will be discussed later in this paper) and therefore can be used as an easy upper bound for $|\phi_f|$:

$$\frac{\cos\frac{\theta+\phi}{2}}{\cos\frac{\theta-\phi}{2}} = \frac{\cos\frac{\theta+\phi_p}{2}}{\cos\frac{\theta-\phi_p}{2}} + \frac{s_f - s_p}{R}. \tag{22}$$

This equation is derived from

$$R_{\text{inner}}(s_f, \phi, 0) + R_{\text{outer}}(s_f, \phi, 0) = R_{\text{inner}}(s_p, \phi_p, 0) + R_{\text{outer}}(s_p, \phi_p, 0). \tag{23}$$

An intuitive interpretation for Eq. (22) is that its solution ϕ, when used by aircraft A_f, is such that the "center" of the projected conflict zone of A_f coincides with the "center" of the projected conflict zone of A_p. The "center" is the point in the control sector whose polar coordinates (referenced by flow 2) are (r, η) with $\eta = 0$ and $r = (R_{\text{inner}}(s, \phi, 0) + R_{\text{outer}}(s, \phi, 0))/2$.

4.4 Existence of heading change maneuvers

We now complete the stability analysis of two intersecting flows of aircraft using heading change maneuvers. The following theorem shows that under appropriate conditions an aircraft entering the sector can always perform a heading change maneuver that results in a conflict-free trajectory, and this maneuver is bounded above. The basic idea of the argument stands close to that used in [11].

Theorem: Consider an angle χ satisfying

$$\chi \in [2\arcsin\frac{D_{\text{sep}}}{2R\sin\frac{\theta}{2}}, \frac{\pi}{2} - \frac{\theta}{2} - \arcsin\frac{D_{\text{sep}}}{2R\sin\frac{\theta}{2}}] \cap [2\arcsin\frac{D_{\text{sep}}}{2R\sin\frac{\theta}{2}}, \frac{\theta}{2}). \tag{24}$$

Assume the protected safety zone $\Phi_f(s_p, \phi_p, \chi)$ is nonempty for any value of the variables $(r_o, \eta_o, s_p, \phi_p)$ satisfying the constraints

$$R_{\text{inner}}(0, -\chi, \eta_o) < r_o < R_{\text{outer}}(0, -\chi, \eta_o), \tag{25}$$

$$0 \leq \eta_o \leq \chi,\ r_o \geq 0, \tag{26}$$

$$r_o = R_{\text{inner}}(s_p, \phi_p, \eta_o), \tag{27}$$

$$\text{and} \quad -\chi \leq \phi_p \leq \chi,\ s_p \geq r_o,\ s_p \geq D_{\text{sep}}. \tag{28}$$

Assume moreover that, under the conditions above, $\Phi_f(s_p, \phi_p, \chi)$ always contains one element ϕ such that $\chi \geq \phi$. Then the heading changes of all aircraft in flows 1 or 2 are bounded above by χ.

Proof: The proof is illustrated in Fig. 9. Consider now any aircraft A_f just entering the sector ($s_f = 0$) and about to make a resolution maneuver. Without loss of generality, let A_f belong to the first aircraft flow. In Fig. 9, rather than plotting A_f at its entry point to the sector, we plot A_f after it has traveled some distance in the sector, thereby simplifying the graphical representations of its projected conflict zone for different headings.

Assume that the heading change of any aircraft entering the sector earlier than A_f is bounded above by χ. If this assumption always implies that the heading change of A_f must be less than or equal to χ, then the heading changes of all aircraft in flows 1 or 2 are bounded above by χ (according to the principle of mathematical induction).

We first hypothesize that there exists no conflict resolution maneuver for A_f with amplitude less than or equal to χ, and then reach a contradiction.

According to the hypothesis, at least one aircraft A_o with polar coordinates (r_o, η_o), is conflicting with the incoming aircraft A_f when aircraft A_f turns to the left with a heading change equal to $-\chi$.

Thus (r_o, η_o) satisfy conditions (25) and (26). According to Proposition 2, A_f must turn further left to find a conflict-free heading. Thus there exists a heading ϕ^{left} such that

$$\phi^{\text{left}} < -\chi \tag{29}$$

$$\text{and} \quad r_o = R_{\text{outer}}(0, \phi^{\text{left}}, \eta_o), \tag{30}$$

simply meaning that the protected safety zone of aircraft A_f undergoing the deviation ϕ^{left} is in just contact with A_o.

We consider next the following two cases on the deviation η_o of aircraft A_o.

Case 1: $\eta_o \leq 0$. Let ϕ be the solution (ϕ^{left}) to (30) for $r_o = 0$ and $\eta_o = 0$. It can be tested that

$$\phi = -2 \arcsin \frac{D_{\text{sep}}}{2R \sin \frac{\theta}{2}}. \tag{31}$$

Further, since $r_o \geq 0$ and $\eta_o \leq 0$, we have $\phi^{\text{left}} \geq \phi$ (according to Proposition 2). From (29) and (31), we get

$$\chi < 2 \arcsin \frac{D_{\text{sep}}}{2R \sin \frac{\theta}{2}}, \tag{32}$$

which contradicts (24).

Case 2: $\eta_o > 0$. For this to happen, an earlier aircraft from flow 1, denoted A_p with polar coordinates (s_p, ϕ_p), must have forced A_o to perform a conflict resolution maneuver. Therefore (s_p, ϕ_p) satisfy (27) and (28).

Since (25)-(28) are satisfied, we know from the assumptions of the theorem that $\Phi_f(s_p, \phi_p, \chi)$ is nonempty and there exists $\phi^{\text{right}} \in \Phi_f(s_p, \phi_p, \chi)$ satisfying $\phi^{\text{right}} \leq \chi$. In other terms, aircraft A_f could have "hidden" behind aircraft A_p with a heading change ϕ^{right} satisfying $\phi^{\text{right}} \in (-\chi, \chi]$ for aircraft A_f. Thus leading to a contradiction. **Q.E.D.**

This theorem appears to be rather unappealing at first glance, since it involves convoluted conditions that must be satisfied by the problem's essential parameters, including the minimum separation distance D_{sep}, the sector size R, and the encounter angle among aircraft θ. It is shown in Appendix how these conditions may easily be checked via a standard Branch-and-Bound algorithm.

Consider the case $R = 80$ nm, $D_{\text{sep}} = 5$ nm, and $\theta = \frac{\pi}{2}$. The simulation shown in Fig. 2 *suggests* that the amplitude of the heading changes performed by all aircraft is bounded above by $\chi = 0.1$ rad. Using the computer-aided approach outlined in the Appendix, we prove that $\chi = 0.1$ is indeed a valid performance bound for any incoming aircraft flows satisfying $R = 80$ nm and $\theta = \frac{\pi}{2}$.

5 Conclusion

This paper provides an approach to prove the stability of intersecting aircraft flows whose conflicts are solved by heading changes. It is shown that under several scenarios of practical interest, it is possible to establish such proofs and therefore ascertain without ambiguity that no instability may occur. The nonlinear nature of heading change maneuvers makes the stability analysis quite convoluted when compared to similar analyses performed with simpler, but less realistic maneuver models. This effort has also led to some interesting and new robustness properties of heading change maneuvers to system uncertainties.

Replacing these simulations with analytic arguments is the object of current research and will be reported elsewhere.

While discussed in the framework of air transportation, it is clear this result applies to a variety of situation involving many mobile and interacting agents.

6 Acknowledgments

This work was supported by NASA Ames Research Center, Office of Naval Research, and the Zakhartchenko Fellowship at MIT.

References

[1] J. -M. Alliot, N. Durand, and G. Granger, "FACES: a free flight autonomous and coordinated embarked solver," Air Traffic Control Quarterly, vol. 8, no. 2, pp. 109-130, 2000.

[2] S. Devasia and G. Meyer, "Automated conflict resolution procedures for air traffic management," Proc. IEEE Conf. Decision and Control, Dec. 1999.

[3] D. Delahaye and S. Puechmorel, "Air traffic complexity: Toward intrinsic metrics," 3rd USA/Europe Air Traffic Management RD Seminar, 2000.

[4] R. Ghosh and C. Tomlin, "Maneuver design for multiple aircraft conflict resolution," Proceedings of American Control Conference, June 2000.

[5] G. Granger, N. Durand, and J. -M. Alliot, "Optimal resolution of en route conflicts," 4th USA/Europe Air Traffic Management RD Seminar, 2001.

[6] J. M. Histon, G. Aigoin, D. Delahaye, R. J. Hansman, and S. Puechmorel, "Introducing structural considerations into complexity metrics," 4th USA/Europe Air Traffic Management RD Seminar, 2001.

[7] J. Hu, M. Prandini, and S. Sastry, "Optimal coordinated maneuvers for three-dimensional aircraft conflict resolution," Journal of Guidance, Control, and Dynamics, vol. 25, no. 5, pp. 888-900, 2002.

[8] J. Krozel and M. Peters, "Strategic conflict detection and resolution for free flight," Proc. IEEE Conf. Decision and Control, San Diego, CA, Dec. 1997.

[9] J. K. Kuchar and L. C. Yang, "A review of conflict detection and resolution modeling methods," IEEE Trans. Intelligent Transportation Systems, vol. 1, no. 4, pp. 179-189, 2000.

[10] Z. -H. Mao and E. Feron, "Stability and performance of intersecting aircraft flows under sequential conflict resolution," Proc. American Control Conference, Arlington, VA, 2001.

[11] Z. -H. Mao, E. Feron, and K. Bilimoria, "Stability and performance of intersecting aircraft flows under decentralized conflict avoidance rules," IEEE Trans. Intelligent Transportation Systems,, vol. 2, no. 2, pp. 101-109, 2001.

[12] R. W. Simpson, Course Notes for 16.72: Air Traffic Control, MIT, 1993.

[13] B. Sridhar, K. S. Seth, and S. Grabbe, "Airspace complexity and its application in air traffic management," 2nd USA/Europe Air Traffic Management RD Seminar, 1998.

[14] C. Tomlin, G. J. Pappas, and S. Sastry, "Conflict resolution for air traffic management: a study in multi-agent hybrid systems," IEEE Trans. Automatic Control, vol. 43, no. 4, pp. 509-521, 1998.

Appendix: A computational procedure to test sufficient conditions for stability

Consider the general problem of proving whether a given function f is positive over a given domain of its argument, that is, proving

$$f(\mathbf{x}) > 0 \text{ for any } \mathbf{x} \equiv (x^{(1)}, ..., x^{(n)}) \in \Omega \subset \mathbf{R}^n, \tag{33}$$

where f is continuous and the domain Ω is bounded.

As will be shown soon, proving the conditions enunciated in the theorem are true can be transformed into solving a problem of the above form.

To test the validity of (33), we follow a "branch-and-bound" procedure: First construct a finite coverage Ω_i, $i = 1, ..., m$, of Ω such that $\bigcup_{1 \le i \le m} \Omega_i \supset \Omega$, and then find both a lower bound, denoted B_i^{lower}, and an upper bound, denoted B_i^{upper}, for the minimum value of $f(\mathbf{x})$ on Ω_i, i.e., $\min_{\mathbf{x} \in \Omega_i} f(\mathbf{x})$, for every $i \in \{1, ..., m\}$. If $B_i^{\text{lower}} > 0$ for all $i \in \{1, ..., m\}$, then we conclude that (33) is true; if $B_i^{\text{upper}} \le 0$ for some $i \in \{1, ..., m\}$, then we say that (33) is not true; if otherwise, i.e., $B_i^{\text{lower}} \le 0$ for some $i \in \{1, ..., m\}$ and $B_i^{\text{upper}} > 0$ for all $i \in \{1, ..., m\}$, then we need to make finer covers or partitions for those Ω_i with $B_i^{\text{lower}} \le 0$, and to repeat the above steps until (33) is answered or some computational tolerance is reached.

There are many ways to construct a coverage of Ω. For instance, we may choose

$$\Omega_i = [x_i^{(1)} - \delta^{(1)}, x_i^{(1)} + \delta^{(1)}] \times \cdots \times [x_i^{(n)} - \delta^{(n)}, x_i^{(n)} + \delta^{(n)}], \tag{34}$$

where $\mathbf{x}_i$, $i = 1, ..., m$, are points on an n-dimensional orthogonal grid with axial spacings $\delta^{(j)} > 0$, $j = 1, ..., n$. The grid points, $\mathbf{x}_i$, $i = 1, ..., m$, are chosen such that $\bigcup_{1 \le i \le m} \Omega_i \supset \Omega$.

We propose to use this procedure to establish whether the conditions enunciated in the theorem are satisfied, therefore leading to a positive conclusion about system stability.

1. Obtain an estimated performance bound χ. This χ can be estimated from simulations such as the one shown in Fig. 2.

2. Recast the problem of testing whether χ satisfies the conditions in the theorem as a problem of the form (33).

3. Test whether (33) is true by following the branch-and-bound procedure described above.

In the rest of this appendix, we consider the orthogonal aircraft flows ($\theta = \frac{\pi}{2}$), and use this scenario as an example to illustrate how to apply the above procedure to test the validity of an estimated heading change bound.

Assume we have an estimated upper bound $\chi \in [2\arcsin\frac{D_{\text{sep}}}{\sqrt{2}R}, \frac{\pi}{4} - \arcsin\frac{D_{\text{sep}}}{\sqrt{2}R}]$.

Since θ equals $\frac{\pi}{2}$, (13) and (14) become

$$R_{\text{inner}}(s,\phi,\eta) = \frac{\sqrt{2}R\sin\frac{\eta+\phi}{2} - D_{\text{sep}}}{\sin\frac{\frac{\pi}{2}-\eta+\phi}{2}} + s \tag{35}$$

$$\text{and} \quad R_{\text{outer}}(s,\phi,\eta) = \frac{\sqrt{2}R\sin\frac{\eta+\phi}{2} + D_{\text{sep}}}{\sin\frac{\frac{\pi}{2}-\eta+\phi}{2}} + s. \tag{36}$$

Let $\mathbf{x} \equiv (r_o, \eta_o, \phi_p)$. According to (27), we may write s_p as a function of $\mathbf{x}$:

$$s_p(\mathbf{x}) = r_o - \frac{\sqrt{2}R\sin\frac{\eta_o+\phi_p}{2} - D_{\text{sep}}}{\sin\frac{\frac{\pi}{2}-\eta_o+\phi_p}{2}}. \tag{37}$$

The following expression, derived from (22) for $\theta = \frac{\pi}{2}$ and $s_f = 0$, defines a ϕ which, very often, belongs to $\Phi_f(s_p, \phi_p, \chi)$:

$$\phi(\mathbf{x}) = \frac{\pi}{2} - 2\arctan(\tan\frac{\frac{\pi}{2}-\phi_p}{2} - \frac{s_p(\mathbf{x})}{R}). \tag{38}$$

Define

$$f_1(\mathbf{x}) \equiv \chi - \phi(\mathbf{x}), \tag{39}$$

$$f_2(\mathbf{x}) \equiv R_{\text{inner}}(0, \phi(\mathbf{x}), \eta_o) - R_{\text{inner}}(s_p(\mathbf{x}), \phi_p, \eta_o), \tag{40}$$

$$\text{and} \quad f_3(\mathbf{x}) \equiv R_{\text{outer}}(s_p(\mathbf{x}), \phi_p, \eta_o) - R_{\text{outer}}(0, \phi(\mathbf{x}), \eta_o). \tag{41}$$

Satisfying the hypotheses of the theorem is equivalent to checking whether

$$\begin{aligned} & f_1(\mathbf{x}) > 0,\ f_2(\mathbf{x}) > 0,\ \text{and}\ f_3(\mathbf{x}) > 0 \\ \text{whenever}\quad & \mathbf{x} \in \Omega = \{(r_o, \eta_o, \phi_p) \,|\, 0 \le \eta_o \le \chi, \\ & \quad R_{\text{inner}}(0, -\chi, \eta_o) < r_o < R_{\text{outer}}(0, -\chi, \eta_o), \\ & \quad r_o \ge 0,\ -\chi \le \phi_p \le \chi,\ s_p(\mathbf{x}) \ge r_o, \\ & \quad \text{and}\ s_p(\mathbf{x}) \ge D_{\text{sep}}\}, \end{aligned}$$

which is a specific instance of (33).

Our last step is to test whether $f_1(\mathbf{x}) > 0$, $f_2(\mathbf{x}) > 0$, and $f_3(\mathbf{x}) > 0$, for all $\mathbf{x} \in \Omega$, following the branch-and-bound procedure.

We construct for Ω a set of covers Ω_i $(i = 1, ..., m)$ of the form (34), where $\mathbf{x}_i = (r_{o,i}, \eta_{o,i}, \phi_{p,i})$ and $(\delta^{(1)}, \delta^{(2)}, \delta^{(3)}) = (\delta^{r_o}, \delta^{\eta_o}, \delta^{\phi_p})$. Since $f_k(\mathbf{x}_i)$ $(k = 1, 2,$ or $3)$ is greater than or equal to $\min_{\mathbf{x}\in\Omega_i} f_k(\mathbf{x})$, we may use it as an upper bound for $\min_{\mathbf{x}\in\Omega_i} f_k(\mathbf{x})$, i.e.,

$$B_{k,i}^{\text{upper}} = f_k(\mathbf{x}_i), \tag{42}$$

for $k = 1, 2, 3$, and $i = 1, ..., m$.

In the following, we construct a lower bound for $\min_{\mathbf{x}\in\Omega_i} f_k(\mathbf{x})$. Define

$$\begin{aligned}
r_{o,i}^{\text{lower}} &= r_{o,i} - \delta^{r_o}, \\
r_{o,i}^{\text{upper}} &= r_{o,i} + \delta^{r_o}, \\
\eta_{o,i}^{\text{lower}} &= \eta_{o,i} - \delta^{\eta_o}, \\
\eta_{o,i}^{\text{upper}} &= \eta_{o,i} + \delta^{\eta_o}, \\
\phi_{p,i}^{\text{lower}} &= \phi_{p,i} - \delta^{\phi_p}, \\
\phi_{p,i}^{\text{upper}} &= \phi_{p,i} + \delta^{\phi_p}, \\
s_{p,i}^{\text{lower}} &= r_{o,i}^{\text{lower}} - \frac{\sqrt{2}R\sin\frac{\eta_{o,i}^{\text{upper}}+\phi_{p,i}^{\text{upper}}}{2} - D_{\text{sep}}}{\sin\frac{\frac{\pi}{2}-\eta_{o,i}^{\text{upper}}+\phi_{p,i}^{\text{upper}}}{2}}, \\
s_{p,i}^{\text{upper}} &= r_{o,i}^{\text{upper}} - \frac{\sqrt{2}R\sin\frac{\eta_{o,i}^{\text{lower}}+\phi_{p,i}^{\text{lower}}}{2} - D_{\text{sep}}}{\sin\frac{\frac{\pi}{2}-\eta_{o,i}^{\text{lower}}+\phi_{p,i}^{\text{lower}}}{2}}, \\
\phi_i^{\text{lower}} &= \frac{\pi}{2} - 2\arctan(\tan\frac{\frac{\pi}{2}-\phi_{p,i}^{\text{lower}}}{2} - \frac{s_{p,i}^{\text{lower}})}{R}), \\
\text{and} \quad \phi_i^{\text{upper}} &= \frac{\pi}{2} - 2\arctan(\tan\frac{\frac{\pi}{2}-\phi_{p,i}^{\text{upper}}}{2} - \frac{s_{p,i}^{\text{upper}})}{R}),
\end{aligned}$$

and define

$$\begin{aligned}
B_{1,i}^{\text{lower}} &= \chi - \phi_i^{\text{upper}}, \\
B_{2,i}^{\text{lower}} &= R_{\text{inner}}(0, \phi_i^{\text{lower}}, \eta_{o,i}^{\text{lower}}) - R_{\text{inner}}(s_{p,i}^{\text{upper}}, \phi_{p,i}^{\text{upper}}, \eta_{o,i}^{\text{upper}}), \\
\text{and} \quad B_{3,i}^{\text{lower}} &= R_{\text{outer}}(s_{p,i}^{\text{lower}}, \phi_{p,i}^{\text{lower}}, \eta_{o,i}^{\text{lower}}) - R_{\text{outer}}(0, \phi_i^{\text{upper}}, \eta_{o,i}^{\text{upper}}).
\end{aligned} \tag{43}$$

Due to the monotone characteristics of $s_p(\mathbf{x})$ (according to Proposition 2), $\phi(\mathbf{x})$ (according to properties of $\tan(u)$ and $\arctan(u)$), $R_{\text{inner}}(s, \phi, \eta)$, and $R_{\text{outer}}(s, \phi, \eta)$ (according to Proposition 2), we can easily show that $B_{k,i}^{\text{lower}}$ $(k = 1, 2,$ or $3)$ defined as above is a lower bound for $\min_{\mathbf{x}\in\Omega_i} f_k(\mathbf{x})$.

Based on the construction of $B_{k,i}^{\text{upper}}$ and $B_{k,i}^{\text{lower}}$, we have

$$\lim_{\max\{\delta^{r_o},\delta^{\eta_o},\delta^{\phi_p}\}\to 0} B_{k,i}^{\text{upper}} = \lim_{\max\{\delta^{r_o},\delta^{\eta_o},\delta^{\phi_p}\}\to 0} B_{k,i}^{\text{lower}} = \lim_{\max\{\delta^{r_o},\delta^{\eta_o},\delta^{\phi_p}\}\to 0} \min_{\mathbf{x}\in\Omega_i} f_k(\mathbf{x}), \tag{44}$$

since $s_p(\mathbf{x})$, $\phi(\mathbf{x})$, $R_{\text{inner}}(s,\phi,\eta)$, and $R_{\text{outer}}(s,\phi,\eta)$ are continuous.

The branch-and-bound algorithm can then be used in our context.

Finally, we run a simulation for the case $R = 80$ nm and $\theta = \frac{\pi}{2}$. Remind that Fig. 2 has empirically suggested that the angle of deviation of the tested aircraft is bounded above by $\chi = 0.1$ rad. In the simulation, we use $\chi = 0.1$ as the estimated performance bound, and follow a construction of Ω_i as suggested by (34) with grid spacings $\delta^{r_o} = 0.002$ nm, $\delta^{\eta_o} = 0.0002$ rad, and $\delta^{\phi_p} = 0.0002$ rad. Then we get $f_1(\mathbf{x}) \geq \min_i B_{1,i}^{\text{lower}} = 0.0027 > 0$, $f_2(\mathbf{x}) \geq \min_i B_{2,i}^{\text{lower}} = 0.0714 > 0$, and $f_3(\mathbf{x}) \geq \min_i B_{3,i}^{\text{lower}} = 0.0924 > 0$, for all $\mathbf{x} \in \Omega$. Hence, we have shown computationally (but rigorously) that $\chi = 0.1$ is a valid performance bound for any scenarios of aircraft flows constrained by $R = 80$ nm and $\theta = \frac{\pi}{2}$.

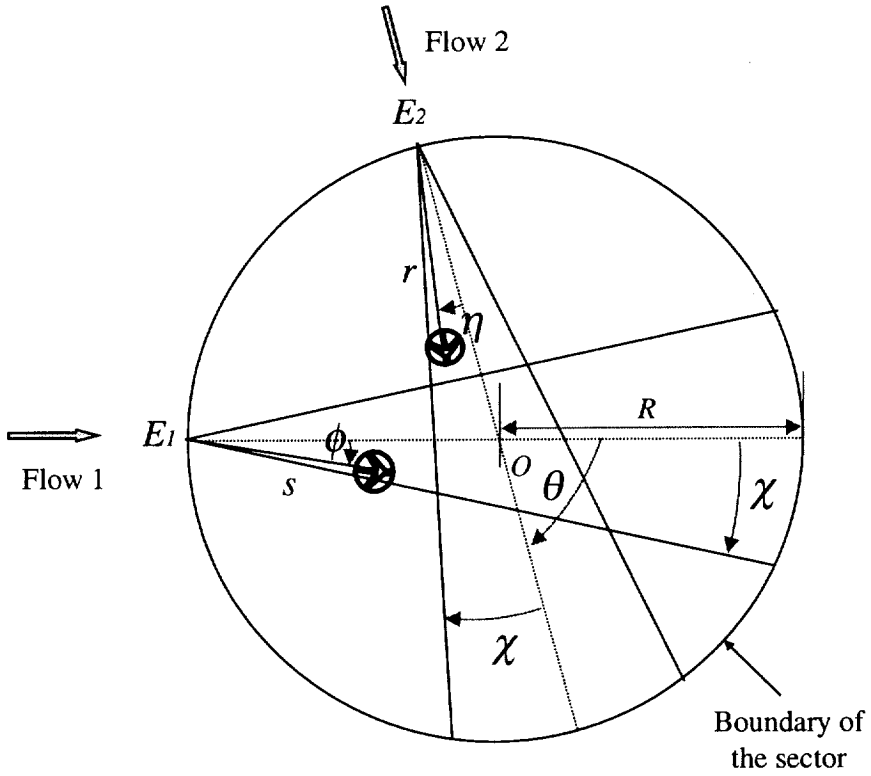

Figure 1: Two flows of aircraft with airway intersection in a circular sector. χ is the decision bound, i.e., allowed largest heading change angle for the aircraft.

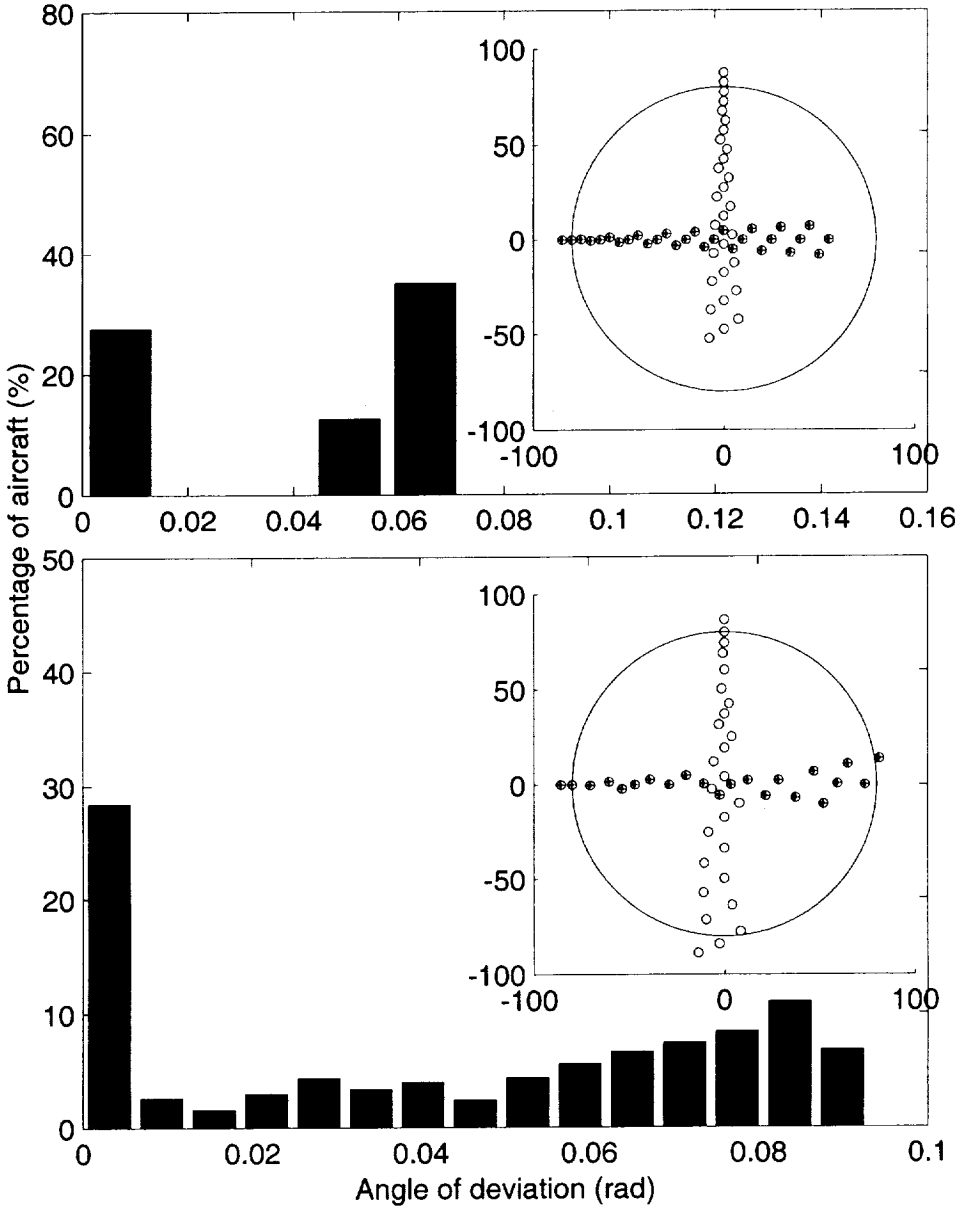

Figure 2: Distributions of angular deviations. Top: Simulation with constant inter-arrival spacing (5 nm). Bottom: Simulation with random inter-arrival spacing (uniform distribution over [5,10] nm).

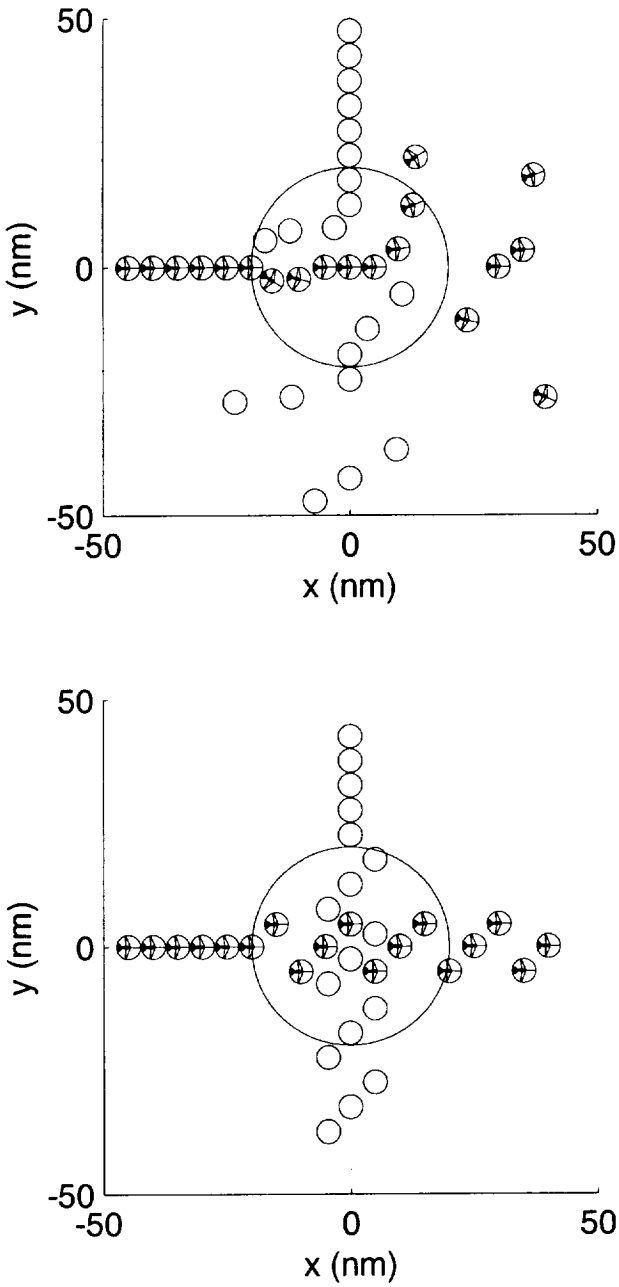

Figure 3: Top: Unstable aircraft flows resulting from heading change maneuvers. Bottom: Stable aircraft flows resulting from offset maneuvers.

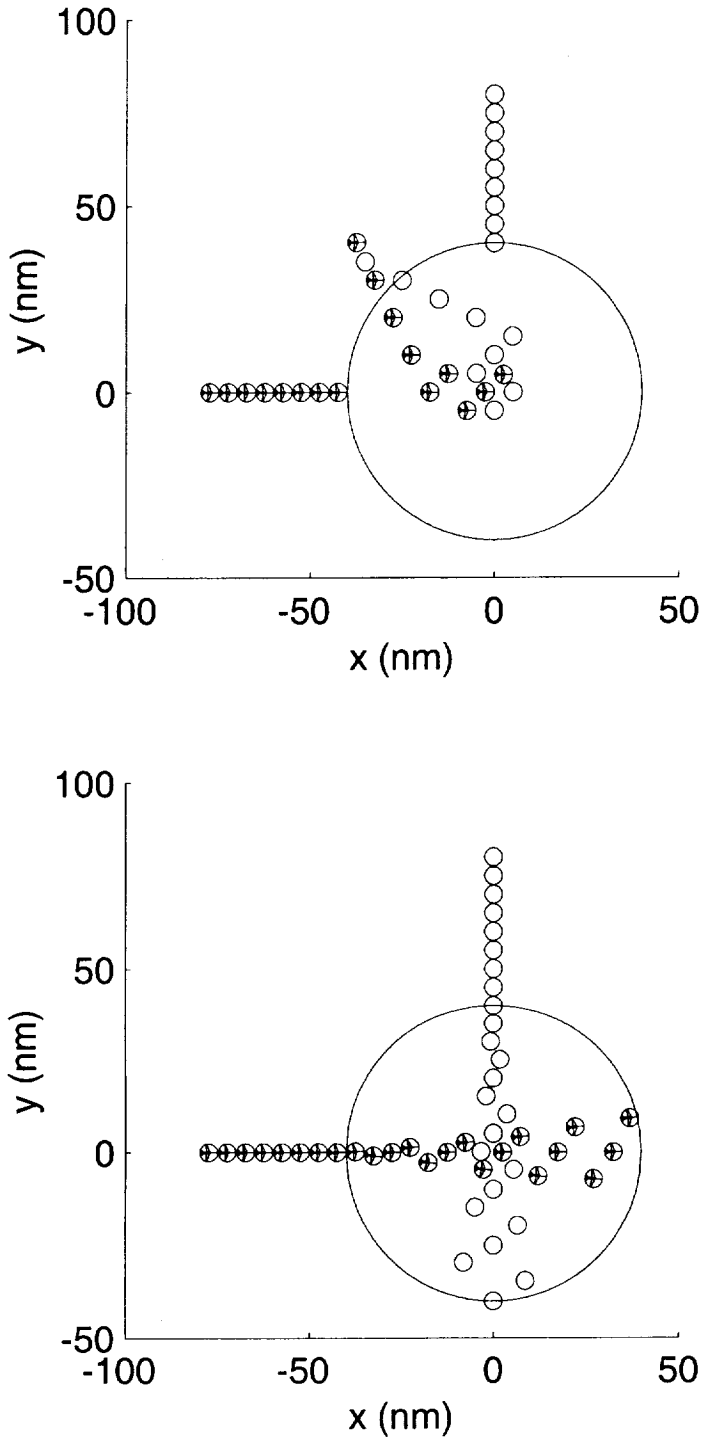

Figure 4: Comparison of offset maneuvers and heading change maneuvers in response to time varying D_{sep}. Top: Using offset maneuvers. Bottom: Using heading change maneuvers.

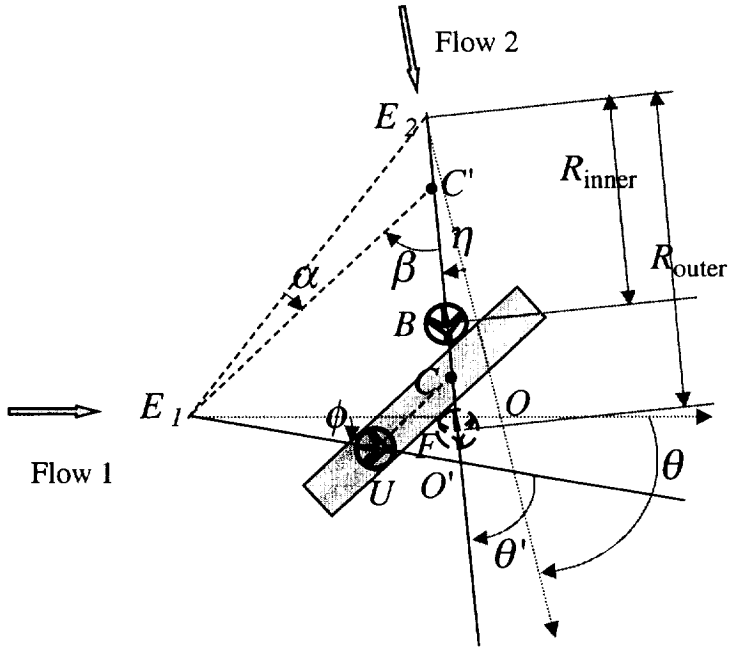

Figure 5: Conflict avoidance conditions on the polar coordinates of a pair of aircraft.

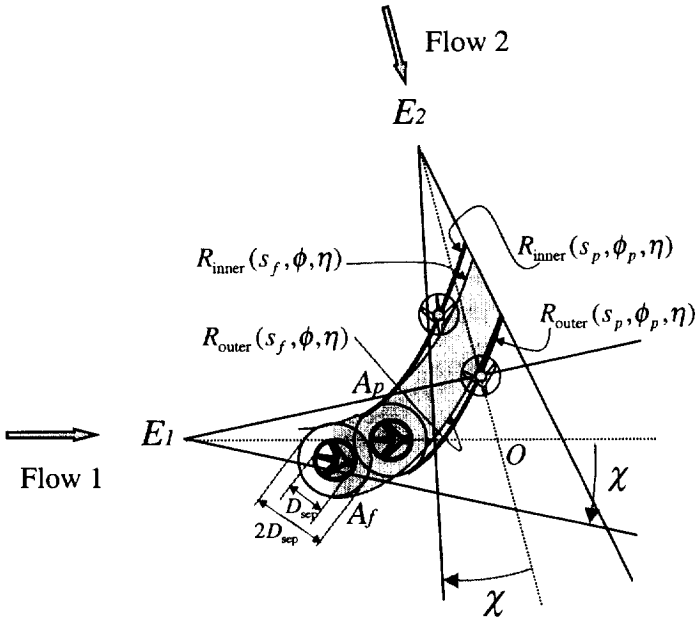

Figure 6: Projected conflict zones for aircraft A_p and A_f, respectively.

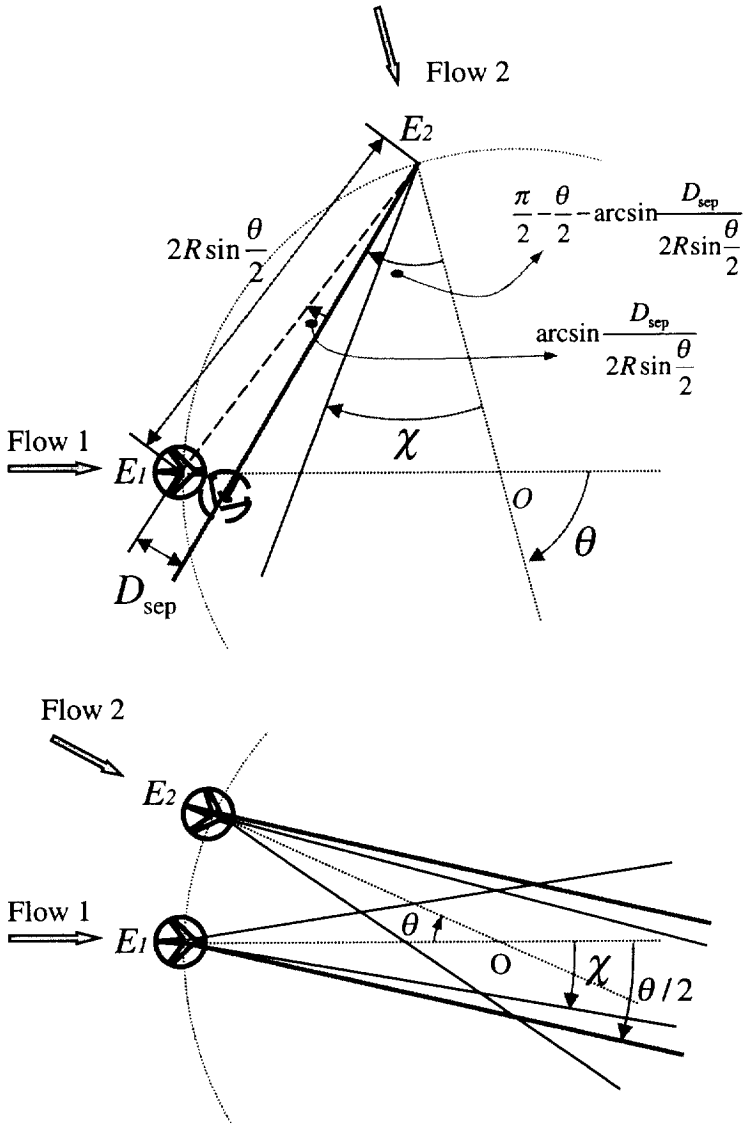

Figure 7: Constraints on the decision bound χ.

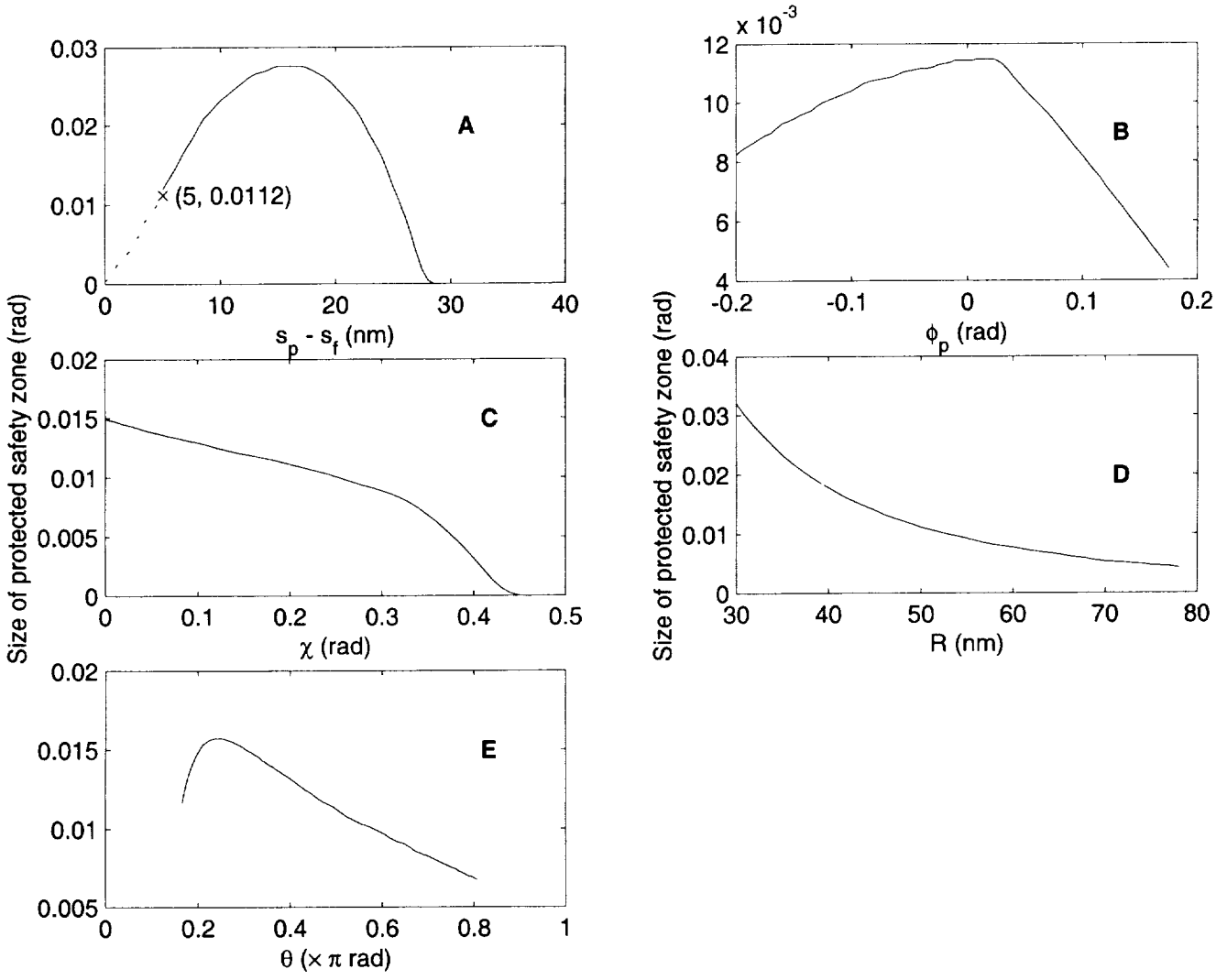

Figure 8: The size of protected safety zone versus various flight parameters. **A**: $R = 50$ (nm), $\theta = \pi/2$ (rad), $s_f = 0$ (nm), $\phi_p = 0$ (rad), and $\chi = 0.2$ (rad). **B**: $R = 50$, $\theta = \pi/2$, $s_f = 0$, $s_p = 5$, and $\chi = 0.2$. **C**: $R = 50$, $\theta = \pi/2$, $s_f = 0$, $s_p = 5$, and $\phi_p = 0$. **D**: $\theta = \pi/2$, $s_f = 0$, $s_p = 5$, $\phi_p = 0$, and $\chi = 0.2$. **E**: $R = 50$, $s_f = 0$, $s_p = 5$, $\phi_p = 0$, and $\chi = 0.2$.

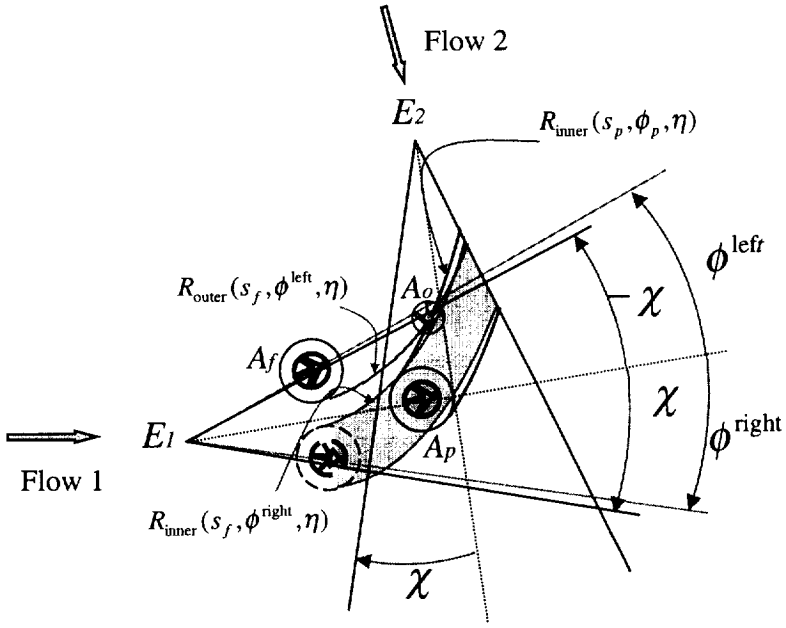

Figure 9: Existence of conflict resolution maneuver with heading change maneuver (see the proof for the theorem).